

UC San Diego

UC San Diego Electronic Theses and Dissertations

Title

Regulation of Myosin VI transport, tethering to actin and cargo binding

Permalink

<https://escholarship.org/uc/item/9nw73120>

Author

Naccache, Samia Nidal

Publication Date

2006

Supplemental Material

<https://escholarship.org/uc/item/9nw73120#supplemental>

Peer reviewed|Thesis/dissertation

UNIVERSITY OF CALIFORNIA, SAN DIEGO

Regulation of Myosin VI transport, tethering to actin and
cargo binding.

A dissertation submitted in partial satisfaction of the requirements of

Doctor of Philosophy in Biology

by

Samia Nidal Naccache

Committee in Charge:

Professor, Eduardo Macagno, Chair
Professor, James Feramisco
Professor, Tama Hasson
Professor, Karen Oegema
Professor, Suresh Subramani

2006

The dissertation of Samia Nidal Naccache is approved, and it is of acceptable quality
and form for publication on microfilm.

University of California, San Diego

2006

DEDICATION

I would like to dedicate this dissertation to my father Albert Naccache and my mother Tina Naccache for their constant support of my academic career, in person but especially over the ether, internet and phone-lines of 7500 miles of distance, to my brother Henri and his wife Jill and my roommate Shimona for their love and support through my graduate years, and to the memory of my grandparents Alberto (1914–2000) Henry (1917-1976) Louisa (1919 -1999) and Marcelle (1920-2005).

TABLE OF CONTENTS

Signature page.....	iii
Dedication.....	iv
Table of Contents.....	v
List of Figures.....	vii
List of Tables.....	x
Acknowledgments.....	xi
Vita.....	xii
Abstract.....	xiv
Introduction.....	1
Chapter One: Myosin VI moves uncoated endocytic vesicles through the cortical actin meshwork.	
Introduction.....	31
Materials and Methods.....	38
Results.....	43
Discussion.....	48
Acknowledgements.....	52
Figures.....	53
Chapter Two: Phosporylation at T406 can switch myosin VI from a motor to a tether.	
Introduction.....	62
Materials and Methods.....	65
Results.....	73
Discussion.....	84

Acknowledgements.....	90
Figures.....	91
Chapter Three: Binding of internalized receptors to the PDZ domain of GIPC/Synectin recruits myosin VI to endocytic vesicles.	
Introduction.....	107
Materials and Methods.....	111
Results.....	120
Discussion.....	132
Acknowledgements.....	138
Figures.....	139
Conclusion.....	158
References.....	162

LIST OF FIGURES

Chapter One:

Figure 1.1. Schematic of GFP tagged myosin VI constructs.....	54
Figure 1.2. The cortical actin meshwork of ARPE-19 cells is depolymerized by nanomolar concentrations of latrunculin.....	55
Figure 1.3. The kinetics of transferrin endocytosis in ARPE-19 cells is not affected by latrunculin A	56
Figure 1.4. The kinetics of transferrin exit from clathrin coated vesicles is not affected by nanomolar concentrations of Latrunculin A.....	57
Figure 1.5. Delivery of transferrin to the early endosome is accelerated by nanomolar quantities of latrunculin A.....	58
Figure 1.6. Delivery of transferrin to the early endosome is accelerated by nanomolar quantities of latrunculin	59
Figure 1.7. Removal of the actin barrier in ARPE-19 cells rescues the trafficking defects seen upon GFP-M6tail and GFP-M6(K157R) expression.....	60

Chapter Two:

Figure 2.1. GFP tagged constructs mimicking myosin VI in the dephosphorylated (GFP-M6(T406A)) or phosphorylated (GFP-M6(T406E)) states localize to peripheral UCVs.....	93
Figure 2.2. Indirect immunofluorescence of ARPE-19 cells expressing GFP-M6(T406A) or GFP-M6(T406E) reveals that they both target to UCV	94
Figure 2.3. Expression levels of GFP-M6, GFP-M6(T406A) and GFP-M6(T406E) are equivalent.....	95
Figure 2.4. Overexpression of GFP-M6(T406A) and GFP-M6(T406E) does not delay the trafficking of transferrin to the early endosome.....	96
Figure 2.5. Movement of GFP-M6(T406A)- and GFP-M6(T406E)-associated vesicles.....	97
Figure 2.6. Actin rearrangements are not due to recruitment of actin polymerizing agents or actin crosslinking.....	99

Figure 2.7. Modification at T406 results in changes in actin filament stability as judged by resistance to cytochalasin D.....	100
Figure 2.8. GFP-M6(T406E)-associated vesicles cluster at actin filament minus ends.....	101
Figure 2.9: Antibody to phosphorylated threonine 406 on myosin VI6 recognizes distal tubules, not mouse kidney proximal tubules.....	103
Figure 2.10: Expression of constitutively active hPak1T423E does not induce myosin VI-associated clusters in ARPE-19 cells expressing GFP-M6.....	104
Figure 2.11: Expression of myosin VI constructs altered at T406 and C442.....	105
Figure 2.12: Video Materials.....	106
Chapter Three:	
Figure 3.1: Myosin VI is not required for the targeting of synectin to UCV.....	140
Figure 3.2: VFP-fused synectin targets to UCV.....	141
Figure 3.3: Both the amino-terminus and PDZ domains of synectin are required for UCV binding.....	142
Figure 3.4: Expression of VFP-syn-NP disrupted trafficking of UCV to the early endosome.....	144
Figure 3.5: Myosin VI binds to the carboxy-terminus of synectin but requires a functional synectin PDZ domain for in situ interaction.....	145
Figure 3.6: PDZ ligand binding regulates myosin VI binding to synectin.....	146
Figure 3.7: Dopamine Receptor 2 targets minimally to the myosin VI associated endocytic vesicle population.	147
Figure 3.8: Proteinuria and altered megalin distribution in synectin-null mice.....	148
Figure 3.9: : Confirmation of the correct targeting of GFP-MegTmT and GFP-MegTmTΔPDZ constructs.....	150
Figure 3.10: Synectin binding to the PBM of megalin is required for synectin and myosin VI recruitment to UCV.....	151

Figure 3.11: Quantification of the collocation of GFP-MegTmT- or GFP-MegTmTΔPDZ ⁻ -and endocytic markers.....	153
Figure 3.12: Confirmation of the correct targeting of GFP-MegTmT and GFP-MegTmTΔPDZ constructs.....	154
Figure 3.13: Scheme of myosin VI docking to UCV and synectin function in kidney proximal tubules	155

LIST OF TABLES

Table 3.1. Synectin constructs expressed in ARPE-19 cells, their expression patterns, and their uptake characteristics (n/a – not applicable).....156

Table 3.2. List of primers used for generation of synectin constructs. Primers for pEYFP-N1-syn-PDZ⁻ and pGFP-MegTmT-ΔPDZ were used for site-directed mutagenesis.....157

ACKNOWLEDGEMENTS

I would like to acknowledge the extensive work of my dissertation advisor and principal investigator Dr. Tama Hasson, and thank her for help encouragement support and advice throughout my graduate career. The text of Chapter One is derived in part from Aschenbrenner, Naccache and Hasson published in the journal *Molecular Biology of the Cell* in 2004 for which Laura Aschenbrenner was the primary researcher. The text of Chapter Two is in part derived from Naccache and Hasson, in press at *Cell Motility and the Cytoskeleton* for which I was the primary researcher. The text of Chapter Three is in part derived from Naccache, Hasson and Horowitz, in press at the *Proceedings of the National Academy of Science*, for which I was one of the primary researchers.

VITA

- 2001 B.A. Biology, Pomona College, CA
- 2002-2005 Teaching Assistant, University of California San Diego
- 2002-2006 Research Assistant, University of California San Diego
- 2006 Ph.D. in Biology, University of California, San Diego

Publications

- Naccache SN and T. Hasson. Myosin VI altered at threonine 406 stabilizes actin filaments *in vivo*. In press, Cell Motility and the Cytoskeleton.
- Naccache SN, Hasson T, and A. Horowitz. Myosin VI docking to endocytic vesicles is regulated by ligand binding to the PDZ domain of GIPC/Synectin. In press, Proceedings of the National Academy of Sciences.
- Aschenbrenner L, Naccache SN, Hasson T. 2004. Uncoated endocytic vesicles require the unconventional myosin, Myo6, for rapid transport through actin barriers. Molecular Biology of the Cell. May;15(5):2253-63.
- Barabe, F., Rollet-Labelle, E., Gilbert, C., Fernandes, M.J., Naccache, S.N., and Naccache, P.H. 2002. Early events in the activation of Fc gamma RIIA in human neutrophils: stimulated insolubilization, translocation to detergent-resistant domains, and degradation of Fc gamma RIIA. J Immunol 168:4042-4049.

Abstracts

- Horowitz, A. Naccache SN, and T. Hasson. 2004. Myosin-VI docking to endocytic vesicles is regulated by ligand binding to the PDZ domain of GIPC/synectin. American Society for Cell Biology, 43rd Annual Meeting. Molecular Biology of the Cell 15(Supplement):632a.
- Naccache, SN and Hasson T. 2004. Motor Domain Phosphorylation Modulates Myosin-VI Function *in vivo*. Supplement to Molecular Biology of the Cell. American Society for Cell Biology, 43rd Annual Meeting. Molecular Biology of the Cell 15(Supplement):45a.
- Naccache SN, Aschenbrenner L, Hasson T. 2003. Myo6 Transports Nascent Endocytic Vesicles Through a Cortical Actin Barrier. American Society for Cell Biology, 43rd Annual Meeting. Molecular Biology of the Cell 14(Supplement) presentation number 12.

Aschenbrenner LM, Naccache SN, Hasson T. 2003. Myo6 Powers the Movement of Nascent Endocytic Vesicles. American Society for Cell Biology, 43rd Annual Meeting. Molecular Biology of the Cell 14(Supplement) presentatin number 1002.

ABSTRACT OF THE DISSERTATION

Regulation of Myosin VI transport, tethering to actin and cargo binding.

by

Samia Nidal Naccache

Doctor of Philosophy, Biology

University of California, San Diego, 2006

Professor Eduardo Macagno, Chair

Myosin VI is a molecular motor that harnesses the conformational changes caused by ATP hydrolysis to generate motion along the actin filament (F-actin). As with all myosins, the motor domain of myosin VI contains an actin binding site and nucleotide binding site. The lever arm of myosin VI is followed by a coiled coil motif that mediates dimerization, and a cargo binding tail domain. Myosin VI is the only myosin that moves to the minus-end of F-actin. It has been implicated in multiple functions in disparate model systems. The ability of myosin VI to move processively across the actin filament provides a role for myosin VI in cargo transport, including uncoated endocytic vesicle (UCV) transport. Alternatively, kinetic studies have shown that myosin VI can be made to spend more of its actomyosin cycle tightly bound to actin when under increased load conditions, allowing myosin VI to also serve as a tension sensor that tethers membrane and protein elements to the actin cytoskeleton. The regulation of myosin VI at the level of the motor for it to act as a motor or tether is an intriguing possibility. In addition, myosin VI is mainly found in a cytoplasmic

pool suggesting that its docking to cargoes is regulated, separately from its interaction with actin. In Chapter One, I show that myosin VI functions to transport uncoated endocytic vesicles (UCV) through the actin meshwork in our model retinal pigmented epithelial cell system, and in doing so demonstrate that the cortical actin meshwork acts as a barrier to uncoated endocytic vesicle trafficking to the pericentriolar region. In Chapter Two, I provide evidence that *in vivo*, myosin VI is regulated to act either as a transporter or a tension sensing anchor to actin following alteration at threonine 406. Finally in Chapter Three, I delineate a mechanism for myosin VI recruitment to the UCV cargo through its adapter GIPC/synectin. I posit that recruitment occurs via activation of the GIPC/synectin PDZ domain by PDZ motif-containing receptors being trafficked through the UCV.

INTRODUCTION

The eukaryotic cell boasts a complex cytoskeleton that provides a dynamic structure mediating cell shape, mechanical strength and cell motility. In addition, the cytoskeleton mediates intracellular organelle transport by providing tracks along which molecular motors can move their cargo.

The cytoskeleton is composed of three distinct interacting filament networks: intermediate filaments, microtubules and microfilaments. All three systems are composed of monomeric building blocks. The intermediate filaments are formed by the assembly of monomers such as desmins, keratins, vimentin and lamins into heterodimers, and provide cells and resulting cell layers with mechanical strength (Kreplak, Aebi et al. 2004). Microtubules are formed by the polymerization of alpha and beta tubulin monomers into long hollow tubes originating from the microtubule-organizing center. Microtubules mediate cell shape, mitosis, cell division, organelle positioning, and cell migration. The microfilaments of the actin network are similarly formed by the polymerization of globular actin monomers (G-Actin) into double stranded helical polymers of G-actin called filamentous actin (F-actin).

The actin cytoskeleton

The actin cytoskeleton is both a highly dynamic and mechanically strong structure. Actin structures can assemble and disassemble quickly and dynamically,

affecting cell shape and morphology, and producing motion. Actin monomers dimerize weakly, but the structure is stabilized when trimerized to nucleate the actin filament. Actin-like molecules such as the Arp2/3 complex help increase the rate of this nucleation at the plus (or barbed) end of the filament, where nucleation occurs. As more G-actin monomers are added to the plus end of the filament, the filament elongates into a helical structure. As the rate of elongation slows, the length of the filament is maintained by depolymerization at the minus end (or pointed end).

The actin filament is thus a polarized structure both biochemically and functionally, a feature which would allow directional motion along the filament. Biochemically, all monomers in the filament point in the same direction. The actin building block, the cytoplasmic G-actin monomer, is a globular protein with two lobes joined by ATP. The ATP binding clefts of all actin monomers of one filament point towards the minus ends. Functionally, the actin filament undergoes net extension at the plus end and net retraction at the minus end. In addition, specialized actin structures provide for physical barriers between cellular compartments, as well as scaffolding for proteins and membranes. The actin filaments in specialized structures are themselves polarized such that the minus ends and plus ends are contiguous. Finally, the polar nature of the actin filament allows molecular motors to move cytoplasmic elements in a directional pattern across the actin networks.

Molecular Motors

While the cytoskeleton performs a mechanical and structural role in cell shape maintenance and other functions, it also provides a physical route along which cargo can travel. This transport is mediated by molecular motors. Kinesins and dyneins have been identified as motors for the microtubule network, and myosins move along the actin network. Generically, molecular motors encompass two important domains: the motor domain that hydrolyzes ATP causing a conformational change resulting in a power stroke, and the tail domain that binds the cargo to be transported across the cytoskeletal structures. While the motor domain remains fairly conserved through families of molecular motors, the tail domains vary greatly to confer cargo specificity.

The Myosin Family

Myosins, originally characterized in muscle, are a gene family of actin filament-based molecular motors. As of today, twenty distinct classes of myosins have been characterized, retaining extensive homology within each class (Krendel and Mooseker 2005). The heavy chain of most myosins are generically divided into three main domains: an N terminal motor domain containing the actin binding site and ATP binding site, a neck domain containing varying numbers of IQ motifs that allow binding to the mainly calmodulin light chain, and a cargo specific tail domain.

Myosins play a role in many actin-based processes such as cell crawling and cytokinesis: (Class II myosins); phagocytosis: (Class I) (Durrwang, Fujita-Becker et

al. 2006), Class VII (Titus 1999), and Class X (Chavrier 2002); granule motility (Class V and VII) (Berg, Powell et al. 2001); secretion (Class V) (Berg, Powell et al. 2001), maintenance of cell shape (Class I and II), as well as more exotic functions such as signal transduction: Class III, IX and VI, (Bahler and Nurse 2001); (Jung, Liu et al. 2006) and actin polymerization: (yeast Class I) (Lechler, Shevchenko et al. 2000).

While their roles in actin mediated force generation vary, the basic actomyosin cycle remains the same for all myosins. The myosin head domain contains both a nucleotide-binding pocket and an actin-binding domain. The interaction of myosin with actin during the actomyosin cycle is controlled by the nucleotide binding state of the myosin. Myosins are weakly bound to actin when ATP or the subsequent transient hydrolyzed product, ADP+phosphate, resides in the nucleotide binding pocket. ATP hydrolysis occurs but phosphate release is slow, which results in trapping the lever arm in a primed or pre-power stroke position (Menetrey, Bahloul et al. 2005). In this state the myosin rapidly attaches and detaches from the actin filament on a submicrosecond scale. The force-generating segment of the actomyosin cycle, or power stroke, occurs when phosphate is released from the pocket, after which the myosin molecule, in the ADP bound or nucleotide free state, is tightly bound to actin. The resulting structural conformation change in the nucleotide pocket is then transferred to the converter region. The lever arm of myosins is thought to transduce the force generated by the structural changes in the nucleotide and actin binding

myosin pockets into larger directional motion along the filament, with the end result of moving towards the plus end of the actin filament. By cycling through weakly bound states and tightly bound states to actin, ATP hydrolysis drives myosin activity (Spudich 2001).

Class VI Myosins

Myosin VI is an actin-based molecular motor that, contrary to other myosins, moves backwards towards the minus end of the actin filament (Wells, Lin et al. 1999). Myosin VI has an N-terminal conserved head domain containing the nucleotide binding pocket and actin binding domain. Between these two structures in the motor are two small unique inserts that contribute to unique kinetic properties of this myosin. Between the motor domain and the converter is another 53 amino acid long unique insert that contributes to the reverse directionality of this myosin. The neck domain follows consisting of the converter domain and the lever arm containing a single IQ motif that can bind the light chain calmodulin. Following this is the tail domain containing a 200 amino acid coiled-coil domain predicted to allow myosin VI to dimerize and move processively, and a C-terminal globular domain (Hasson and Mooseker 1994) allowing binding to cargo.

Kinetic properties of myosin VI

Analysis of nucleotide and actin binding kinetics have shown that myosin VI spends most of its time in the actomyosin cycle bound to actin (Robblee, Olivares et al. 2004) making it a high duty ratio motor (Yoshimura, Homma et al. 2001). Myosin VI thus has a weaker binding affinity to ATP than other myosins and a higher affinity for ADP, which results in myosin being in a strongly bound state to actin for most of the actomyosin cycle (Yoshimura, Homma et al. 2001). ADP binds tightly with slow dissociation kinetics and binds five times faster than ATP at equivalent concentrations (Robblee, Olivares et al. 2004). While phosphate release is the rate limiting step of the myosin VI cycle in the absence of actin, ADP release is rate limiting in the presence of actin (De La Cruz, Ostap et al. 2001). It is thought that the unique amino acid insert near the nucleotide-binding site interferes with nucleotide binding. From studies in which the unique insert was deleted, it was shown that the insert is responsible for slowed ADP release, and ATP induced dissociation from actin. The insert most likely reduces the mobility of Switch 1 which is important for Mg^{++} binding and γ Phosphate binding, so that it becomes difficult to release ADP, and also reduces affinity of ATP by hindering the pocket (Menetrey, Bahloul et al. 2005).

Myosin VI is a processive motor

The role of myosin VI in transport is contingent on its ability to move processively. Because myosin VI spends most of the actomyosin cycle bound to actin,

in the context of a double headed motor the trailing head can spend enough time bound to actin to allow the leading head to find the next actin binding site before falling off the actin filament. Double headed myosin VI is a processive motor that can take three to five steps before coming off the actin filament (Rock, Rice et al. 2001). Myosin VI has multiple preferred binding sites on the actin filament, although the predominant ones are 36 nanometers apart. This results in a few step sizes that are smaller than the 36 nanometers, in both directions on the filament. The latest biophysical data suggests that double-headed myosin VI walks hand over hand on the actin filament. The current theory is that the working stroke is responsible for part of the step size, followed by a diffusive search that allows the leading head to find the next binding site, as the lever arm of myosin VI is too short to reach the next site without the search (Rock, Rice et al. 2001); (Rock, Ramamurthy et al. 2005); (Okten, Churchman et al. 2004); (Yildiz, Park et al. 2004). Biased Brownian motion has also been proposed to explain how biased thermal diffusion of the myosin heads along actin result in motion along the filament (Nishikawa, Homma et al. 2002).

Existence as a dimer is essential for myosin VI's processivity. Based on a heptad repeat sequence in the tail domain of myosin VI, it has been assumed that this region of the tail would form a stable helical coiled coil. However, constructs used for biophysical studies of myosin VI have been forced into the dimer form by the inclusion of a C-terminal leucine zipper, or myosin II rod domain, known to initiate dimerization. Surprisingly, it was shown that myosin VI exists in the cytoplasm

primarily as a monomer (Lister, Schmitz et al. 2004). Recently, however, it was shown that monomeric myosin VI can dimerize in vitro only when in very close proximity to another myosin VI molecule or when at a sufficiently high, and non-physiologic, concentration (Park, Ramamurthy et al. 2006). The resultant dimer can move processively. Myosin VI dimerization was inhibited by the myosin VI cargo binding domain in vitro, indicating that a cargo binding-dependent mechanism is required for proximity based dimerization.

The behavior of myosin VI under load

As myosins function to transport cargo along actin, backward load inflicted on the myosin affects the forward stepping dynamics of myosin VI. It was shown that a two pico-newton load applied to myosin VI had the surprising effect of stalling the myosin molecule onto the actin filament, thus transforming myosin VI into an anchor onto actin rather than a transporter (Altman, Sweeney et al. 2004). This load was above what would be encountered physiologically, but the effect of progressively larger backward loads on the kinetics of myosin VI allowing this anchoring was studied. At physiological concentrations of ATP and ADP it was shown that load enhances the ADP association rate of myosin VI, thus pushing myosin VI to be bound to actin for even longer than usual. Whilst in the absence of load, the rate of ADP release is rate limiting, with load the rate of ADP association increases. The rate of ATP association decreases under load so that myosin VI is in the actin bound state for

longer, and ATP binding becomes rate limiting. This suggests that myosin VI could bind tightly to actin filaments if the tail is bound to structures that provide resistance, such as membrane, and would provide a mechanism to anchor cellular components to actin (Altman, Sweeney et al. 2004).

Reverse directionality

A structural hallmark of myosin VI is that it is the only myosin that moves to the minus end of the actin filament. Myosin VI was found to exhibit reverse directionality and *in vitro* has been shown to move to the minus end of actin filaments (Wells, Lin et al. 1999). The unique insert directly before the converter domain was found to be responsible for this directionality. The insert was surprisingly found to bind the calmodulin molecule (Bahloul, Chevreux et al. 2004) allowing it to make specific interactions with the nearby converter, as a result the IQ helix and its traditional bound calmodulin is reoriented (relative to other myosins) about 120°. This redirects the lever arm towards the minus end of the actin filament (Menetrey, Bahloul et al. 2005). In this fashion, structural changes at the core of the conserved motor domain result in rotating the lever arm in the opposite direction on actin to other myosins (Wells, Lin et al. 1999).

Myosin VI in deafness

The physiological significance of myosin VI has emerged as myosin VI has been genetically linked to proper auditory function. The Snell's Waltzer mouse, which carries a deletion for the myosin VI gene (Avraham, Hasson et al. 1997), is deaf and exhibits vestibular dysfunction. The stereocilia of this mouse are severely deformed, indicating that myosin VI is required for proper formation of the stereocilia of the inner ear hair cells, and thus proper hearing. In addition, progressive sensorineural dominant deafness in a human family was shown to be due to single nonsense mutation in the motor domain of myosin VI (C442Y) (Melchionda, Ahituv et al. 2001). This cysteine residue is in a domain highly conserved among most Class VI myosins. The C442Y mutation causes an increase in the rate of ADP release while actin gliding velocity is decreased (Sato, White et al. 2004). The nonsense mutation (R1166X) in the tail domain of myosin VI as well as the missense mutation (E216V) are linked to autosomal recessive deafness (Ahmed, Morell et al. 2003). Finally, the missense mutation H246R in the motor domain of myosin VI is linked to both dominant human sensorineural deafness, as well as to familial hypercardiomyopathy (Mohiddin, Ahmed et al. 2004), a disorder more commonly caused by mutations in genes encoding sarcomeric proteins.

Myosin VI *in vivo*

The specific kinetic characteristics of myosin VI, namely its processivity, reverse directionality, and its reaction to high backward force allow for the prospect that *in vivo* myosin VI would act both as a transporter to the minus ends of F-actin, and a tension sensor that anchors proteins and membrane to actin. Forays into the nature of myosin VI function *in vivo*, however, have proved confusing as to the true nature of myosin VI activity. Myosin VI is found in most organism from *C. elegans* to humans and ubiquitously throughout various tissues. It is unfortunately lacking in yeast. At the time of writing, the effect of mutations in myosin VI on a plethora of model systems point to sometimes overlapping roles for myosin VI. Briefly, myosin VI may be involved in membrane and protein complex tethering onto actin, maintenance of actin mediated barriers and transport of particles between asymmetrically dividing cells, cell migration, and movement of endocytic cargo.

Role for myosin VI in tethering to actin

Myosin VI is required for maintaining the structural integrity of inner ear hair cells, which explains the linkage of myosin VI to deafness. The inner ear hair cell is a specialized sensory cell that carries out auditory and vestibular transduction. The stereocilia are microvilli-like cellular processes containing cross-linked actin filament bundles that are highly polarized with the plus end at the top and the minus end into the cell cytoplasm. Multiple stereocilia of a single hair cell cluster together in a single

hair bundle that can be deflected by sound waves. The deflections open or close transduction channels that transmit the mechanical information to the nervous system. Another specialized actin feature of inner ear hair cells is the cuticular plate, which is formed of a random meshwork of cross-linked actin filaments. Myosin VI is enriched at the base of the stereocilia where the stereocilia taper into the cuticular plate. It is also enriched at the pericuticular necklace, a region largely free of actin (Hasson, Gillespie et al. 1997) but enriched in endocytic vesicles. In Snell's Waltzer mice lacking myosin VI expression, stereocilia are intact at birth but gradually fuse together and become disorganized. This indicates that myosin VI is needed for the maintenance of stereocilia morphology (Self, Sobe et al. 1999). In addition, the inner ear hair cells of zebra fish lacking myosin VI exhibit similar abnormalities in stereocilia formation as myosin VI seems to be necessary for the structural integrity of the apical surface of inner ear hair cells (Seiler, Ben-David et al. 2004). Finally, a zebra fish myosin VI deletion results in abrogation of the mechano-electrical transduction of the affected inner ear hair cells (Kappler, Starr et al. 2004).

The precise role myosin VI is playing in stereocilia development is unknown. The current theory is that myosin VI anchors the membrane around the stereocilia to actin by translocating along the polarized stereocilia towards the cell cytoplasm whilst bound to a protein or membrane cargo through its tail domain. Once the proper tension is established for membrane to anchor around the stereocilia, myosin VI then anchors to the actin filament, effectively maintaining this tension in the membrane and

maintaining the proper shape of the stereocilia (Altman, Sweeney et al. 2004). However, due to its localization to endocytic hotspots at the base of the stereocilia, its participation in endocytic events required for the proper formation of stereocilia cannot be discounted.

Another myosin VI-dependent process explained by a role for myosin VI in anchoring elements to the cytoskeleton is *Drosophila* spermatid individualization. After undergoing multiple rounds of mitosis and meiosis, spermatids exist in a syncytium, with nuclei separated from each other by a network of cytoplasmic ridges. Spermatids individualize in an actin dependent process that requires myosin VI (Hicks, Deng et al. 1999). During individualization, the syncytial membrane is reorganized around 64 spermatids, and an actin complex or cone organizes around the spermatid nuclei, moving away from the nucleus down the tails of the spermatids. In the process the membrane is remodeled and cytoplasm extruded. Myosin VI is concentrated at the junction between the motile actin structure performing the extrusion, and a zone of membrane remodeling (Rogat and Miller 2002). The actin density in the wild-type progressing cone increases with time, but in the myosin VI mutant it decreases (Noguchi, Lenartowska et al. 2006). Since the turnover rate of the actin filaments is not affected by myosin VI, it is more likely that myosin VI affects actin accumulation. Most importantly, myosin VI localizes to the actin cones through the motor domain and not the tail domain, and remains stalled on actin for minutes, indicating that myosin VI here is acting as an anchor onto actin. Myosin VI collocates

with Arp2/3 and cortactin, and myosin VI depletion results in the mislocalization of both proteins (Rogat and Miller 2002). Myosin VI anchoring to actin might thus be important for the asymmetric localization and stabilization of proteins involved in actin assembly during the individualization step of spermatogenesis.

A similar role for myosin VI in oogenesis in stabilizing protein complexes was extrapolated from the fact that myosin VI, Arm (*Drosophila* Beta catenin) and E-cadherin co-immunoprecipitate from ovarian extracts. Since the depletion of myosin VI does not affect E-cadherin endocytosis, but did decrease the abundance of E-cadherin, myosin VI was hypothesized to be more likely to maintain E-cadherin and Arm (*Drosophila* Beta catenin) in a complex that would protect them from degradation during oogenesis (Geisbrecht and Montell 2002).

Finally, myosin VI localizes to the Golgi of A431 and NRK cells (Buss, Kendrick-Jones et al. 1998). Cells lacking myosin VI exhibit severely reduced golgi size, as well as impaired secretion of a secreted form of alkaline phosphatase (Warner, Stewart et al. 2003). The actin network surrounding the golgi is thought to be oriented with the minus end away from the golgi. Myosin VI at the golgi could thus act as an anchor that extends the golgi structure across the actin cytoskeleton, explaining why the absence of myosin VI results in a reduction in golgi size. Myosin VI at the golgi, however, exists in two pools, one bound to actin, the other to membranes, most likely via a receptor (Warner, Stewart et al. 2003). Optineurin, for example links myosin VI to the golgi by binding Rab8 on the golgi and the tail domain of myosin VI

(Sahlender, Roberts et al. 2005), providing myosin VI with a potential role in vesicle sorting.

Role of myosin VI in asymmetrical cell fate determinant compartmentalization

Myosin VI may be needed to establish a barrier between asymmetrically dividing cells which require that cell fate determinants be positioned differentially between the resulting cell progeny. *Drosophila* neuroblasts undergo asymmetrical cell division to form a neuroblast and a ganglion mother cell. In this process, cell fate determinants segregate differentially into the daughter cells and are packaged in apical or basal compartments. One such determinant is Miranda, which co-immunoprecipitates with myosin VI (Petritsch, Tavosanis et al. 2003). Myosin VI depletion results in incorrect mitotic spindle orientation and the improper distribution of Miranda. Myosin VI might cause this distribution by trafficking Miranda into the basolateral compartment (Petritsch, Tavosanis et al. 2003).

In the *Drosophila* embryo, myosin VI is responsible for the proper formation of the actin-based metaphase furrows formed between adjacent mitotic spindles in the syncytial blastoderm. Either myosin VI transports particles to these furrows that are necessary for their formation, or myosin VI directly mediates their formation by interacting with actin (Mermall and Miller 1995). Interestingly, in the first visualization of an unconventional myosin transporting particles, cell cycle dependent

motility of cytoplasmic particles in the *Drosophila* embryo was ATP dependant and catalyzed by myosin VI (Mermall, McNally et al. 1994).

Similarly, during *Drosophila* oogenesis, myosin VI is associated with motile cytoplasmic particles in the nurse cell actin rich cortex (Bohrmann 1997). In the *Drosophila* ovarian follicle, 15 nurse cells surround the oocyte and are connected to it by ring canals. Cytoplasmic particles associated with myosin VI were observed to pass from nurse cells through the ring canal into the oocyte (Bohrmann 1997).

Finally, in *C. elegans*, myosin VI depletion causes a defect in spermatogenesis. Myosin VI plays a role in asymmetric division and proper partitioning of cytoskeletal elements and organelles between the spermatocyte and the residual body (Kelleher, Mandell et al. 2000). Contrary to the previous examples where active trafficking by myosin VI would be required to cause a differential accumulation of cell fate determinants, myosin VI in *C. elegans* spermatogenesis is suggested to cause this partitioning by anchoring components to actin and essentially creating a barrier. The result is that asymmetrically positioned components cannot move from one region to another during spermatid budding.

Role of myosin VI in cell migration

Border cell migration , which refers to the migration of a group of follicle cells, depends on myosin VI. Disruption in myosin VI expression during oogenesis results in defects in follicle cell migration and follicle cell epithelium morphogenesis which

eventually results in the degeneration of the egg chambers (Deng, Leaper et al. 1999). In addition myosin VI is crucial for the dorsal closure of *Drosophila* embryo as mutations in myosin VI result in a defect in epithelial cell migration. Myosin VI is enriched at the leading edge of the migrating epithelial sheet causing dorsal closure, and if myosin VI is depleted, the epithelial sheet is ridged and cells detach and the underlying actin cables are also destroyed (Millo, Leaper et al. 2004). The precise role of myosin VI in this migration is still unknown, although a role in stabilizing protein complexes has been theorized.

Receptor mediated endocytosis

Myosin VI is a processive motor that has been thought to participate in cargo transport. In this vein myosin VI was implicated in the transport of endocytic vesicles. Endocytosis is the process by which extracellular material is internalized through the cytoplasmic membrane. In receptor-mediated endocytosis, a receptor with extracellular ligand binding domains is engaged by a ligand. In some cases receptors then cluster and a clathrin-coated pit is formed on the cytosolic surface of the pit. The pit invaginates and pinches off to form a clathrin-coated vesicle. This vesicle is now an endocytic vesicle, transporting ligand-bound receptors such that the ligand binding domains are contained within the vesicle, and the cytoplasmic domain is still in the cytoplasm. Clathrin then uncoats to form an uncoated endocytic vesicle (UCV). These vesicles are eventually delivered to fuse with the early endosome. One function of the

endocytic system is to properly sort and deliver internalized ligands, and from the early endosome some receptors are recycled back to the cytoplasm, whereas others are transported to late endosomes and lysosomes for degradation.

Role of actin in endocytosis

Endocytosis has been linked to the cytoskeleton because both clathrin-coated vesicle formation and uncoating occur immediately under the plasma membrane, where there is a cortical actin cytoskeletal layer. Cortical actin filaments are polarized with their plus ends at the plasma membrane and their minus ends facing inward. Whereas in some cell types actin is an absolute requirement for endocytosis, in others the role of actin is not as clear (Fujimoto, Roth et al. 2000). For example, the actin cytoskeleton can localize clathrin coated pits to certain domains of the membrane (Gaidarov, Santini et al. 1999). In this case actin may act as a physical barrier to free diffusion of the clathrin-coated pit, or as a direct anchor to part of the endocytic machinery. In addition, actin may be involved in clathrin coated pit dynamics, (Gottlieb, Ivanov et al. 1993); (Fujimoto, Roth et al. 2000); (Merrifield, Perrais et al. 2005) although the requirement for actin varies between the apical and basolateral membrane of polarized epithelial cells (Gottlieb, Ivanov et al. 1993); (Jackman, Shurety et al. 1994)); (Shurety, Stewart et al. 1998); (Apodaca 2001), (Sheff, Kroschewski et al. 2002). Alternatively, force generated by actin polymerization against the invaginating coated pit could liberate the coated pit from the membrane

(Lamaze, Fujimoto et al. 1997; Merrifield, Moss et al. 1999); (Taunton, Rowning et al. 2000). Cortical actin has also been shown to be a physical barrier to exocytic vesicles during the final stages of vesicle secretion. Finally the early endosome is transported to the pericentriolar region by microtubule based transport.

Actin filaments in epithelial cells are organized with the plus end of filaments at the membrane and the minus end towards the interior of the cell. A minus end directed motor would thus be ideal to transport endocytic vesicles from their origination site at the membrane to the early endosome. As such, myosin VI has been characterized to transport endocytic vesicles.

Other myosins have been implicated in endocytosis as Class I ameboid myosins and Class I myosins of lower eukaryotes locate to the sites of the dense cortical meshwork (called actin patches in yeast) responsible for endocytosis. However their role seems to be more structural with regards to actin, for example, myosin I recruits Arp2/3 to regions of endocytosis (Soldati 2003).

Role of myosin VI in endocytosis

Due initially to its localization, direction of movement along the actin filament, and recently to in depth analysis on the effect of myosin VI on endocytosed receptors, myosin VI has been implicated in the transport of endocytic vesicles.

The role of myosin VI in endocytosis has been well elucidated. Myosin VI is found in endocytic hotspots. In sensory hair cells of the inner ear, myosin VI is

enriched in the pericuticular necklace (Hasson, Gillespie et al. 1997), a region of the hair cell that is rich in clathrin and vesicles and clathrin, and the sole site of endocytosis for the hair cell (Kachar, Battaglia et al. 1997).

Myosin VI is also enriched at the apical brush border of proximal tubule kidney cells. Blood is filtered through the nephron's Bowman's capsule and the filtrate, composed of water and waste products, passes through the proximal tubule where sodium, water amino acids vitamins and glucose are reabsorbed. The filtrate then flows on towards the distal tubule. The kidney proximal tubule consists of a mass of polarized epithelial cells containing an extensive apical endocytic apparatus which consists of a network of clathrin coated pits and small coated and uncoated endosomal vesicles. This apical endocytic system is involved in re-absorption of molecules that were filtered through the glomeruli. Scavenger receptors, such as megalin, are involved in this function, and mediate the endocytosis of a large variety of ligands. Myosin VI is enriched at the apical brush border of proximal tubule kidney cells, and specifically at the intermicrovillar region (Biemesderfer, Mentone et al. 2002), a region at the base of the microvilli that is enriched with receptors during endocytosis. The intermicrovillar region is the beginning of the endocytic pathway in proximal tubule microvillar cells there is an enrichment in clathrin rich crypts at the base of the brush border microvilli. Dab2 and GIPC/synectin, both myosin VI adaptors, as well as megalin are enriched in this region (Biemesderfer, Mentone et al. 2002).

In addition, myosin VI also localizes to the terminal web of the intestinal brush border, also an endocytic hotspot (Heintzelman, Hasson et al. 1994).

Myosin VI can target to clathrin coated pits in polarized intestinal epithelial cell types. This localization might indicate a role in endocytosis as overexpression of the dominant negative tail domain inhibited endocytosis (Buss, Arden et al. 2001). In all cell types investigated myosin VI was also found to localize to uncoated endocytic vesicles. Staining with an antibody to myosin VI revealed a peripheral enrichment of myosin VI-associated vesicles coinciding with the region of densest cortical actin (Aschenbrenner, Lee et al. 2003).

Myosin VI localization to the uncoated endocytic was determined by an analysis of the kinetics of transferrin receptor-mediated endocytosis. The transferrin receptor is a constitutively recycling ligand binding receptor. At two minutes following the initiation of endocytosis, fluorescently-labeled transferrin has left the clathrin coated pits and vesicles (as defined by a lack of collocation of transferrin with clathrin or its adaptor AP-2) and has not yet entered the early endosome (as defined by a lack of collocation with the early endosome marker EEA1), indicating that transferrin is at the uncoated vesicle. At this two minute timepoint, fluorescently-labeled transferrin collocates with endogenous myosin VI. Green fluorescent protein tagged (GFP-tagged) myosin VI as well as GFP-tagged myosin VI tail only targeted to these uncoated endocytic vesicles (Aschenbrenner, Lee et al. 2003). Overexpression of the GFP-tagged version of the tail domain of myosin VI did not inhibit endocytosis, but

inhibited transferrin trafficking to the pericentriolar endosome in cultured ARPE-19 cells, a model epithelial cell system. This implicated myosin VI in endocytic vesicle trafficking (Aschenbrenner, Lee et al. 2003). Interestingly, in all cell types observed, myosin VI targeted to uncoated endocytic vesicles, but it was required for uncoated vesicle traffic only in cell types that contained a rich cortical actin meshwork. In Chapter One of my dissertation, I explore the ability of myosin VI to transport uncoated endocytic vesicles across the actin meshwork.

Receptors utilizing on myosin VI for endocytic processes:

Cystic Fibrosis Transmembrane Regulator (CFTR), the AMPA-receptor, the glucose transporter (Glut1) and the sodium proton exchanger (NHE3) have been described to rely on myosin VI for endocytic processes, such as internalization, receptor recycling and trafficking down the microvilli. Different adaptor proteins between the receptors and myosin VI might be at play in each case.

Endocytosis of the cystic fibrosis transmembrane conductance regulator (CFTR) is facilitated by myosin VI (Swiatecka-Urban, Boyd et al. 2004). CFTR is a chloride channel that mediates chloride transport in a transepithelial manner in airway cells, testis, pancreas intestine and other tissues. While the endocytosis of CFTR is actin dependent, it is yet unknown if actin is necessary for clustering of CFTR into clathrin-coated pits or for clathrin-coated pit budding. CFTR interacts with myosin VI, the myosin VI adaptor protein Dab2, and clathrin. In addition, overexpression of dominant

negative GFP-tagged myosin VI tail results in inhibited CFTR endocytosis and an increase in the CFTR receptor at the membrane.

AMPA and AMPA-type glutamate receptor internalization, which occurs via clathrin mediated endocytosis has been found to be myosin VI dependent. AMPA and AMPA-type glutamate receptor endocytosis was decreased in Snell's Waltzer cultured hippocampal neurons (Osterweil, Wells et al. 2005). Myosin VI in this system is enriched at the synapse. Finally, myosin VI immunoprecipitates with Sap97, another myosin VI adaptor protein, as well as AP-2 and the AMPA receptor.

In addition, proper recycling of the glucose transporter Glut1 was shown to be dependent on myosin VI (Reed, Cefalu et al. 2005). Myosin VI binds Glut1 via yet another adaptor protein, GIPC/Synectin.

Finally, myosin VI is thought to transport the sodium proton exchanger NHE3 down the microvillus during acute renal hypertension (Yang, Maunsbach et al. 2005). Acute hypertension results in the retraction of the Na⁺/H⁺ exchanger isoform 3 (NHE3) from the top of proximal tubule microvilli to the base of the microvilli, and myosin VI itself also retracts to the base of the microvilli during hypertension.

It should by now be apparent that many layers of regulation are expected to operate on myosin VI to allow such a highly conserved protein to interact differently on various specialized actin structures. This regulation would be hypothesized to involve the motor domain of myosin VI, and is the subject of Chapter Two of my dissertation. Another layer of regulation involving the tail domain of myosin VI would

be required to allow myosin VI to target to a variety of adaptor proteins and cargo molecules. Aspects of the mechanism of myosin VI recruitment to cargo is tackled in Chapter Three of my dissertation.

Role of TEDS rule in regulating myosin activity

In Chapter Two of this dissertation, I explore the possibility that myosin VI is regulated to be a transporter or a tether onto actin. The method for this regulation could coincide with a conserved mode of regulating the motor activities of other myosins. The cardiomyopathy loop is a surface loop in the myosin motor domain that is thought to form part of the actin binding interphase. Almost all myosins have either a glutamate or aspartate at this site. Class I and VI myosins have a highly conserved threonine or serine residue at this surface loop instead, and since serines and threonines can become negatively charged by phosphorylation, phosphorylation there was thought to regulate myosin enzymatic activity (Yamashita and May 1998). Known as the TEDs rule site, it is conserved as a serine in three *Acanthamoeba*, five *Dictyostelium*, two *Saccharomyces*, one *Aspergillus* and one *Emericella* Class I myosin (Wang, Wang et al. 1998). All Class VI myosins to date carry a conserved threonine residue at that site. This gave rise to the suggestion that a negative charge at the TEDS site provided by an acidic amino acid, or a phosphorylated hydroxyamino acid would be required to regulate ATPase activity (Bement and Mooseker 1995).

This prediction has turned out to be true in Class I myosins. The TEDS site is phosphorylated to control ATPase activity and actin motility in ameboid Class I myosins (Lee, Egelhoff et al. 1996), (Wu, Lytvyn et al. 1997), (Novak and Titus 1998; Yamashita and May 1998) (Wang, Harvey et al. 2000), (Brzeska, Young et al. 2001) (Grosshans, Grotsch et al. 2006). PAK kinases are thought to mediate the phosphorylation of the TEDs site in ameboid myosin I, (Lee, Egelhoff et al. 1996), (Brzeska, Young et al. 1999), (Barylko, Binns et al. 2000). This suggests that PAK may regulate phosphorylation at the TEDs site in myosin VI as well.

Several indirect lines of evidence have led us to believe that myosin VI could be phosphorylated in vivo at the TEDS site, specifically by P21 activated kinase (PAK). In the epidermoid cell line A431, myosin VI is phosphorylated at the head domain upon EGF stimulation (Buss, Kendrick-Jones et al. 1998). Immunoprecipitated myosin VI was also phosphorylated by PAK in the head domain. This phosphorylation mapped to between the myosin VI amino acids 308 and 631 , and the flanking sequences are PAK recognition sites (De La Cruz, Ostap et al. 2001). PAK1 and PAK2 kinases were capable of phosphorylating myosin VI in vitro, and this phosphorylation was diminished but not abolished when myosin VI was bound to actin, indicating that other sites not on the actin face of myosin VI might also be phosphorylated (Aschenbrenner 2004). Finally, PAK3, a neuronal kinase, can phosphorylate threonine 406 in vitro (Yoshimura, Homma et al. 2001), and this phosphorylation facilitates the actin translocation of myosin VI.

Cargo docking mechanism of myosins

The cargo docking mechanisms for most myosins via their tail domain has not been determined. The single headed Class I myosin binds directly to anionic membrane phospholipids via positively charged tail domains in vitro (Hayden, Wolenski et al. 1990), and phospholipid interactions are assumed to be behind the cargo docking mechanism of myosin I. However most membranes are free of myosin I (Coluccio 1997) 1997), suggesting a regulatory mechanism is required to target myosin I to its cargo (Barylko, Jung et al. 2005). Myosin I tail-binding proteins that could mediate this regulation have been identified in lower eukaryotes (Xu, Mitchelhill et al. 1997); (Anderson, Boldogh et al. 1998); (Lechler, Shevchenko et al. 2000); (Evangelista, Klebl et al. 2000); (Jung, Remmert et al. 2001) although it is not known if these proteins play a role in anchoring myosin I to the membrane and none have been identified in vertebrates.

Myosins from Classes I, V, VI, VII, and X participate in intracellular organelle trafficking including endocytosis and exocytosis. However the cargo docking mechanism for myosin Va is the only one fully elucidated. Myosin V cargo sorting is mediated by organelle-specific Rab GTPases which reside on the organelle surface and interact with myosin V either directly or via an adapter protein (Wu, Rao et al. 2001; Fukuda, Kuroda et al. 2002; Wu, Wang et al. 2002; Westbroek, Lambert et al. 2003; Boldogh, Ramcharan et al. 2004). For example Rab27a, involved in exocytic

vesicle sorting, is the receptor for myosin V on the melanocyte surface, and recruits melanophilin, an adaptor protein that can also link to the actin cytoskeleton, in a GTPase dependent manner. The carboxy-terminus of melanophilin can then recruit myosin Va to the Rab27a-melanophilin complex. In addition, tail phosphorylation has been shown to regulate myosin V release from cargo (Karcher, Roland et al. 2001). However, the regulation of myosin V recruitment to its cargo is still unknown.

Cargo docking mechanism of myosin VI

Some information is already known about myosin VI recruitment to its endocytic cargo. Two leads were established, one that different isoforms of myosin VI with varying inserts in the tail domain might dictate myosin VI targeting, the other that since myosin VI interacts with various adaptors the adaptors might dictate the recruitment of myosin VI to cargo.

Myosin VI recruitment to cargo via different tail splice variants

Different splice variants containing varying insert sizes in the tail domain of myosin VI have been identified, and the size of the insert was implicated in determining myosin VI targeting to its cargo (Buss, Arden et al. 2001) (Dance, Miller et al. 2004). It has also been hypothesized that as epithelial cells differentiate, different isoforms are expressed to allow myosin VI to clathrin coated pits when myosin VI is needed at the endocytic sites of the fully differentiated cells. Caco2 cells

for example require around seven days for full differentiation into a monolayer with fully functional microvilli and subsequent endocytic domains at their base. It has been reported that the myosin VI small insert isoform and the isoform with no insert are expressed when the Caco2 monolayer is non-polarized, whereas the large insert is expressed when polarized (Buss, Arden et al. 2001). In tandem, it was found that myosin VI collocates with clathrin coated vesicles in fully differentiated Caco2 cells. Unfortunately we have been consistently unable to repeat this result. In our hands we rarely see myosin VI naturally targeting to clathrin coated vesicles in other cell types except in NRK cells (Buss, Arden et al. 2001); (Dance, Miller et al. 2004) as explained below.

Myosin VI recruitment to cargo via adaptor proteins

Dab2, an adaptor protein that binds the clathrin adaptor AP2 via its central motif, and acts as an inhibitor to the Ras cascade, binds to the myosin VI tail via its C-terminus (Morris, Arden et al. 2002); (Inoue, Sato et al. 2002). Dab2 binds myosin VI *in vivo* and *in vitro* and is believed to be the its adaptor onto clathrin coated pits (Morris, Arden et al. 2002). In cell types with high Dab2 content such as in NRK cells, myosin VI is also recruited to clathrin coated pits. In these cell types splice variants in the tail affect the extent of myosin VI targeting to clathrin as the large insert targeted to clathrin coated pits. Modulation of targeting was only evident in the context of the full-length myosin VI. All splice forms target to UCV in ARPE-19 cells, which

exhibit low Dab2 content. Over-expression of Dab2 in ARPE-19 cells reroutes myosin VI to clathrin coated pits, suggesting that Dab2 at sufficient concentrations causes myosin VI targeting to clathrin coated pits.

GIPC/Synectin is another myosin VI adaptor protein, and is thought to mediate the interaction of myosin VI with the UCV (Aschenbrenner, Lee et al. 2003); (Dance, Miller et al. 2004). GIPC (GAIP interacting protein, C terminus) is composed of an N terminus that serves to homo-dimerize the molecule (Bunn, Jensen et al. 1999) (Gao, Li et al. 2000). Following is a central type three PDZ (Postsynaptic density 95, Disk large, Zona occludens-1) domain defined by its ability to bind C-terminal PDZ motifs in various proteins (reviewed in (van Ham and Hendriks 2003)). The PDZ domain is a sequence repeat of around ninety amino acids and PDZ target specificity is dependent on the C-terminal PDZ binding motif of interacting proteins. Twenty eight PDZ ligands to GIPC/Synectin have been defined to date, some are serine/threonine kinase receptors (Blobe, Liu et al. 2001), others tyrosine kinase receptors (Booth, Cummings et al. 2002), integrins (El Mourabit, Poinat et al. 2002), transporters (Bunn, Jensen et al. 1999), G protein coupled receptors (Hirakawa, Galet et al. 2003), scavenger receptors (Gotthardt, Trommsdorff et al. 2000), cytoplasmic proteins (Bunn, Jensen et al. 1999), chemotactic receptors (Cai and Reed 1999) and glycoproteins (Gao, Li et al. 2000). Finally, GIPC/Synectin binds myosin VI via its C-terminus (Bunn, Jensen et al. 1999). This suggests that GIPC/Synectin can mediate between endocytosing receptors binding via the PDZ domain of GIPC/Synectin, and myosin recruitment.

Myosin VI targets to uncoated endocytic vesicles in all cell types and it is co-assembled with GIPC/Synectin in all of them (Dance, Miller et al. 2004). In ARPE-19 cells, myosin VI and GIPC/Synectin target to the UCV and fluorescently tagged versions of myosin VI and GIPC/Synectin constructs also target properly to the UCV. In addition we know that GIPC/Synectin contains a PDZ motif that can bind PDZ binding motifs on endocytosed receptors. This provides us with the opportunity to analyze the mechanism of recruitment of myosin VI and GIPC/Synectin to the uncoated endocytic vesicle specifically, in the context of receptor mediated endocytosis.

Dissertation Aims

The aim of this dissertation is to further our knowledge of myosin VI function in trafficking endocytic vesicles across the actin cytoskeleton. The following questions are tackled in the three chapters of this dissertation. In Chapter One we ascertain that myosin VI functions to traffic cargo across through the cortical actin meshwork. In Chapter Two we reconcile the role of myosin VI in transporting cargo across the actin meshwork with its role in anchoring protein and membrane elements to actin by elucidating the mechanism of regulation of myosin VI interaction with actin. Finally in Chapter Three we analyze the mechanism by which myosin VI is recruited to its cargo for transport across the actin meshwork.

CHAPTER ONE: Myosin VI moves uncoated endocytic vesicles through the cortical actin meshwork.

INTRODUCTION

Myosin VI is a molecular motor that harnesses the conformational changes precipitated by ATP hydrolysis to provide motion along the actin filament. Biophysical analysis of myosin VI has shown that double-headed myosin VI can move processively along the actin filament for up to six steps before falling off the actin filament, raising the possibility that myosin VI is utilized by the cell to transport its cargo. We have shown that myosin VI targets to uncoated endocytic vesicles in our model system, the retinal pigmented epithelial cell line ARPE-19 (Aschenbrenner, Lee et al. 2003). We then directly tested the role of myosin VI in vesicle transport and cargo trafficking. This was achieved by characterizing the motile properties of uncoated vesicles using GFP-tagged versions of myosin VI as markers. I then tested the importance of cortical F-actin in endocytic vesicle trafficking to determine whether actin was a barrier to myosin VI associated vesicle trafficking, and if myosin VI was the motor used to cross that barrier. Our conclusion, outlined in this chapter, is that actin is a barrier to inward endocytic vesicle movement and that myosin VI is specifically recruited to the vesicle surface to move vesicles through this barrier.

Clathrin-dependent receptor-mediated endocytosis is a multi-step process resulting in the delivery of internalized ligand-receptor complexes to the early endosome. The first step is clathrin-coated vesicle formation, a process that requires the action of a growing array of accessory proteins and the GTPase, dynamin (reviewed in (Schmid 1997; Higgins and McMahon 2002)). After clathrin uncoating, Rab5, a series of Rab5 effectors, and PI3-kinase are recruited to facilitate early endosome antigen 1 (EEA1)-mediated docking and uncoated vesicle fusion with the early endosome (reviewed in (Clague 1998); (Gruenberg 2001)). While budding and fusion processes have been well characterized, the mechanism whereby the short-lived uncoated vesicles are transported to the early endosome for fusion has received less attention and up until recently there were no reliable markers distinguishing uncoated vesicles from other transient intermediary vesicles.

Recently, the actin-based molecular motor myosin VI has been shown to associate with uncoated vesicles (Aschenbrenner, Lee et al. 2003). Unlike other unconventional myosins, myosin VI travels toward the minus end of actin filaments (Wells, Lin et al. 1999). This directionality of movement suggests that, if the actin cortex were a barrier to uncoated vesicle trafficking, then myosin VI could be used to overcome this barrier. The structural domains of myosin VI can be summarized as such: an N-terminal conserved motor domain containing the nucleotide binding pocket and actin binding domain, followed by a converter region then an insert unique to Class VI myosins that binds calmodulin and mediates myosin VI's reverse

directionality, followed by the lever arm containing a conventional IQ motif that binds a single calmodulin light chain, followed by a coiled-coil region mediating dimerization, and a C-terminal globular domain that is the cargo-binding domain. This globular tail targets myosin VI to uncoated endocytic vesicles (Aschenbrenner, Lee et al. 2003).

A number of proteins have been transiently found as uncoated vesicle components. For example, both the small GTPase Rab5 and the transferrin receptor can be detected on uncoated vesicles, but in both cases this reflects only a small fraction of the total vesicle population. The majority of Rab5 is either cytoplasmic, in a guanine-nucleotide dissociation inhibitor (GDI)-complexed form (Pfeffer, Dirac-Svejstrup et al. 1995) or is associated with early endosomes (Gorvel, Chavrier et al. 1991); reviewed in (Zerial and McBride 2001), whereas the transferrin receptor is evident in the membrane of all endocytic and exocytic compartments with an enrichment in the recycling endosome (Hopkins 1983);(Hanover, Willingham et al. 1984);(Eskelinen, Kok et al. 1991); (Trischler, Stoorvogel et al. 1999); reviewed in (Mukherjee, Ghosh et al. 1997). A similar heterogeneous distribution exists for GIPC/synectin, an adapter protein for myosin VI, which is also evident on coated vesicles, the Golgi, and on other small vesicles found throughout the cell cytoplasm ((De Vries, Lou et al. 1998); (Liu, Kandala et al. 2001); (Aschenbrenner, Lee et al. 2003), (Dance, Miller et al. 2004).

Previous work in our lab (Aschenbrenner, Lee et al. 2003) showed that myosin VI is recruited to endocytic vesicles after clathrin uncoating. GIPC/synectin is associated with myosin VI-decorated vesicles and may link myosin VI to these vesicles. When transferrin-containing vesicles fuse with early endosomes, myosin VI and GIPC/synectin are released, and the endosomes are transported by a presumed microtubule-mediated motility to the pericentriolar region.

Both clathrin-coated vesicle formation and uncoating occur immediately under the plasma membrane, where there is a cortical actin cytoskeletal layer. Cortical actin filaments are polarized with their plus ends at the plasma membrane and their minus ends facing inward and are further cross-linked into a meshwork by actin-binding proteins such as the spectrin family (Harsfalvi, Fesus et al. 1991) and myosin II (Van Dijk, Furch et al. 1999). The role of actin in endocytosis is cell specific (Fujimoto, Roth et al. 2000). The actin cytoskeleton can localize clathrin coated pits to certain domains of the membrane (Gaidarov, Santini et al. 1999). In this case actin may act as a physical barrier to free diffusion of the clathrin coated pit, or as a direct anchor to part of the endocytic machinery. In addition, actin may be involved in clathrin coated pit dynamics, (Gottlieb, Ivanov et al. 1993); (Fujimoto, Roth et al. 2000); (Merrifield, Perrais et al. 2005) although the requirement for actin varies between the apical and basolateral membrane of polarized epithelial cells (Gottlieb, Ivanov et al. 1993); (Jackman, Shurety et al. 1994); (Shurety, Stewart et al. 1998); (Apodaca 2001); (Sheff, Kroschewski et al. 2002). Alternatively, force generated by actin

polymerization against the invaginating coated pit could liberate the coated pit from the membrane (Lamaze, Fujimoto et al. 1997; Merrifield, Moss et al. 1999); (Taunton, Rowning et al. 2000). Cortical actin has also been shown to be a physical barrier to exocytic vesicles during the final stages of vesicle secretion. This has been hypothesized to be overcome either by actin depolymerization, (Trifaro, Rose et al. 2000), or by the molecular motor myosin V (Schott, Collins et al. 2002); (Desnos, Schonn et al. 2003); (Varadi, Tsuboi et al. 2005). We have posited that myosin VI performs a similar role, to extricate vesicles out of the cortical meshwork on their way inwards to the early endosome.

In many cell types, the actin meshwork is sufficiently dense that it was predicted to be a barrier to the transport of the recently uncoated endocytic vesicles toward the more centrally located early endosome (reviewed in(Qualmann, Kessels et al. 2000);(Qualmann, Kessels et al. 2000); (Hasson 2003)). However, it had not been possible to test this hypothesis directly because of the lack of a specific uncoated vesicle marker.

We utilized GFP-tagged myosin VI (GFP-M6) constructs to dissect the role of myosin VI in uncoated vesicle trafficking. Over-expression of the globular tail domain of myosin VI (GFP-M6Tail) displaces the endogenous myosin VI from uncoated vesicles and delays transferrin trafficking to the early endosome due to an accumulation of uncoated vesicles in actin-rich cell peripheries (Aschenbrenner, Lee

et al. 2003). These vesicles lacked EEA1, suggesting that they were en route to the early endosome but had not yet fused with it.

To ascertain that myosin VI was recruited to uncoated endocytic vesicles in order to move them, we conducted time-lapse experiments utilizing a series of GFP tagged constructs. GFP-M6-associated vesicles exhibited net movement toward the cell interior at a velocity consistent with that observed for myosin VI in vitro (Aschenbrenner, Naccache et al. 2004). This is the first example of myosin VI-based movement in vivo.

The expression of GFP-M6Tail produced vesicles capable only of Brownian motion. Since the actin-binding domain of myosin VI is lacking in these constructs, we concluded that the vesicles are stranded in the actin meshwork but not irreversibly bound to the actin.

To further investigate the necessity of a functional Myosin VI motor in endosomal traffic, a mutation causing myosin rigor binding to actin (K157R) was introduced into GFP-M6. K157R is a mutation in a universally conserved P loop domain that binds the terminal phosphate of ATP (Ruppel and Spudich 1996). Mutations in the myosin P loop in *Dictyostelium discoideum*, *C. elegans* and other organisms have shown that these myosins are deficient in ATP binding and exhibit neither ATPase activity nor movement in filament motility assays (Ruppel and Spudich 1996). The rigor mutant targeted to uncoated endocytic vesicles. Similarly to GFP-M6Tail, GFP-M6(K157R) inhibited transferrin trafficking, resulting in a block at

the uncoated vesicle stage which distinguished from the tail construct, was irreversible. Time-lapse observation of GFP-M6(K157R)-associated vesicles showed that they were irreversibly immobile (Aschenbrenner, Naccache et al. 2004). This suggests that the motor properties of myosin VI are indeed required to move nascent vesicles out of actin-rich peripheries and that actin is a barrier to this trafficking.

We concluded that the movements seen for GFP-M6-associated vesicles were due to the intrinsic motor activity of myosin VI and that no other actin-based motor was associated with these vesicles. This also substantiated the hypothesis that actin in ARPE-19 cells, our model system, was acting as a barrier to uncoated endocytic vesicles.

We thus predicted that eliminating the actin network would rescue trafficking in myosin VI mutant expressing cells. Latrunculin A (Lat A) was utilized to depolymerize F-actin. Lat A is a potent actin depolymerizing agent which operates by sequestering G-actin, thus shifting actin monomer equilibrium towards the depolymerization state (Yarmola, Somasundaram et al. 2000). First, however, we had to ascertain that latrunculin A would not affect prior endocytic events, as the role of actin in endocytosis had not been investigated in ARPE-19, the cell type used in our model system. We predicted that actin depolymerization would only affect the uncoated vesicle trafficking stage.

MATERIALS and METHODS

Cell Culture and Transfection

Retinal Pigmented Epithelial Cells (ARPE-19 cells) (Dunn, Aotaki-Keen et al. 1996) were grown at 37°C with 5% CO₂ in DMEM-F12 media with 10% FBS, , 0.25m g/ ml fungizone, and 2mM L-glutamine and transfected with GFP-tagged myosin VI constructs using Transit (Mirus) transfection reagent. Transit was used as recommended and utilizing a ratio of 1:3 DNA (in micrograms) to Transit (in microliters).

Antibodies for immunofluorescence

Antibodies used in this study were from the following sources: antibody to Early Endosome Antigen 1 (EEA1): BD Transduction Laboratories (Lexington, KY) used at 1:200; FITC- and rhodamine-conjugated donkey anti-rabbit and anti-mouse antibodies used at 1:100: Jackson ImmunoResearch Laboratories (West Grove, PA):. Antibody to the clathrin adapter AP-2 was generously provided by Dr. Sandra Schmid (The Scripps Research Institute, La Jolla, CA).

Treatment of ARPE-19 cells with Latrunculin A

Latrunculin A was purchased from Biomol (Plymouth Meeting, PA) or Calbiochem (San Diego, CA). Latrunculin A was diluted in DMSO and then into DMEM-F12 serum free media. The latrunculin A concentration and incubation

timepoint which would eliminate the cortical actin meshwork of ARPE-19 cells while causing the mildest effect on cell shape was determined to be 0.015 μM latrunculin A for 30 minutes at 37° C (DMEM-F12/LatA). Its solvent dimethylsulfoxide (DMEM-F12/DMSO.) was utilized as a control.

Quantification of Transferrin Endocytosis Using an ELISA Assay

ARPE-19 cells were serum-starved in DMEM-F12 media without serum and incubated for an additional 30 min at 37°C in DMEM-F12 media containing 0.015 μM latrunculin A (DMEM-F12/LatA), or its solvent dimethylsulfoxide (DMEM-F12/DMSO). The cells were chilled on ice for 20 min, and the medium was replaced with ice-cold DMEM-F12/LatA or DMEM-F12/DMSO containing 25 $\mu\text{g/ml}$ human biotinylated transferrin (Sigma) and incubated on ice for an additional 1 h to label surface receptors. Cells were washed twice with 0.5% BSA in PBS at 4°C before placing the cells back at 37°C for 0–15 min with the appropriate DMEM-F12 medium.

To quantify transferrin endocytosis, transferrin still bound to the cell surface was stripped by washing twice for 30 s each with 10 mM HCl + 150 mM NaCl. Cells were then washed with PBS before removal from the culture dish using PBS containing 5 mM EDTA. Cells were lysed in PBS containing 1% TX-100, and protein concentrations were determined using a BCA assay (Pierce Chemical Co., Rockford, IL). The amount of transferrin taken up by each cell culture was quantified using an ELISA-based assay as described (Smythe, Redelmeier et al. 1992). A 1:10,000

dilution of rabbit anti transferrin antibody (United States Biological, Swampscott, MA) was used to coat the ELISA plates. Streptavidin-HRP (Molecular Probes) was used at 1 $\mu\text{g}/\text{ml}$. After color development, the absorbance at 492 nm read using a Versamax tunable microplate reader (VersaLogic, Eugene, OR).

Steady State Uptake Assay for Endocytosis in the presence of Latrunculin.

Steady state uptakes were undertaken and quantified as described (Aschenbrenner et al., 2003). Briefly, ARPE-19 cells were serum starved for 2 hours in DMEM-F12 media without serum at 37°C. After serum starvation cells were further incubated for 30 min at 37°C in DMEM-F12/LatA or DMEM-F12/DMSO (as described above). The medium was replaced with DMEM-F12 containing 35 $\mu\text{g}/\text{ml}$ rhodamine-conjugated transferrin (R-Tsfn; Molecular Probes, Eugene, OR), and uptake was allowed to proceed at 37°C for 1–30 min. Uptake was stopped by fixation in 4% PFA in PBS. Cells were visualized with a Leica DMR upright light microscope fitted with a Hamamatsu ORCA 10bit CCD Digital Camera and processed as described (Aschenbrenner, Lee et al. 2003).

Pulse-chase Uptake of R-Tsfn

Pulse-chase uptakes were undertaken as described (Aschenbrenner, Lee et al. 2003). Briefly, for pulse-chase experiments in the presence of DMSO or LatA, following 1.5-h serum starvation, the cells were incubated for 30 min in DMEM-

F12/LatA or DMEM-F12/DMSO at 37°C. The cells were then incubated on ice for 30 min in the appropriate media before an additional 1 h on ice with 35 $\mu\text{g/ml}$ R-Tsfn in DMEM-F12/LatA or DMEM-F12/DMSO media. Cells were washed at 4°C with DMEM-F12 to remove unbound transferrin, before transferring to 37°C for 1–30 min to allow uptake to proceed. Uptake was stopped by fixation in 4% PFA in PBS, and cells were permeabilized in 0.1%TX-100 in 4% PFA in PBS. Cells were then stained for immunofluorescence utilizing anti-EEA1 or anti-AP2 antibodies followed by the appropriate mouse secondary FITC conjugated antibodies. Cells were visualized as above. Percent overlap between EEA1 or AP2 and rhodamine transferrin was determined by scoring the then number of EEA1 or AP2 positive vesicles that were also rhodamine transferrin positive. Three cells for which 100 vesicles positive for EEA1 or AP2 each were scored for each condition.

Quantification of Trafficking Using Fluorescence

Quantification of steady state R-Tsfn uptake to the pericentriolar endosome and quantification of percent overlap between GFP-tagged constructs, R-Tsfn, and endocytic markers was done as described (Aschenbrenner, Lee et al. 2003).

Published pulse-chase experiments in ARPE-19 cells have confirmed that after exit from the myosin VI-positive uncoated vesicle compartment, R-Tsfn enters peripheral early endosomes that are EEA1-positive (Aschenbrenner, Lee et al. 2003). For experiments undertaken in the presence of DMSO or LatA, quantification of this

delivery was accomplished by using the fact that given longer chase times in ARPE-19 cells, the EEA1-positive pericentriolar region receives the endocytosed transferrin. Of note, at these later pulse-chase time points, overlap between the endocytosed transferrin and myosin VI is no longer seen confirming complete delivery of the transferrin to the early endosome compartment (Aschenbrenner, Lee et al. 2003). Therefore to quantify delivery of transferrin from the uncoated vesicles to the early endosome in DMSO- or Lat A-treated cell, the cells were scored as positive for delivery to the early endosome if any pericentriolar R-Tsfn was evident. In some experiments, the position of the early endosome was confirmed by staining for EEA1 during quantification of early endosome delivery. Error bars represent the SD from three experiments.

RESULTS

We hypothesized that wild type myosin VI acts to move uncoated endocytic vesicles across the actin meshwork. Implicit to this hypothesis, we predicted that actin acts a barrier to myosin VI mediated vesicle trafficking.

Our analysis of myosin VI mutants suggested that actin was a barrier slowing uncoated vesicle traffic to the early endosome. GFP-M6(Tail), a myosin VI construct lacking the motor domain, and GFP-M6(K157R) (Figure 1.1), a myosin VI construct mutated to be in a terminal state of rigor binding to actin result in an abrogation of myosin VI-associated vesicle motility. I predicted that eliminating the actin network would rescue trafficking in cells expressing the myosin VI mutants. I also predicted that actin depolymerization would accelerate the rate of transferrin delivery to the early endosome.

Depolymerizing the cortical actin meshwork

We used the F-actin–depolymerizing drug latrunculin A (LatA)(Spector, Shochet et al. 1983), which sequester G-actin monomers. Titration experiments revealed that nanomolar LatA concentrations were sufficient to remove the peripheral actin meshwork from ARPE-19 epithelial cells without significantly altering cell attachment or cell shape (Figure 1.2A). The effect of depolymerizing the cortical actin meshwork on uncoated vesicle localization was studied.

We found that Lat A reduced myosin VI-associated vesicle recruitment to actin at the ARPE-19 cell peripheries. When treated with low concentrations of Lat A (0.01-0.025 μ M), cortical actin filaments as well as stress fibers are depolymerized in ARPE-19 cells (Figure 1.2A). In addition, myosin VI redistributed in the presence of Lat A (Figure 1.3B). Immunofluorescence imaging using a polyclonal myosin VI antibody revealed that myosin VI is normally enriched at the periphery in a punctate pattern and in an area colocalizing with cortical actin. The addition of Lat A caused a disruption of the punctate pattern of peripheral Myosin VI (Figure 1.2B). This change in myosin VI location suggested that the targeting of myosin VI to vesicles in the periphery is dependent on the presence of filamentous actin at the periphery.

Since actin has been implicated in different stages of endocytosis and vesicle trafficking, and since the particular role of actin and extent to which this role is important varies depending on cell type, we had to at first determine the effect of actin depolymerization on the stages of endocytosis in ARPE-19 cells prior to the delivery of cargo to the early endosome. For this purpose we measured the effect of Lat A on receptor mediated trafficking of transferrin over three endocytic vesicle stages: endocytosis, clathrin coated vesicle formation, and clathrin uncoating.

Effect of Latrunculin A on endocytosis

We evaluated the effect of Lat A on clathrin-coated pit formation utilizing an ELISA based assay (Fujimoto, Roth et al. 2000); (Buss, Arden et al. 2001). This direct

sandwich ELISA compared the amount of biotinylated transferrin taken up by ARPE-19 cells at various timepoints in the presence of DMSO or LatA (Figure 1.3).

Treatment with 0.015 μ M LatA had no effect on the rate of transferrin endocytosis in ARPE-19 cells.

Effect of Latrunculin A on clathrin coated pit uncoating

We then determined whether clathrin coated pits could still be uncoated within the proper timeframe in the presence of latrunculin A. This was conducted by visualizing whether transferrin could still exit clathrin coated pits within two minutes of uptake. Pulse-chase experiments following R-Tsfn (rhodamine transferrin) and comparing its location to clathrin over a seven minute time-course were conducted (Figure 1.4). Treatment with LatA had no effect on the rate of transferrin exit from clathrin-coated pits and vesicles (Figure 1.4). Therefore, depolymerizing the peripheral actin cytoskeleton had no effect on clathrin-coated vesicle formation or uncoating, allowing us to directly test the effects of LatA on the next step, the delivery of components to the early endosome.

Effect of Latrunculin on delivery to the early endosome

To determine early endosome delivery kinetics, we allowed cells treated with DMSO or Latrunculin A (LatA) to endocytose R-Tsfn for fixed time periods ranging from 1 to 15 min at 37°C and then quantified the percent of cells where R-Tsfn had

reached the pericentriolar early endosome (see MATERIALS AND METHODS for quantification methodology) (Figure 1.5). In DMSO-treated cells, R-Tsfn maximally reached the early endosome after 5–7 min (Figure 1.5). In LatA-treated cells, R-Tsfn delivery to the early endosome was accelerated, reaching the pericentriolar region within 2–3 min ($p < 0.001$). A similar acceleration was observed in LatA-treated cells when the location of endocytosed transferrin was compared with the vesicles associated with the early endosome marker, EEA1 (Figure 1.6). This acceleration suggests that actin is a barrier to uncoated vesicle trafficking to the early endosome and that actin's presence causes a 3–5-min delay in endosome delivery equivalent to the normal uncoated vesicle lifetime.

Effect of cortical actin depolymerization on myosin VI-based uncoated vesicle delivery to the pericentriolar region

Transferrin-containing vesicles accumulate in peripheral actin-rich regions of GFP-M6tail– and GFP-M6(K157R)–expressing cells, thereby blocking delivery to the early endosome (Aschenbrenner, Naccache et al. 2004). We hypothesized that F-actin depolymerization should rescue this phenotype. We first evaluated the effects of actin depolymerization on cells transfected with GFP and GFP-M6. These control experiments revealed that the presence of DMSO coupled with the exposure to transfection reagent resulted in a slower net rate of steady state transferrin uptake compared with untransfected controls. After 15 min of uptake in the presence of

DMSO or LatA, 60–75% of GFP- or GFP-M6–transfected cells exhibited a pericentriolar R-Tsfn accumulation, a number significantly less than the ~95% seen for untransfected cells after 15 min (Figure 1.7). Although trafficking was slower, in the presence of DMSO, cells transfected with GFP-M6tail and GFP-M6(K157R) still exhibited a significant block in transferrin trafficking, with only 32.7 ± 7.1 and $34.1 \pm 4.5\%$ of cells exhibiting a pericentriolar accumulation, respectively. After treatment with LatA, however, $57.0 \pm 7.3\%$ of GFP-M6tail–transfected cells and $57.9 \pm 7.3\%$ of GFP-M6(K157R)–transfected cells exhibited pericentriolar transferrin accumulation, levels equivalent to those seen in wild-type controls. Therefore the block in trafficking seen upon GFP-M6Tail and GFP-M6(K157R) over-expression is due to trapping in the actin cytoskeleton, and this block can be released by removing the F-actin barrier.

DISCUSSION

Previous studies using pulse-chase methods in cultured cell lines had suggested that there was a short-lived uncoated vesicle population found near the plasma membrane that ultimately fused with the early endosome (Hopkins 1983); (Hanover, Willingham et al. 1984); (Eskelinen, Kok et al. 1991); (Eskelinen, Kok et al. 1991). In this study we present the first characterization of these nascent uncoated endocytic vesicles, showing that they are motile, exhibiting net movement into the cell. A myosin, myosin VI, is responsible for their movement. In the absence of a myosin VI motor, only slow diffusion-based vesicle movement to the early endosome is evident, a movement that was not due to retrograde actin flow.

Depolymerizing this actin meshwork resulted in an attenuation of the trafficking defect imposed by myosin VI mutants. Therefore, actin is a barrier to vesicle trafficking, but myosin VI as a minus-end-directed motor takes advantage of the features of this barrier to transport uncoated vesicles to the early endosome for fusion.

Cultured retinal pigmented epithelial cells (ARPE-19) are semi-polarized when grown on glass. Myosin VI is enriched in a peripheral region associated with the cortical actin network in these cells, which we have shown reflects association with nascent endocytic vesicles (Aschenbrenner, Lee et al. 2003). There has been a debate in the literature as to the role of actin in the endocytic cycle in different cell types. In retinal pigmented epithelial cells, we have shown that at least at nanomolar quantities

of LatA, depolymerization of the cortical actin meshwork does not affect the initial stages of endocytosis.

Myosin VI is enriched in various regions of endocytic activity. In epithelial cells with microvilli, myosin VI localizes to the base of the microvillus, to the terminal web, and to vesicle rich regions (Biemesderfer, Mentone et al. 2002);(Heintzelman, Hasson et al. 1994); (Hasson, Gillespie et al. 1997); (Buss, Arden et al. 2001). In secretory cell types, the cortical actin network is a barrier to exocytosis at the plasma membrane (reviewed in(Eitzen 2003)). In these systems, actin serves a scaffolding role and is required to anchor secretory vesicles as a readily releasable pool (Sankaranarayanan, Atluri et al. 2003). In some cases, this anchoring requires a myosin (Rose, Lejen et al. 2002); (Rudolf, Kogel et al. 2003) whereas in other cases, such as GLUT4 delivery to the adipocyte plasma membrane, a plus-end-directed unconventional myosin, myo1C, may play a role in vesicle delivery across the barrier toward the plasma membrane (Bose, Guilherme et al. 2002). In peripheral regions there is a higher percentage of plus ends facing outward so a plus-end-directed myosin would be appropriate for vesicle trafficking outward for exocytosis. As a minus-end-directed motor, myosin VI is suited to play the opposite role, moving uncoated vesicles inward away from the plasma membrane for fusion with the early endosome.

The uncoated vesicles analyzed in our time-lapse studies took a circuitous route to exit the actin-rich periphery. They did not appear to move along one specific actin track to exit the actin mesh nor did the vesicles in each area appear to have preset

endosomal destinations (online supplementary materials (Aschenbrenner, Naccache et al. 2004). Instead, the uncoated vesicles apparently switched between actin tracks.

This type of motility is consistent with the kinetic analysis of myosin VI movement *in vitro*, which predicted short processive runs interspersed with pauses (Rock, Rice et al. 2001) and also with modeling of motor-assisted transport of particles in situations of mixed filament polarities and a minus-end-directed motor (Smith and Simmons 2001). Because actin at the plasma membrane is biased with minus-ends inward, this start-and-stop motility by myosin VI would eventually lead to vesicle exit from the actin meshwork.

Wild-type myosin VI is thought to be a monomer and non-processive if not bound to cargo. It has been suggested that myosin VI dimerizes on the UCV following cargo binding (Jim Spudich pers. Comm). In addition, very recently that when it is in the proper viscous environment (such as would be found in the actin meshwork), and when bound to cargo, myosin VI can move processively as a monomer because it would not be able to diffuse away from the actin filament (Iwaki, Tanaka et al. 2006).

Uncoated vesicles are universally present in all cells as an intermediate in endocytic trafficking between clathrin-coated vesicles and the early endosome. In some cell types, such as polarized epithelial cells with a terminal web domain, actin would serve as a barrier to uncoated vesicle delivery. Therefore we would propose that epithelia present in Snell's waltzer mice, which lack myosin VI, must utilize vesicle diffusion followed by endosome capture as the major mechanism for delivery to the

early endosome. In other cell types, such as fibroblasts, which lack dense actin-rich regions, there would not be a barrier, and endosome delivery could occur unimpeded. Indeed, we have found that expression of myosin VI mutants has no effect on trafficking in fibroblasts, confirming that myosin VI is specifically involved in trafficking through actin-rich regions only (our unpublished results). It is relevant to mention that while cultured cell types appear generally to function properly without myosin VI, myosin VI is essential for the normal retinal electrophysiology of retinal cells (Kitamoto, Libby et al. 2005).

We have shown that actin is a physical barrier to uncoated vesicle trafficking. Accelerated vesicle movement out of the actin mesh is due to myosin VI motor activity and results in a short vesicle lifetime. Therefore the molecular motor myosin VI is specifically recruited to extricate nascent vesicles from the actin mesh to allow for timely early endosome fusion.

ACKNOWLEDGEMENTS

The text of Chapter one is in part derived from Aschenbrenner, Naccache and Hasson published in the journal *Molecular Biology of the Cell* in 2004 for which Laura Aschenbrenner was the primary researcher. For the portion included in the result section of this manuscript, the dissertation author was the primary researcher. Dawn Jolson and Jennifer Stubbs are acknowledged for their help with setting up the endocytosis assay.

FIGURES

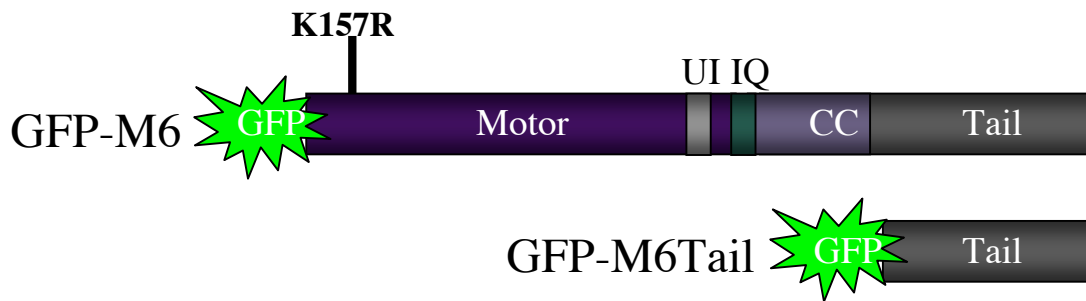


Figure 1.1. Schematic of GFP tagged myosin VI constructs. The motor domain is followed by a converter region that is bordered by an insert unique to myosin VI (UI), and a neck region that contains a single IQ motif. This is followed by a coiled coil motif (CC) then a globular tail. The K157R alteration is represented.

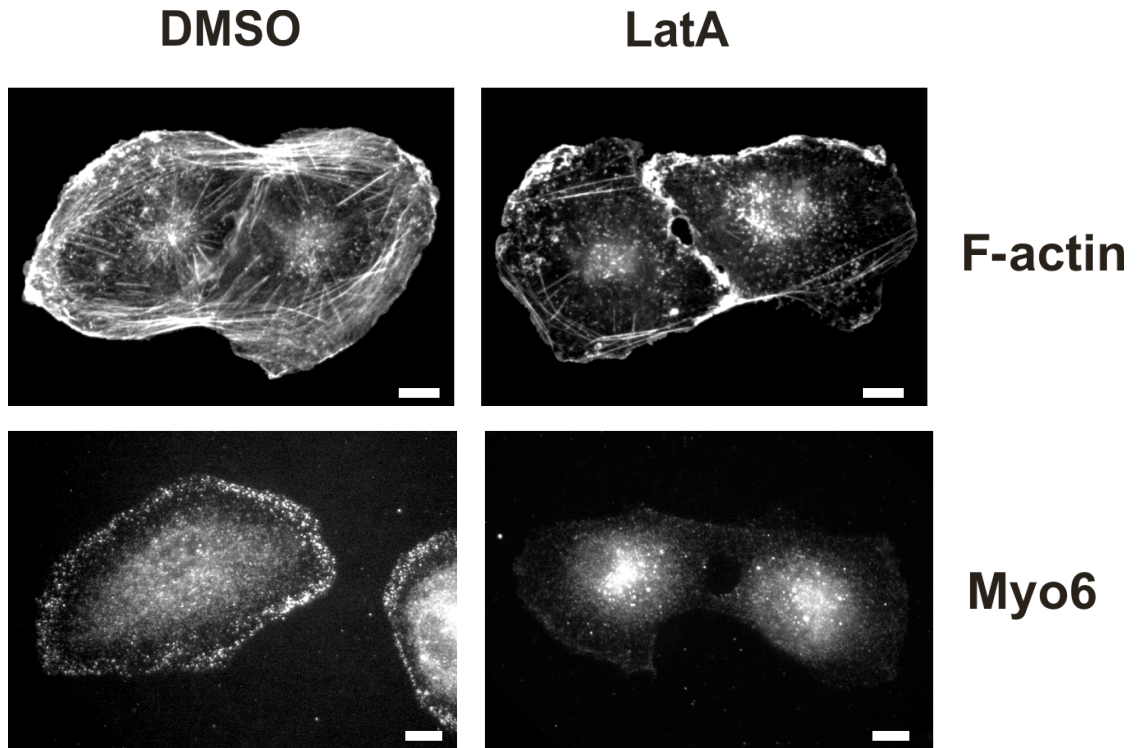


Figure 1.2. The cortical actin meshwork of ARPE-19 cells is depolymerized by nanomolar concentrations of latrunculin. Cells treated for 30 min with DMSO or 0.015 μM latrunculin A (LatA) were fixed and stained with rhodamine-phalloidin or antibodies to myosin VI. Scale bars, 10 μm .

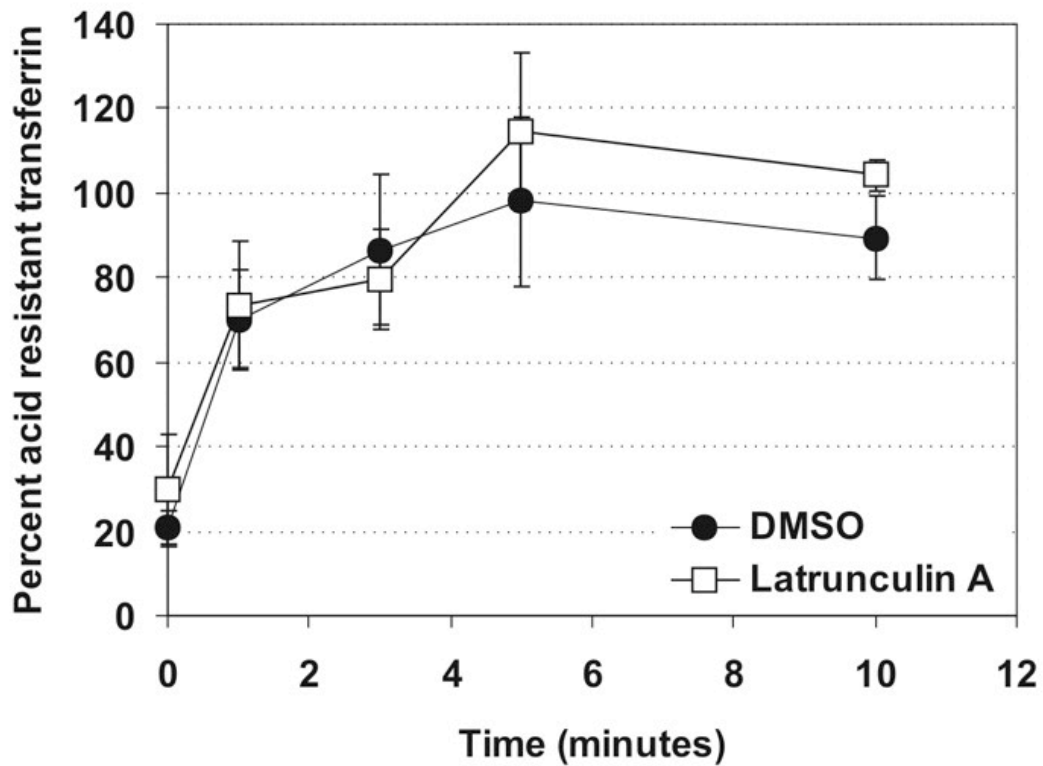


Figure 1.3. The kinetics of transferrin endocytosis in ARPE-19 cells is not affected by latrunculin A. Quantification of the endocytosis of biotinylated transferrin. ARPE-19 cells treated with DMSO (circle) or Latrunculin A (square) were incubated in biotinylated transferrin followed by uptake at 0, 1, 5, 7 and 10 minutes at 37°C. Shown is a representative example of four experiments.

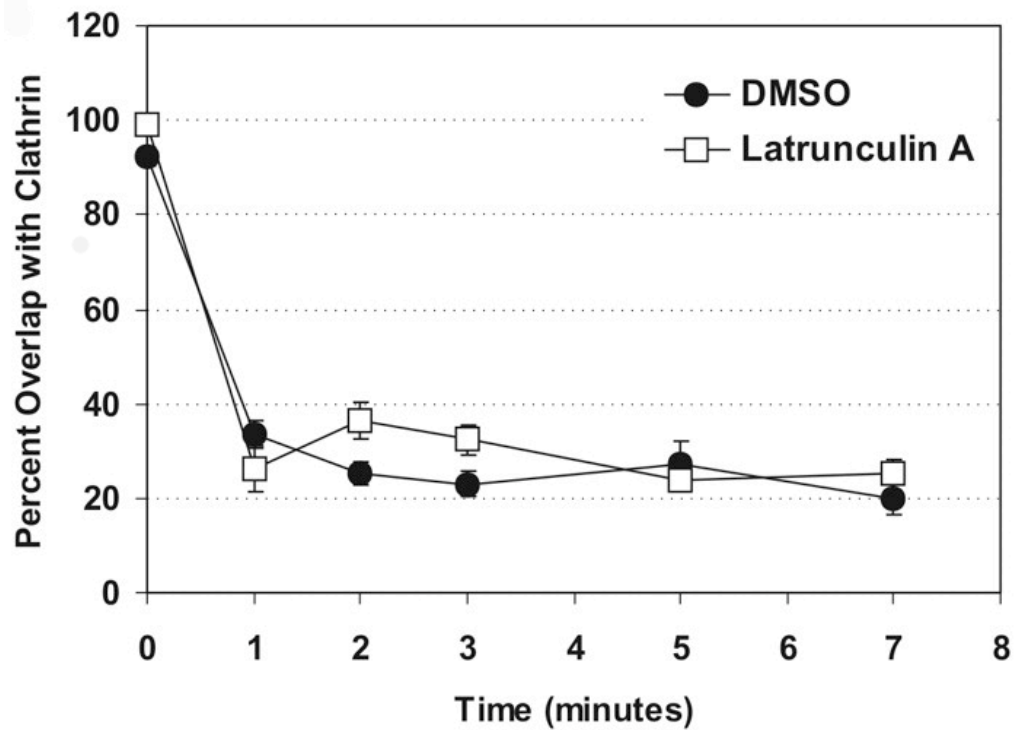


Figure 1.4. The kinetics of transferrin exit from clathrin coated vesicles is not affected by nanomolar concentrations of Latrunculin A. Pulse-chase of rhodamine transferrin in cells incubated in the presence of DMSO (circle) or latrunculin A (square). Cells were stained with AP-2, a marker for clathrin. Percent overlap of AP-2 with transferrin was measured by counting one hundred AP-2-positive vesicles from three separate cells for each condition and determining the number of those vesicles that were also positive for rhodamine transferrin.

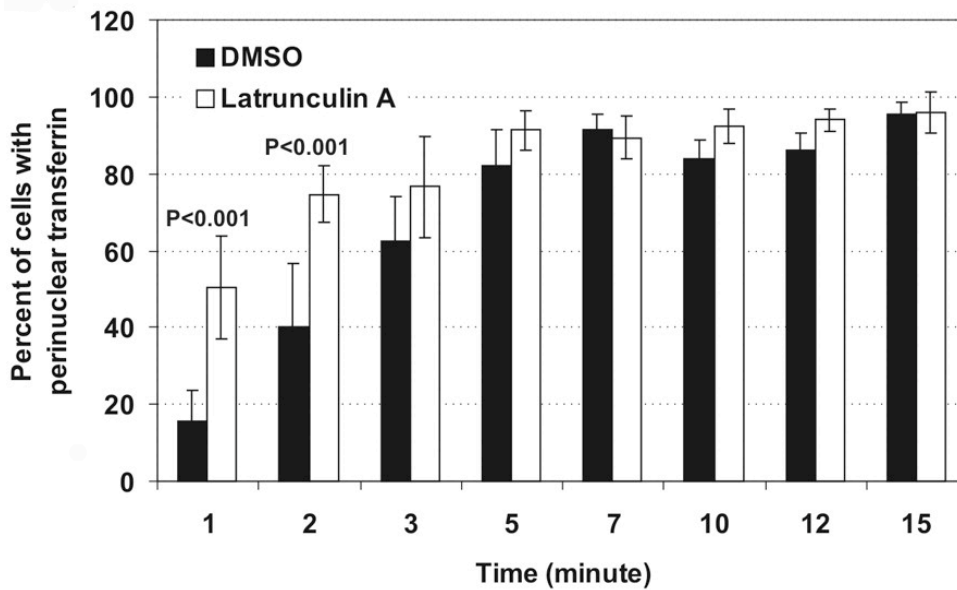


Figure 1.5. Delivery of transferrin to the early endosome is accelerated by nanomolar quantities of latrunculin A. Delivery of transferrin to the pericentriolar early endosome was judged by steady state uptake experiments in the presence of DMSO (black bars) or latrunculin A (white bars). The histogram shows the percent of cells exhibiting delivery of R-Tsfn to the pericentriolar early endosome at fixed uptake times. More than 600 cells were counted per time point.

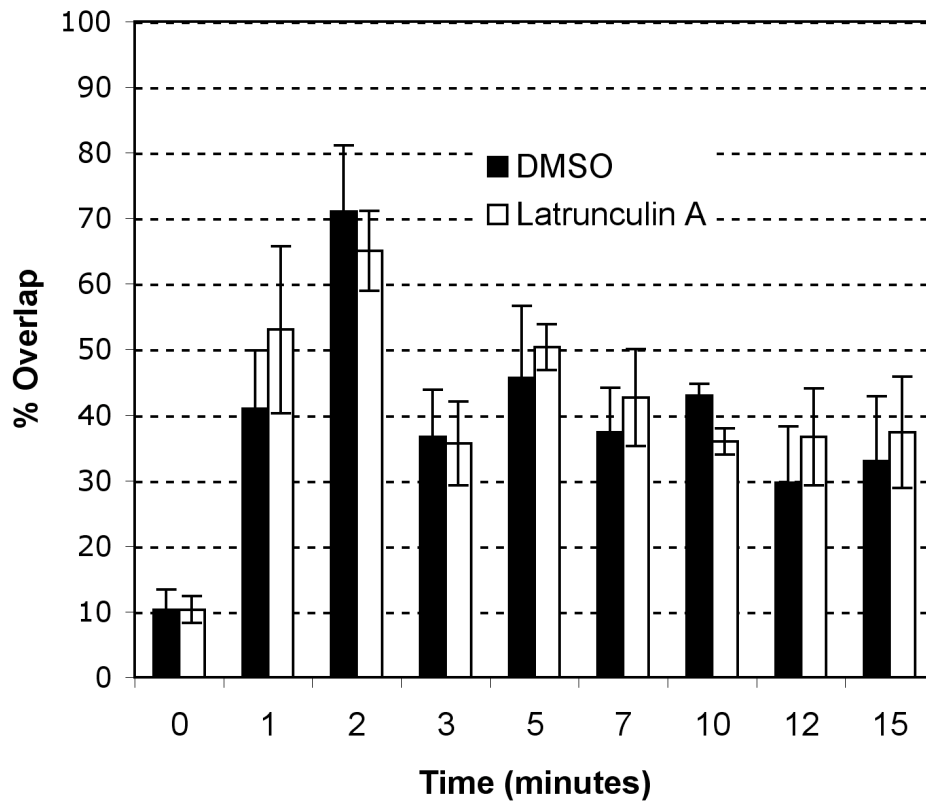
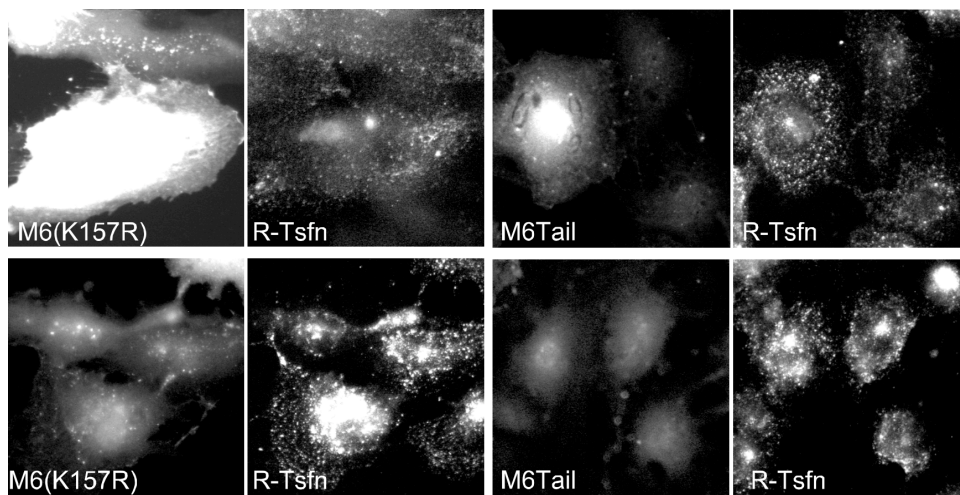
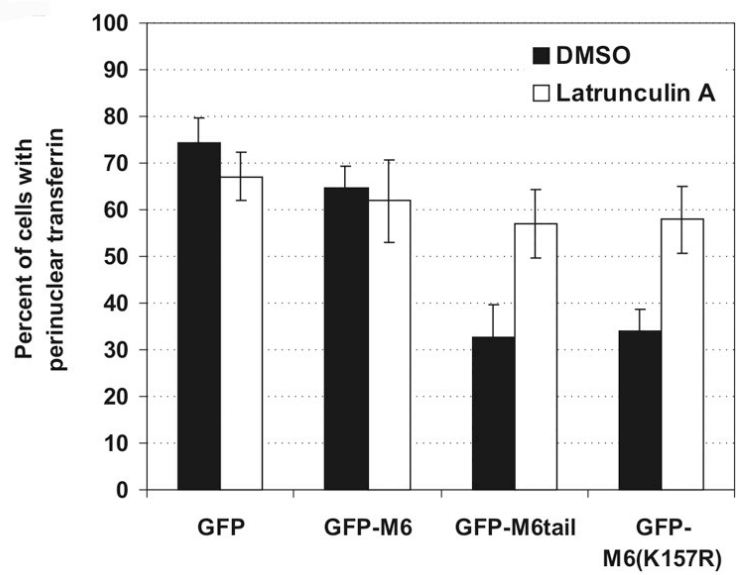


Figure 1.6. Delivery of transferrin to the early endosome is accelerated by nanomolar quantities of latrunculin A. Delivery of transferrin to the pericentriolar early endosome was judged by pulse chase experiments in the presence of DMSO (black bars) or latrunculin A (white bars). Cells were stained with an antibody to EEA1, a marker for early endosomes. Percent overlap of EEA1 with transferrin was measured by counting one hundred EEA1-positive vesicles from three separate cells for each condition and determining the number of those vesicles that were also positive for rhodamine transferrin.

Figure 1.7. Removal of the actin barrier in ARPE-19 cells rescues the trafficking defects seen upon GFP-M6tail and GFP-M6(K157R) expression. (A) ARPE-19 cells transfected with GFP-M6, GFP-M6(K157R), or GFP-M6Tail (Green) were treated with DMSO or latrunculin A for 30 minutes before a 15 minute steady state uptake of rhodamine transferrin. (B) Histogram showing the percent of transfected cells exhibiting delivery of endocytosed R-Tsfn to the pericentriolar early endosome after 15 min of uptake. More than 500 cells were counted per construct.

A.**B.**

CHAPTER TWO: Myosin VI altered at threonine 406 stabilizes actin filaments *in vivo*.

INTRODUCTION

Myosins are a large family of molecular motors that transport components along the actin cytoskeleton. Of these, the unconventional myosin, myosin VI, is unique as it travels towards the minus end of actin filaments, rather than towards the plus end as is seen for all other characterized myosins. Actin filaments are often oriented with their minus ends towards the interior of the cell, and in keeping myosin VI is required for inwards transport during endocytosis.

The actomyosin cycle has the net effect of converting ATP hydrolysis into force generation. In the absence of ATP, myosin is tightly bound to actin in a state termed rigor bound. Myosin is weakly bound to actin when its nucleotide-binding pocket is occupied by ATP or the hydrolysis product ADP plus Phosphate, and in this state flutters on and off the actin filament. In the meantime, the lever arm of myosin is in the pre-powerstroke conformation with respect to the head domain. Binding to actin results in phosphate release. The conformational change in the head domain core resulting from phosphate release is amplified through the lever arm of myosin and results in a power stroke. If the cargo-binding domain of myosin is secured, the

net result is actin filament displacement, if not the net result is cargo displacement.

Myosin VI is rare amongst the myosin superfamily in that it spends most of its time in the ADP bound state (Robblee, Olivares et al. 2004) tightly bound to actin. In the context of a double headed myosin moving along an actin filament, this allows the trailing head of myosin VI enough time tightly bound to the actin filament so that the leading head can find the next actin binding site, resulting in processive motion such that myosin VI can take up to six steps on the actin filament before falling off it (Altman, Sweeney et al. 2004).

Recent kinetic studies have suggested that myosin VI is not only a molecular motor capable of processive transport, but can also serve as a regulated tether capable of sensing and responding to tension exerted on the head domain by cargo. ADP dissociation from the nucleotide binding pocket is the rate limiting step during the actomyosin VI cycle . As the ADP-bound form binds tightly to F-actin, this feature allows two-headed myosin VI to move processively with an average run length of 300nm over a period of 1 second. In response to increased backwards force however, myosin VI's kinetic cycle is altered; ADP release rates are increased and the affinity for ATP is dramatically reduced making ATP association the rate limiting step in the actomyosin VI cycle (Altman, Sweeney et al. 2004). As a result, under increasing load the myosin remains bound to actin. This property allows the head of myosin VI to sense and respond to tension applied from the cargo at the cargo binding domain. The mechanism for modulating this change between stepping and stalling kinetics *in vivo*

is unknown.

Both Class I and VI myosins have a highly conserved threonine or serine residue at a surface loop on the actin-binding face of the motor. Phosphorylation at this site is required to activate ATPase activity and actin motility in ameboid class I myosins . We theorized that phosphorylation at the equivalent site in myosin VI, threonine 406 (T406), could serve as the motor – to – tether signal.

The impact of phosphorylation at T406 has been analyzed kinetically using baculovirus-expressed myosin VI fragments either phosphorylated *in vitro* with PAK3, or modified at T406 to mimic the phosphorylated or dephosphorylated state . These studies suggested that phosphorylation at T406 does not dramatically affect the ATPase activity of unloaded myosin VI. However, alteration of T406 to glutamate (T406E) to mimic phosphorylation increased the rate of phosphate release of unloaded myosin VI, pushing it into the ADP bound state without affecting the rate of ADP dissociation (De La Cruz, Ostap et al. 2001). This is analogous to the role of the TEDS site in increasing the rate of phosphate release from the actin bound *Acanthamoeba* myosin I-C (Ostap, Lin et al. 2002). We envisioned that any modification that pushed myosin VI into a tightly bound state may be sufficient to act as the *in vivo* signal to switch myosin VI from a motor to a tether under load.

Here we test this hypothesis by analyzing the *in vivo* effects of expression of GFP tagged versions of myosin VI altered at position T406 to mimic the phosphorylated or dephosphorylated state. We find that phosphorylation at T406 does

not affect the basic motor activity of myosin VI as assayed by monitoring the transport of uncoated endocytic vesicles (UCVs). However, this alteration affects the route taken by myosin VI cargo and leads to tight binding to F-actin, supporting the theory that phosphorylation at T406 may be a mechanism to switch myosin VI from a motor to a tether.

MATERIALS and METHODS

Cell Culture and Transfection

ARPE-19 cells were grown as described and transfected (Aschenbrenner, Lee et al. 2003) utilizing Transit (Mirus). Quick Change XL site directed mutagenesis kit (Clontech) was utilized to create GFP-M6(T406E) and GFP-M6(T406A) using full length porcine myosin VI fused to GFP (GFP-M6) (Aschenbrenner, Lee et al. 2003). GFP-M6+LI(T406A) and GFP-M6+LI (T406E) were created from full length human myosin VI containing both the small and large tail domain splice insertions fused to GFP, (GFP-M6+LI) . Primers used are listed in the Supplementary Materials. When two constructs were co-expressed, 2 micrograms of each construct was utilized for transfection. Constructs were allowed to express for 26 hours, the optimal time for GFP-M6(T406E)-associated vesicle cluster formation.

Site-directed mutagenesis and constructs used

The primers used for site directed mutagenesis are as listed below. The mutation in the primer set is underlined. Isolated clones were subcloned and sequenced to verify that the point mutation was incorporated and that no other mutations were introduced by PCR.

For GFP-M6(T406A):

5'-GGGGGCGCCAAAGGAGCAGTTATAAAGGTGCCC-3' and

5'-GGGCACCTTTATAACTGCTCCTTTGGCGCCCC-3'.

For GFP-M6(T406E)

5'-GGGGGCGCCAAAGGAGAAAGTTATAAAGGTGCCC and

5'-GGGCACCTTTATAACTTCTCCTTTGGCGCCCC-3'

For GFPM6+LI (T406A)

5'-GGGGCACCAAAGGAGCAGTTATAAAGGTACCT-3' and

5'-GAGGTACCTTTATAACTTGCTCCTTTGGTGCCCC-3'

For GFPM6+LI (T406E)

5'-CAGGGGGGCACCAAAGGAGAAAGTTATAAAGGTACCTCTGAAA-3'

and

5'-TTTCAGAGGTACCTTTATAACTTTCTCCTTTGGTGCCC CCTG-3'.

GFP-M6(C442Y) was created by Lori Aschenbrenner utilizing site directed mutagenesis kit. To create GFP-M6(C442Y)-(T406E) and GFP-M6(C442Y)-(T406A), GFP-M6(C442Y) was cut with SmaI and KpnI then ligated into GFP-M6(T406A) or GFP-M6(T406E). Constructs were confirmed by sequencing and protein size was confirmed in immunoblot analysis with antibody to green fluorescent protein GFP or antibody to the tail domain of myosin (Aschenbrenner et al 2003). pCMV6m/hPak1-T423E(constitutivel active PAK), was generously provided by Dr. Gary Bokoch (Scripps Research Institute).

Antibodies

Antibody to GIPC/synectin was used as described . Antibody to the clathrin adapter AP-2 was generously provided by Dr. Sandra Schmid (The Scripps Research Institute). anti-Arp3 was from Upstate Biotech. Anti α -actinin was from Sigma. Antibodies to myosin VI were as described in Aschenbrenner et al 2003. Affinity-purified rabbit and mouse anti-myo6 tail domain antibodies were used as described previously (Hasson and Mooseker 1994). Mouse antibodies to GFP were from MBL. Antibody to M6 phospho T406 utilized at 1:100 was generously provided by Dr. Mitsuo Ikebe (Yoshimura, Homma et al. 2001) antibody to PAK1: Santa Cruz used at 1:80. Myc anti rabbit antibody was obtained from Santa Cruz.

Fixation of mouse kidneys

Mouse kidneys were fixed by Dr. Arie Horowitz. Mice were anesthetized by injection of avertin and perfused through the left ventricle with phosphate buffered saline (PBS), followed by 4% paraformaldehyde (PFA) in PBS. Kidneys were excised and the cortex was cut into $\sim 2 \times 2$ mm blocks and fixed in PBS containing 20 mM EGTA and 4% PFA for 5 min. After rinsing in PBS/20 mM EGTA, tissue blocks were quenched in 0.05% NaBH₄/PBS/EGTA for 10 min and infiltrated with 1 M sucrose/PBS/EGTA for 2 hrs on ice. Tissue blocks were embedded in OCT (Tissue-Tek) and frozen in liquid nitrogen.

Immunofluorescence and Time-lapse Video Microscopy

Coverslip grown cells were processed for immunofluorescence in six-well plates as described . Affinity-purified rabbit anti-myosin VI tail domain antibodies are as described . All secondary antibodies were from Jackson Immunochemicals. Samples were observed with a Leica DMR upright light microscope fitted with a Hamamatsu ORCA 10bit CCD Digital Camera unless otherwise stated.

GFP-labeled vesicles were monitored at 25°C using the Leica DMR fitted with a Plan Apochromat 100X 1.4NA oil immersion objective as described in detail in . Images were captured at a rate of one frame every 10 sec. Openlab software was used to control shutters and filter wheels. All cells were monitored for a minimum of 13 min, and cell health was checked by phase-contrast microscopy. Any cells exhibiting contraction were eliminated from the analysis.

The position of distinct vesicles that were initially positioned within 10 μ m of the cell edge was manually determined in successive frames using Openlab measurements software as described (Aschenbrenner, Naccache et al. 2004). 100 vesicles were tracked for each GFP-construct studied. Each construct was analyzed in 10 separate experiments and 8-11 cells minimum per experiment were recorded. For each experiment tracking cells expressing an altered version of myosin VI, a wildtype GFP-M6 control was also tracked to assure cell health. The Openlab software recorded the (x,y) coordinates of the fluorescent particles at each given time, calculated vesicle trajectories and calculated the instantaneous velocity ($\Delta d/\Delta t$). The displacement vector

analysis was plotted using Canvas 6.0 utilizing the x,y coordinates. Plots and statistical analyses of vesicle properties were generated with Microsoft Excel 2000.

Kidney sections: frozen kidney blocks were cryo-sectioned with a Microm HM525 cryostat to a thickness of 4 μ m, and placed on microscope slides. OCT was removed by immersion in acetone at -20°C for 5 min, and the sections were transferred to room temperature and rehydrated by 0.5% BSA/PBS. Sections were blocked in 2% BSA/PBS for 20 min, incubated with primary antibodies for 1 hr, washed by 0.5% BSA/PBS, incubated with secondary antibodies, washed again, and incubated with rhodamine phalloidin for 20 min. After a final wash, sections were mounted with coverslips and Vectashield. Sections were imaged as above.

Pulse-chase and steady-state uptake assay for endocytosis

Pulse-chase and steady-state uptakes of R-Tsfn were undertaken and quantified as described in the materials and methods section of chapter 1.

Staining and transfection of Caco-2 cells

Caco-2 cells (ATCC) were grown at 37°C with 5% CO_2 in DMEM (GIBCO) with 10% FBS, 1.5g/l NaHCO_3 , 2mM L-glutamine, 1% Fungizone and 0.001% human transferrin (Sigma). The eGFP-C2-rat-esp1 2B construct was generously provided by Dr. Jim Bartles (Northwestern University Medical School) (Loomis, Zheng et al. 2003). Cells were transfected with Lipofectamine. (Invitrogen) For semi-

differentiated cultures on filters or coverslips, cells were analyzed 24 hours after transfection. For differentiated cultures, cells were analyzed 3 days after transfection. The cells were fixed with 4% formaldehyde in 1xPBS for 20minutes, and permeabilized with 1%Triton-X100 in 1xPBS with 4% formaldehyde for 10 minutes. Coverslips were blocked for 30 minutes in 3%BSA in 1xPBS before staining with rhodamine-phalloidin and visualized as described for ARPE-19 cell experiments.

Visualization of actin filament minus ends

DNaseI was utilized to visualize free actin minus ends using a method adapted from . ARPE-19 cells were grown on coverslips and transfected as above with 2-4 μ g DNA per well. 25.5 hours later, the cells were washed with buffer B (5 mM KCl, 137 mM NaCl, 4 mM NaHCO₃, 0.4 mM KH₂PO₄, 1.1 mM Na₂HPO₄, 2 mM MgCl₂, 5 mM Pipes, and 5.5 mM glucose, pH 7.2). Cells were permeabilized with a saponin extraction buffer consisting of buffer B containing 0.05% saponin, 20 μ M phalloidin, and 4 mM EGTA for 45 seconds. Cells were washed 3 times for 30 seconds each in an F-actin stabilization buffer consisting of Buffer B containing 20 μ M phalloidin and 4 mM EGTA to remove all G-actin. Cells were incubated with 1 μ M rhodamine-conjugated DNase I (DNase I-rho; 1mM stock kindly donated by Dr. Robert Fischer, The Scripps Research Institute, La Jolla, CA) diluted in 10 mM imidazole-acetate, pH7.5, 3.25 mM Tris-acetate, 51 mM KCl, 2.24 mM Mg-Acetate, 0.54 mM BSA, 4.93 mM Mn-acetate and 0.5 μ M cytochalasin D (ICN Biomedical) for 17 min. Cells were lastly washed with buffer B containing 20 μ M phalloidin and 4 mM EGTA to remove

DNase I-rho not bound to the actin cytoskeleton. Cells were fixed with 3.7% formaldehyde in buffer B for 10 min. Actin was visualized utilizing rhodamine-phalloidin (Molecular Probes) or coumarin-phalloidin (Sigma).

DnaseI stained coverslips were mounted in Vectashield (Vector Labs) and observed with a Nipkow spinning disk confocal scan head (QLC100, VisiTech) attached to a Nikon Eclipse E600 microscope equipped with a 40x/0.8 NA Plan Apo DIC objective and a Cooke Sensicam QE CCD camera. Images were captured using Image Pro Plus.

Cytochalasin Treatment

ARPE-19 cells were grown on coverslips and transfected with 2 μ g DNA per well. 25.5 hours later, cells were incubated in DMEM-F12 media containing 50 μ M cytochalasin D at 37°C for 5 minutes. The cells were then fixed and permeabilized as above and the F-actin visualized using rhodamine-phalloidin (Molecular Probes).

Determining level of ectopic expression of GFP-tagged constructs

ARPE-19 cells were grown as described in 6 well plates and transfected with 4 micrograms of GFP, GFP-M6T406A, GFP-M6(T406E), GFP-M6 per well utilizing Transit. Cells were scraped in 5mM EDTA in 1xPBS, spun down at 1000rpm for 2 minutes, and resuspended 5x sample buffer. Western blot analysis utilizing rabbit anti myosin VI antibody at 1microgram/ml followed.

Timelapse movies

Movies 1-3 (Figure 2.12) monitor the motility of GFP-M6(T406A) and GFP-M6(T406E)-associated UCVs. Movies can be found both at <http://www.interscience.wiley.com/jpages/0886-1544/suppmat> and as supplementary materials to this dissertation.

RESULTS

Targeting of GFP-M6(T406E) and GFP-M6(T406A)

GFP tagged myosin VI (GFP-M6) recreates the function of endogenous myosin VI and transports uncoated endocytic vesicles (UCV). To mimic the phosphorylated and dephosphorylated state, threonine 406 of GFP-M6 was altered to glutamate (GFP-M6(T406E)) and to alanine (GFP-M6(T406A)) respectively (Figure 2.1A).

When expressed in ARPE-19 epithelial cells, both GFP-M6(T406A) and GFP-M6(T406E) targeted to UCVs (Figure 2.1B) and associated with the UCV adapter protein, GIPC/synectin but not the adaptor to clathrin, AP-2. (Figure 2.2A and B). Ectopically expressed myosin VI altered at T406 did not locate to other compartments in the endocytic pathway (unpublished data). GFP-M6, GFP-M6(T406A) and GFP-M6(T406E) were expressed at similar levels in transiently transfected ARP-19 cells (Figure 2.3). The T406 alterations did not dramatically disrupt function as both constructs did not delay proper trafficking of transferrin to the early endosome (Figure 2.4).

Motility of GFP-M6(T406E) and GFP-M6(T406A) associated vesicles

Changing the phosphorylation state of threonine 406 was hypothesized to result in an effect on the motor properties of myosin VI. We analyzed the motility of

GFP-M6(T406A) and GFP-M6(T406E) associated vesicles using time lapse video microscopy (Figure 2.5). Tracking the fate of individual vesicles present in GFP-M6(T406A)-expressing cells (Figure 2.5A; movie 1-Figure 2.12) revealed a pattern similar to that observed in cells expressing wild type GFP-M6 . Vesicles moved from exterior regions towards the interior before disappearing upon endosome fusion. This transport pattern was also observed for vesicles associated with GFP-M6(T406E) (Figure 2.5B panel b; movie 2-Figure 2.12). Analysis of 100 vesicles for each construct revealed that maximal velocity was similar to that observed for GFP-tagged wildtype myosin VI (38.4 ± 16.6 nm/s; with the average at 45.7 ± 24.1 nm/s for GFP-M6(T406A)-associated vesicles, and 37.5 ± 21.6 nm/s for GFP-M6(T406E)-associated vesicles (Figure 2.5C). Therefore, *in vivo* the motor activity of myosin VI is intact regardless of phosphorylation state.

Surprisingly, at later times a subset of GFP-M6(T406E)-associated vesicles followed an alternate route through the peripheral actin cytoskeleton. Instead of moving inwards, the vesicles moved laterally at the cell periphery and aggregated into clusters at distinct sites (Figure 2.1B; Figure 2.5B, panels c-e; movies 3-Figure 2.12). 37% of GFP-M6(T406E) expressing cells exhibited this vesicle clustering phenotype by 24 hours after transfection (Figure 2.1C) with the percentage of cells exhibiting this phenotype increasing to near 60% at later times after transfection (unpublished data). This phenotype was not prevalent in control transfected cells or in cells expressing GFP-M6(T406A) (Figure 2.1C).

Analysis of the tracks taken by individual GFP-M6(T406E)-associated vesicles suggested that these vesicles were capable of exiting the actin meshwork and reaching the early endosomes at early times before significant cluster formation (Figure 2.5B, panels b, d). However at later times, essentially all peripheral vesicles in the region of the clusters trafficked towards the cluster rather than towards the cell interior (Figure 2.5B, panels c, e). This change in path did not reflect a change in velocity; there was no statistically significant difference in average velocity between vesicles that trafficked inwards and those that trafficked into clusters (Figure 2.5D).

Effect of M6-T406E on the actin cytoskeleton

As GFP-M6(T406E)-associated vesicles exhibited a change in path we investigated whether the underlying actin cytoskeleton was altered. Rhodamine-phalloidin staining revealed that the actin cytoskeleton was dramatically increased in density at the position of the vesicle clusters (Figure 2.1B). Interestingly, the density of actin in the region of the clusters appeared to increase over time; newly formed clusters with fewer vesicles (arrowheads in Figure 2.1B) had less dense F-actin filaments in the area when compared to more mature clusters comprised of greater numbers of vesicles (arrows in Figure 2.1B).

A number of possible mechanisms that could cause an increase in actin filament number were explored. First we asked if the actin rearrangements were due to the redistribution of the actin polymerization machinery. In *Drosophila*, myosin VI

modulates actin dynamics during spermatogenesis by promoting the localization of the Arp2/3 complex, an actin nucleator (Rogat and Miller 2002). We stained for Arp3 in GFP-M6(T406E) expressing cells. Arp3 did not colocalize with the actin enrichments or GFP-M6(T406E)-associated vesicle clusters (Figure 2.6A), indicating that the change in the actin cytoskeleton seen here was not due to recruitment of the actin polymerization machinery to the vesicle surface.

Next we asked if the increase in actin filament density was due to the recruitment of actin cross-linking agents or an increase in myosin VI cross-linking activity. GIPC/synectin, the myosin VI adaptor protein which associated with myosin VI on UCVs, has been shown to bind α -actinin by yeast two hybrid (Bunn et al, 1999). As α -actinin is a potent actin filament cross-linker we investigated whether this protein could be stabilizing filaments in the regions containing myosin VI-associated vesicle clusters. Staining for α -actinin revealed that it was excluded from the actin-dense vesicle cluster sites (Figure 2.6B), however, eliminating this possibility.

Over-expression of proteins that bind to the sides of actin filaments, such as villin and espin, can lead to stabilization of polarized actin filament bundles. In addition, myosin-II in vitro can decorate filaments and inhibit their depolymerization . To test whether GFP-M6(T406E) was exhibiting a similar activity, we expressed it in Caco-2 cells, a polarized intestinal epithelial cell line with abundant apical microvilli. Expression of a GFP-tagged espin in Caco-2 cells resulted in a significant lengthening of the apical actin bundles as judged by phalloidin staining (Figure 2.6C). This result

is similar to that observed when espin was overexpressed in the renal epithelial cell line, LLC-PK (Loomis, Zheng et al. 2003). Expression of GFP-M6(T406E) in Caco-2 cells, in contrast, had no effect on microvillar length (Figure 2.6C). Identical results were observed when Caco-2 cells were grown on coverslips or on filters and in both semi-differentiated cells (as shown in Figure 2.6C) or cells fully differentiated after 10 days in culture. Expression of GFP-M6(T406A) also had no effect.

To eliminate the possibility that alternative splicing of the tail domain might play a role in targeting myosin VI to the appropriate cargo in Caco-2 cells, GFP-M6+LI(T406E) containing the large tail splice insert was also assayed. Inclusion of the spliced domain also did not have any effect on microvillar length (data not shown). Therefore modification at T406 is not simply producing a myosin that is stabilizing filaments by binding non-specifically to F-actin.

Since myosin VI is working as a minus end directed motor in our *in vivo* assay, we theorized that if it was binding tightly at the minus ends, this could be a mechanism to stabilize filaments if binding inhibited depolymerization of these normally dynamic filaments.

If the minus ends were tightly bound by myosin VI, then these filaments should be resistant to cytochalasin D, a drug that depolymerizes actin by capping the plus end. Titration studies confirmed that after 5 minutes of treatment with 50 μ m cytochalasin D, F-actin was effectively depolymerized in cells expressing wild type GFP-M6 (Figure 2.7A). In GFP-M6(T406E)-expressing cells, however, actin

filaments associated with the vesicle clusters were found to be resistant to depolymerization (Figure 2.7B).

To test whether GFP-M6(T406E) was tethering at actin filaments minus ends we used fluorescently conjugated DNase I, which binds to G-actin and the minus end of F-actin. To specifically visualize the minus ends, G-actin was removed by permeabilization of live cells in the presence of an F-actin stabilization buffer (see Materials and Methods). As an internal control for extraction, cells were co-transfected with CFP, a protein of a similar size to G-actin. CFP was efficiently extracted from transfected cells (Figure 2.8A), as was the soluble GFP-tagged myosin, however the vesicle-associated myosin remained in place. Only cells where CFP was fully extracted were utilized for further analysis. As expected, extraction of cells did not disrupt the actin cytoskeleton (Figure 2.8B).

The DNase I staining pattern, when compared to the F-actin pattern, revealed that actin filaments are not organized with a consistent polarity in ARPE-19 cells (Figure 2.8C, panel b,c). The presence of dense filaments did not result in the uniform binding of DNase I to that region. Instead, DNase I staining was consistently seen as a punctuate pattern throughout the cytoplasm in cells not expressing GFP-M6(T406E). In cells expressing this construct, however, DNase I bound to filament ends found preferentially at the sites of GFP-M6(T406E)-associated vesicle clusters (Figure 2.6C, panel a). This was not due to nonspecific sticking of DNase I to UCVs, as vesicles present in GFP-M6 expressing cells did not retain bound DNase I (Figure 2.8C, panel

b). The DNase I staining was also evident in the occasional ruffle present in the ARPE-19 cells, where UCVs were not present (Figure 2.8C, panel b). Taken together these data suggests that F-actin binding of cargo-bound GFP-M6(T406E) inhibits depolymerization from the minus ends producing stabilized filaments. Add: minus ends were accessible indicating myosin VI was not altering actin dynamics by binding to the minus end of actin.

Is myosin VI phosphorylated at threonine 406

Thus far we have shown that mimicking phosphorylation at T406 in myosin VI causes myosin VI to stabilize actin filaments in a manner suggesting myosin VI is now acting as an anchor. However, we have not determined whether this behavior is reflective of myosin VI T406 phosphorylation *in vivo*. One tool available to us was a pre-existing antibody to myosin VI directly generated to the phosphorylated version of threonine 406 of myosin VI (Anti M6PhosphoT406) (Yoshimura, Homma et al. 2001). Having no access to positive controls for this antibody, this antibody had to be used in a model system where we suspected myosin VI to phosphorylated at T406. Myosin VI functions to transport uncoated endocytic vesicles in ARPE-19 cells. In this capacity endogenous myosin VI is not required to function as an anchor or tension provider between the membrane and cytoskeletal elements. We thus predicted that myosin VI would not be phosphorylated in our system. However it has been hypothesized that in inner ear hair cells, myosin VI provides a tension sensing role that would result in the proper anchoring of stereocilia into the actin rich cuticular plate of inner ear hair cells.

In chick cochlea it was found that myosin VI is phosphorylated at the motor domain, but it wasn't determined on which amino acid (Aschenbrenner 2004). This model system was currently unavailable to us.

A similar system is kidney proximal tubule epithelial cells. Myosin VI is highly concentrated at the base of microvilli in these cells, and myosin VI could have a potential role in anchoring these microvilli. Since the antibody to the phosphorylated version of myosin VI was raised in rabbits, we could not utilize our rabbit- anti myosin VI antibody to double stain kidney proximal tubules. Instead we utilized antibody to the motor domain of myosin VI generated in mouse (Aschenbrenner, Lee et al. 2003) which had an identical staining pattern to the rabbit anti myosin VI (data not shown). The myosin VI antibody stained the region under the actin rich microvilli in kidney sections (Figure 2.9A). Included in our cryosection of proximal microtubules were contaminants in the form of the distal microtubules, as the nephron proceeds from the proximal to the distal tubule. Distal microtubules stained for actin and myosin VI show that neither is concentrated in the apical region of the distal tubule cells (Figure 2.9B). Anti M6PhosphoT406, on the other hand, did not recognize a concentration of myosin VI at the base of the microvilli (closed arrows Figure 2.9C).

This would indicate that myosin VI was not concentrated in kidney, however, the antibody did recognize the apical region of distal microtubules (open arrows Figure 2.9C). This would indicate that the antibody is not specific to myosin VI. In addition, in ARPE-19 cells, the mouse motor myosin VI antibody recognized the same

vesicles as the anti tail myosin VI antibody. The M6phosphoT406 antibody on the other hand recognized entirely different vesicles than the anti motor myosin VI antibody (Data not shown). Finally, in western blots, the antibody recognized many nonspecific bands, none of which were myosin VI, so it was decided not to utilize this antibody for further experimentation.

Is PAK upstream of myosin VI

We turned, then, to circuitous methods of determining whether myosin VI was regulated by phosphorylation. It has been hypothesized that PAK is the kinase *in vivo* for the myosin VI motor. We hypothesized that expression of activated PAK would result in the phosphorylation of myosin VI at T406 in our model system. The readout for this putative phosphorylation would be that expressed GFP-M6 activated by PAK would exhibit the same phenotype as GFP-M6(T406E) in ARPE-19 cells. Co-expression of deactivated PAK and GFP-M6(T406E) should have no effect if PAK were the upstream signal for myosin VI phosphorylation.

In order to determine if PAK operated upstream of myosin VI, we co-expressed the constitutively activated PAK(Pak-T423E) and our GFP tagged myosin VI construct. If the clustering phenotype were due to direct or indirect PAK mediated phosphorylation at threonine 406, we would expect to visualize a clustering of GFP-M6-associated vesicles similar in formation as that of GFP-M6(T406E).

We first needed to detect exogenous PAK expression utilizing anti myc antibodies, however utilizing a panel of anti-myc antibodies did not allow us to detect any difference between transfected and untransfected cells, even when the permeabilization conditions and fixing conditions were titrated for ARPE-19 cells. We then utilized an antibody to PAK1, which made it clear which cells were over-expressing the PAK constructs beyond endogenous background levels. These cells corresponded to those also expressing GFP-M6, as in general cells expressing one construct express the other when co-expressing. Expression of constitutively active PAK resulted in PAK targeting to focal adhesions and ruffling membrane (Figure 2.10A). However PAK expression was not accompanied by a change in GFP-M6 expression pattern to that closer to a GFP-M6(T406E) pattern (Figure 2.10B), a result corroborated by viewing over 50 cells. Thus PAK mediated phosphorylation does not result in a GFP-M6(T406E) like phenotype.

Effect of C442Y on T406E phenotype

We finally turned to an approach that would help us relate the effect of putative phosphorylation at T406 to a physiological effect *in vivo*, such as one that would cause damage to the proper anchoring of stereocilia. The missense C442Y mutation in myosin VI has been identified as a point mutation in humans responsible for dominant negative deafness (Melchionda, Ahituv et al. 2001). GFP-M6(C442Y) when expressed in ARPE-19 cells exhibits the same clustering of GFP-M6-associated

vesicles as GFP-M6(T406E). Given the proximity of myosin VI C442 and myosin VI T406 and the potential for interaction between their adjacent domains (see Discussion) it is possible that an alteration at C442Y affects T406 in such a way as to allow phosphorylation to occur at that site. The effect of both mutations would have the net result of modifying the interaction with phosphate release following actin binding. This would give C442Y the same phenotype as T406. It is also possible that alterations at both those sites result in the same cumulative phenotype due to new domain interactions. In order to investigate these possibilities we constructed GFP-M6(C442Y)-(T406E) and GFP-M6(C442Y)-(T406A).

We expected that GFP-M6(C442Y)-(T406A) would not exhibit clusters if the C442Y phenotype was due to hyperphosphorylation at T406. GFP-M6(C442Y)-(T406A) still exhibited clustering (Figure 2.11). However, a larger number of cells expressing GFP-M6(C442Y)-(T406E) exhibited clustering than GFP-M6(C442Y) alone or GFP-M6(T406E) alone, indicating that effect of alterations at C442 and T406 is additive and most likely due to the same change in myosin VI interaction with the nucleotide or motor domain.

DISCUSSION

Altering the motor domain of myosin VI at threonine 406 to glutamate produces a myosin with an altered functionality. While GFP-M6(T406E) still targets to uncoated endocytic vesicles and transports them at wildtype velocities, their route is changed. Instead of trafficking towards the center of the cell to the early endosome, a subset of GFP-M6(T406E)-associated vesicles move laterally and accumulate at fixed peripheral sites. As the T406E alteration is a mimic of phosphorylation at T406 (Wang, Wang et al. 1998); (Yamashita and May 1998);(Liu, Osheroov et al. 2001), this suggests that phosphorylation at T406 is an *in vivo* mechanism to switch myosin VI between its roles as a motor and a tether. In addition to tethering vesicles, expression of GFP-M6(T406E) also results in actin filament changes. GFP-M6(T406E)-bound filaments are resistant to cytochalasin and are oriented with clustered minus ends. As cytochalasin acts to depolymerize actin by capping the plus end of the actin filament, stabilization of the actin filament in the presence of cytochalasin suggests that myosin VI binds tightly to the minus end of the filament. Myosin VI does not cap the actual end of actin filaments as they remain accessible to DNaseI. Our analysis suggests that binding of cargo-bound GFP-M6(T406E) to the sides of actin inhibits depolymerization from the minus ends, producing stabilized filaments. Therefore myosin VI may serve an additional role as a regulator of actin dynamics.

The movement of GFP-M6-associated vesicles is characteristic of a motor that is only processive over short time periods. Following movement, the vesicle falls off

the filament and exhibits Brownian type motion until movement on the next filament commences (Aschenbrenner, Naccache et al. 2004). This ‘start and stop’ type of motion coupled with the inherent bias of actin filaments with their minus ends oriented inwards allows myosin VI to act transport uncoated vesicles out of cell peripheries (Aschenbrenner, Naccache et al. 2004). It is interesting, therefore, to consider the possibility that the change in path of endocytosed vesicles seen in GFP-M6(T406E)-expressing cells may be the result of a change in motor processivity. When analyzed *in vitro*, the modification T406E increases the amount of time myosin VI remains in the ADP-bound state where tight binding to actin is favored . The linear motion of GFP-M6(T406E)-associated vesicles along the filament suggests that the increased time spent on the filament allows for increased processivity *in vivo*. Further analysis will be required to test whether modification at T406 does indeed increase processivity *in vitro*.

We have already shown that myosin VI-associated UCVs can fuse to each other before reaching the early endosomes (Aschenbrenner, Naccache et al. 2004). Fusion would create vesicles that would present increased load to the myosin VI motor, a situation which has been shown to increase the tethering capabilities of this myosin . Because so many vesicles are present at the filament minus ends in GFP-M6(T406E)-expressing cells, fusion events between UCVs may occur, further increasing myosin VI’s affinity for F-actin at these sites. Our studies suggest that if there is fusion, it is not extensive, however. When GFP-M6(T406E)-expressing cells

with clusters are allowed to endocytose R-Tsfn, it is delivered to the edges of the vesicle clusters (data not shown) and does not fully penetrate the interior indicating that all vesicles in the cluster are not fused. However these peripheral fusion events may be sufficient to increase load, thereby increasing the tethering capabilities of myosin VI at these sites.

The clustering of actin filament minus ends seen during GFP-M6(T406E) expression is a unique phenomena that may reflect polarity sorting of filaments by myosin VI. Polarity sorting of actin has only been observed *in vitro* under conditions of very high concentration of a double-headed plus-end directed myosin and in these cases the plus ends were grouped together. It is possible that vesicle clustering produces high local concentrations of myosin VI sufficient to induce polarity sorting such that the minus-ends are further brought together.

Actin-based motility is at the heart of myosin VI's function in trafficking of receptors and uncoated vesicles across the peripheral actin cytoskeleton in cultured epithelial cells (Aschenbrenner, Naccache et al. 2004) (Aschenbrenner, Lee et al. 2003) (Swiatecka-Urban, Boyd et al. 2004) and movement of components down proximal tubule microvilli. (Yang, Maunsbach et al. 2005). In other examples, however, actin based motility does not fully explain the role of myosin VI nor the phenotype resulting from its loss. Genetic studies suggest Myosin VI is required for tethering and/or positioning of organelles during *Drosophila* neuroblast cell division and ovary border cell migration , and as a part of Golgi positioning in mouse

fibroblasts (Warner, Stewart et al. 2003). Most recently, it was shown that during *Drosophila* spermatogenesis, myosin VI binds the actin rich growth cone instrumental in spermatid individualization through the motor domain, and remains stalled on actin for minutes (Noguchi, Lenartowska et al. 2006). Therefore, depending on the system of study, myosin VI has been implicated as either a motor or a tether. In agreement with these roles for myosin VI, our results indicate that myosin VI *in vivo* can be made to act as a tether to the minus end of actin filaments if modified to mimic phosphorylation at T406.

Threonine 406 is found in the cardiomyopathy loop of myosin VI, which is important for actin binding. The Switch II loop is domain of the myosin motor that mediates a direct effect on the ATP binding pocket. A long conserved alpha helix embedded in the myosin 50 kD subdomain connects the cardiomyopathy loop and the Switch II loop. The missense mutation C442Y is putatively at the end of this conserved alpha helix, and is responsible for dominant deafness in humans (Melchionda, Ahituv et al. 2001). Threonine 406 and Cysteine 442 are in interacting domains according to the solved crystal structure of myosin VI, and the mechanisms mediating the effect of the C442Y mutation might be linked to that of T406 phosphorylation, as shown by our results that the C442Y and T406E mutations are additive.

We have not been able to establish whether myosin VI is phosphorylated at T406 *in vivo*. PAK kinase homologs are thought to mediate the phosphorylation of the

TEDs site in ameboid myosin I , (Barylko, Binns et al. 2000) (Lee, Egelhoff et al. 1996), (Brzeska, Young et al. 1999). This suggests that PAK may regulate phosphorylation at the TEDs site in myosin VI as well. In addition, PAK1 kinase is downstream from the small G proteins Rac, Rho, and Cdc42, which are known to rearrange and control the structure of the actin cytoskeleton (Tapon and Hall 1997). Baculovirus expressed myosin VI can be phosphorylated by PAK3 (Yoshimura, Homma et al. 2001), and PAK1 (Buss, Arden et al. 2001) *in vitro*. *In vivo*, however myosin VI was observed to be phosphorylated at the head domain upon EGF stimulation in the epidermoid cell line A431(Buss, Kendrick-Jones et al. 1998), but it is not known at what site. In other cell systems, myosin VI is phosphorylated *in vivo* in LLCPK cells (Aschenbrenner 2004), but only on serine residues, precluding phosphorylation at T406. In chick cochlea, however, myosin VI was phosphorylated on threonine residues, although it was technically impossible to establish which threonines they were (Aschenbrenner 2004). PAK expression increased coincidentally with developmental increases in threonine phosphorylation. Yoshimura et al 2001 have used a myosin VI threonine 406 phospho specific antibody to detect phosphorylation at T406 due to PAK3. We initiated a detailed analysis of this antibody and, unfortunately, found no evidence that this antibody actually recognizes myosin VI isolated from tissues or cell lines as judged by western blot and immunocytochemistry. Thus far we have been unable to identify myosin VI phosphorylated at T406 *in vivo*. It will be interesting to determine whether

phosphorylated myosin VI is present in systems where the myosin is predicted to serve a tethering role such as myosin VI associated with the Golgi, in the inner ear, or during *Drosophila* spermatogenesis.

In sum, our data support the hypothesis that modification of T406 by mimicking phosphorylation produces a myosin VI molecule primed to act as a tether. Once bound to cargo and under load, phosphorylated myosin VI would be sufficient to inhibit further depolymerization of that filament, leading to filament stabilization. Therefore, the tethering function of myosin VI is also consistent with a role for myosin VI as a regulator of F-actin dynamics. This is supported by the EM analyses of inner ear phenotypes seen in myosin VI knockout mice, which suggest that myosin VI is required for regulated F-actin assembly in sensory hair cells, and in *Drosophila* spermatogenesis where myosin VI knockouts do not exhibit the same actin density at growth cones as wild-type.

ACKNOWLEDGEMENTS

The text of Chapter two is in part derived from Naccache and Hasson, in press at Cell Motility and the Cytoskeleton. I was the only researcher on this project. Dr. Arie Horowitz is acknowledged for providing fixed kidney. Dr. Gary Bokosh is acknowledged for providing PAK constructs. Dr. Colin Jamora as well as Pedro Lee and Luke Denly are acknowledged for providing lab space for continuing this project, as well as excellent technical and moral support, and the use of their cryostat. Dr. Mitsuo Ikebe is acknowledged for providing the phosphoT406 M6 antibody. Jeff Keil is acknowledged for providing gradient gels.

FIGURES

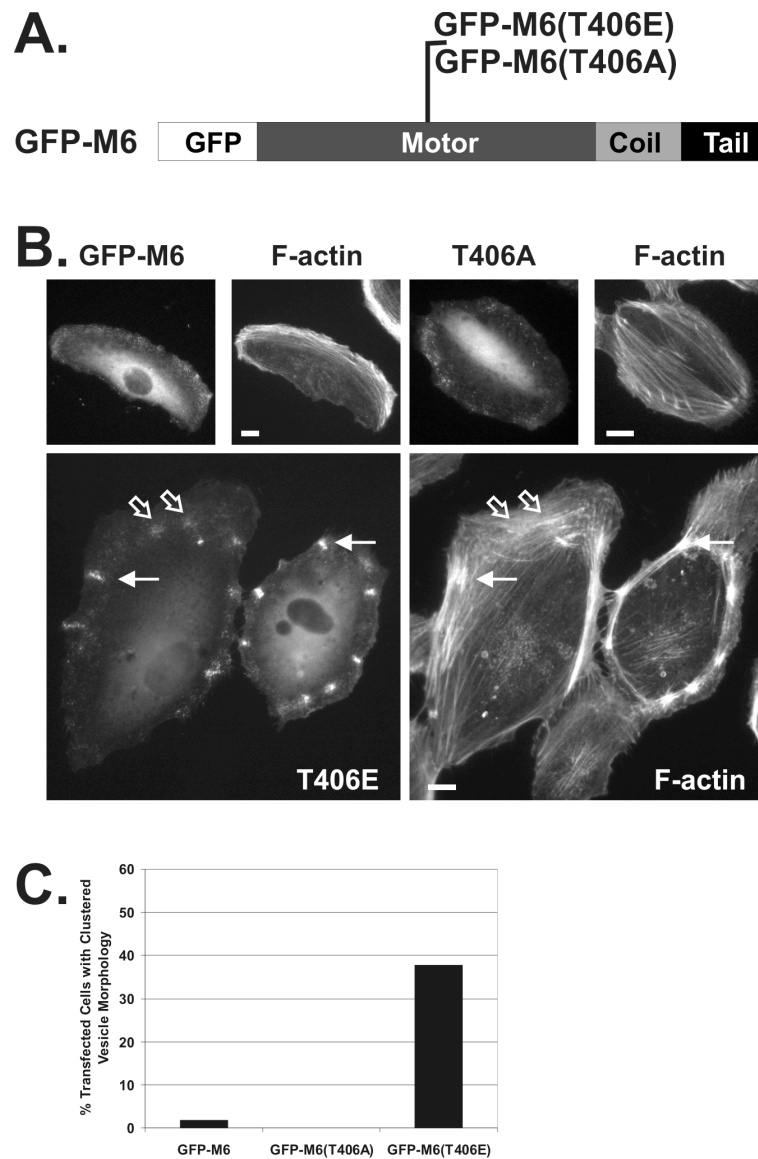


Figure 2.1. GFP tagged constructs mimicking myosin VI in the dephosphorylated (GFP-M6(T406A)) or phosphorylated (GFP-M6(T406E)) states localize to peripheral UCVs. (A) Schematic of the GFP-M6 constructs used in this study. (B) ARPE-19 cells transfected with the GFP fusion constructs counterstained for F-actin with rhodamine-conjugated phalloidin. Open arrows: vesicle clusters lacking dense actin accumulations. Closed arrows: vesicle clusters that correlate with dense F-actin. (C) Histogram depicting the percentage of cells expressing GFP-M6, GFP-M6(T406A) or GFP-M6(T406E) that demonstrate a vesicle clustering phenotype 24 hours after transfection. Scale bars = 10 μ m.

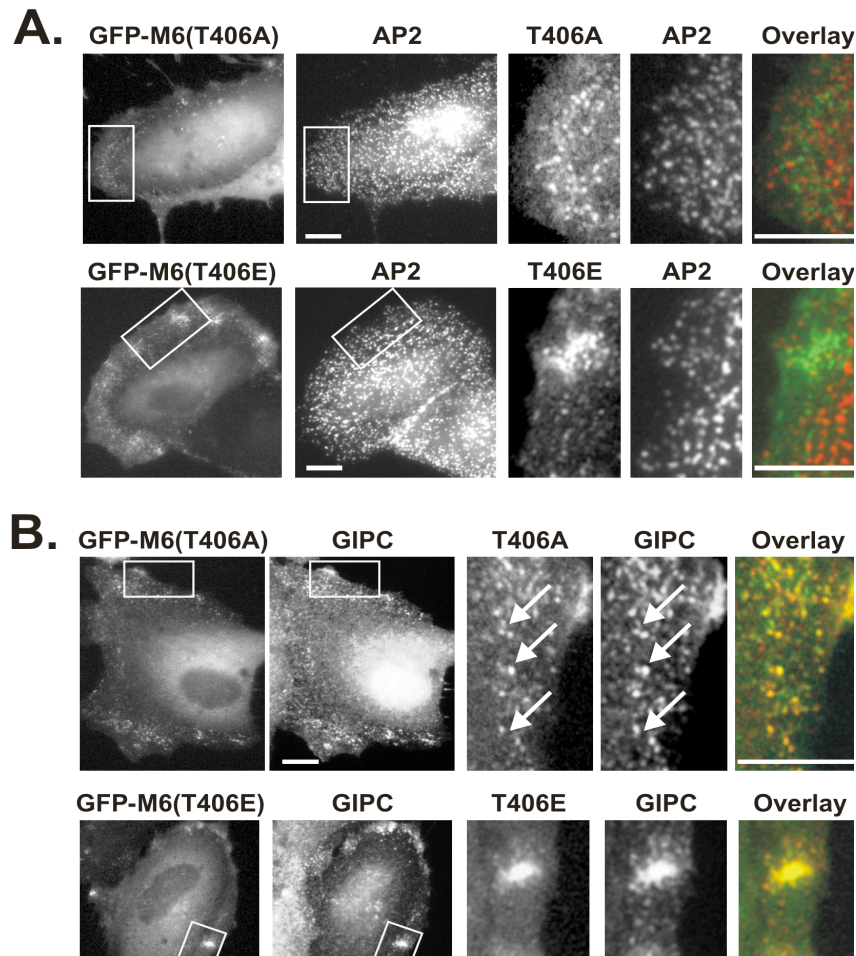


Figure 2.2. Indirect immunofluorescence of ARPE-19 cells expressing GFP-M6(T406A) or GFP-M6(T406E) reveals that they both target to UCVs. The boxed area in the left hand panels is enlarged in the right hand panels. The GFP construct is presented in green in the overlays. (A) Staining for the clathrin adaptor AP-2 (red), a marker for clathrin coated vesicles and pits. Staining reveals no significant overlap (<2%). (B) Staining for GIPC/synectin, a marker for UCVs (Dance *et al.*, 2004). Essentially all GFP-M6-associated vesicles stain positively for GIPC/synectin. Examples of overlap between the GFP-M6 constructs and GIPC/synectin is indicated by arrows. Scale bars = 10 μ m.

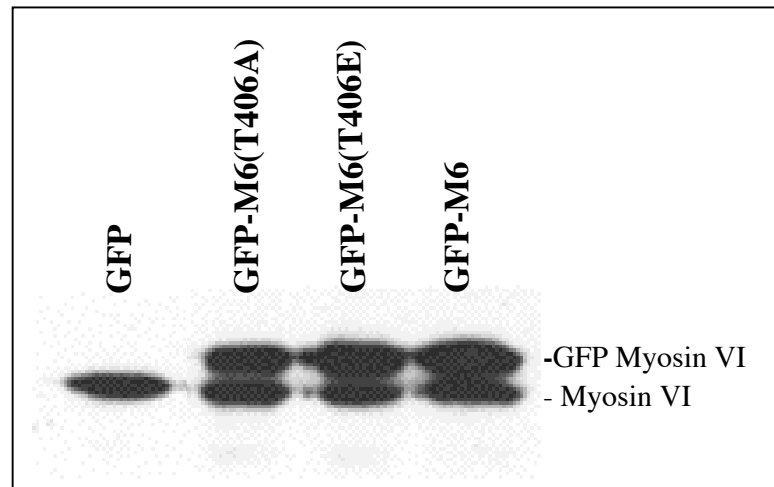


Figure 2.3. Expression levels of GFP-M6, GFP-M6(T406A) and GFP-M6(T406E) are equivalent. Myosin VI immunoblot of ARPE-19 cell lysates transfected with GFP-M6, GFP-M6(T406A) and GFP-M6(T406E).

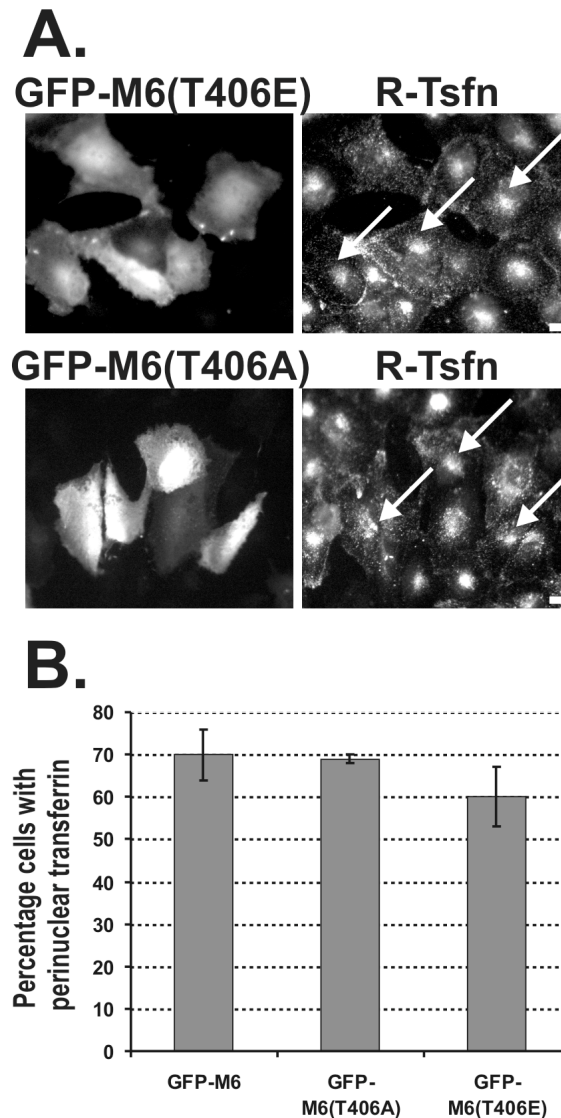
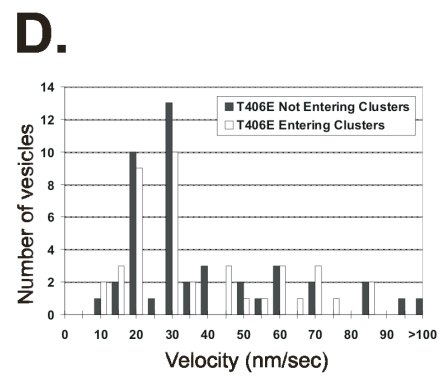
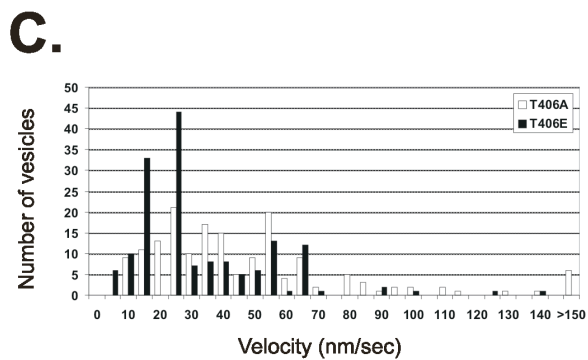
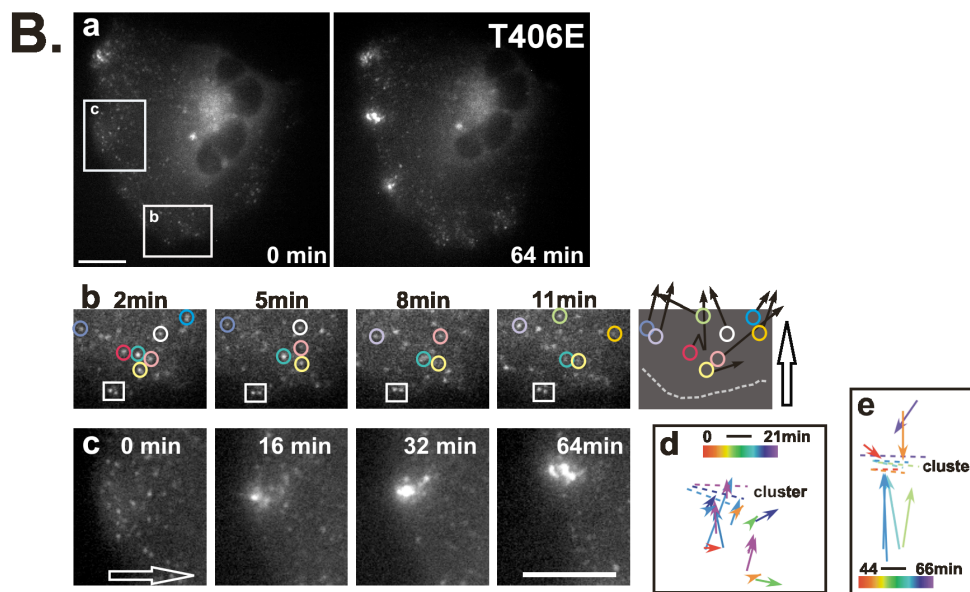
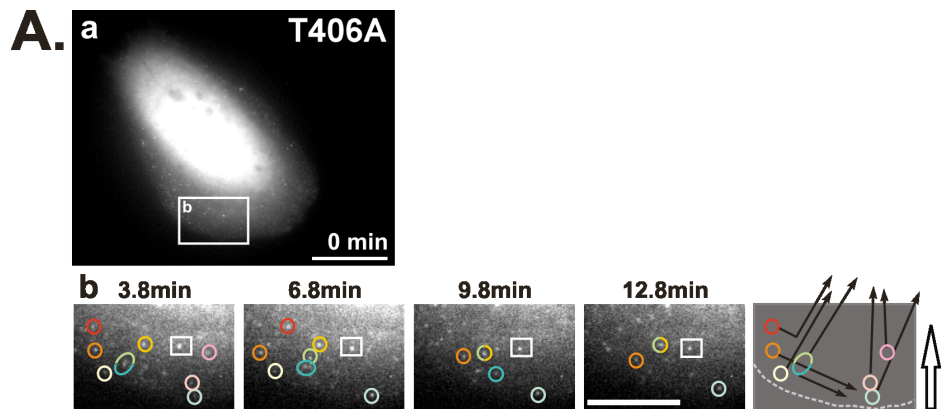


Figure 2.4. Over-expression of GFP-M6(T406A) and GFP-M6(T406E) does not delay the trafficking of transferrin to the early endosome. (A) ARPE-19 cells transfected with GFP-M6, GFP-M6(T406A) or GFP-M6(T406E) were incubated with R-Tsfn at 37°C for 15 minutes, a timepoint at which GFP-tagged myosin VI mutants block transferrin trafficking (Aschenbrenner *et al.*, 2003; Aschenbrenner *et al.*, 2004). Transfected cells that do not exhibit pericentriolar staining are indicated by open arrows, whereas cells exhibiting pericentriolar staining are indicated by closed arrows. Scale bars= 10 μ m. (B) Histogram quantifying the percentage of transfected cells (n=300) in which transferrin reached the pericentriolar region. Standard deviation represents the average of three experiments.

Figure 2.5. Movement of GFP-M6(T406A)- and GFP-M6(T406E)-associated vesicles. ARPE-19 cells expressing GFP-M6(T406A) or GFP-M6(T406E) were analyzed by time-lapse video microscopy. (A) corresponds to timelapse movie 1 for GFP-M6(T406A)-associated vesicles. (B) corresponds to timelapse movies 2 (low mag) and 3 (higher mag) of GFP-M6(T406E)-associated vesicles. The boxed area(s) in panel (a) for (A) and (B) are enlarged in (b) or (c) as labeled. The relative timing of each image is shown in minutes. In panel (b) for (A) and (B) individual vesicles are outlined to allow tracking between panels. The cell edge is towards the bottom for A(b) and B(b), and towards the left for panel B(c) and in some panels is depicted as a dotted line. Net direction of movement necessary to achieve delivery to the early endosomes is shown with an open arrow. The right panels in A(b) and B(b) are a schematic showing the overall movement of circled vesicles, with the direction of movement depicted as an arrow. Note that the vesicles track in a direction consistent with delivery to the early endosomes. B(c) presents an example of the formation of a GFP-M6(T406E)-associated vesicle cluster. Note that the cluster itself moves over time. B(d,e) depicts the movement of a representative subset of distinct GFP-M6(T406E)-associated vesicles in the region of the vesicle cluster shown in B(c). Each vesicle is represented by a displacement vector (arrow) which shows the position of the vesicle, the direction traveled, and the distance covered over the vesicle's lifetime, in some cases culminating with entry into the cluster. B(d) presents the vesicles that appear early in the timelapse movie and reach their destination (either the early endosomes or the cluster) within the first 21 minutes of the movie, with destination time reflected in the coloring of the arrow. Dotted lines represent the position of the cluster over time, which appears approximately 11 minutes into the movie. Panel (e) presents vesicles that appear late in the timelapse movie, and that reach their destination within 44-66 minutes after initiation of the timelapse. At this time, essentially all vesicles enter the clusters. Scale bars = 10 μm . (C, D) Histograms of maximal instantaneous velocities of GFP-associated vesicles in nm/s. (C) Vesicles were tracked in cells expressing GFP-M6(T406A) (white bars) or GFP-M6(T406E) (black bars). n=160. (D) A comparison of the maximal velocity of 40 vesicles that trafficked into the cell interior (T406E Not Entering Clusters; black bars) to those that trafficked into vesicle clusters (T406E Entering Clusters; white bars).



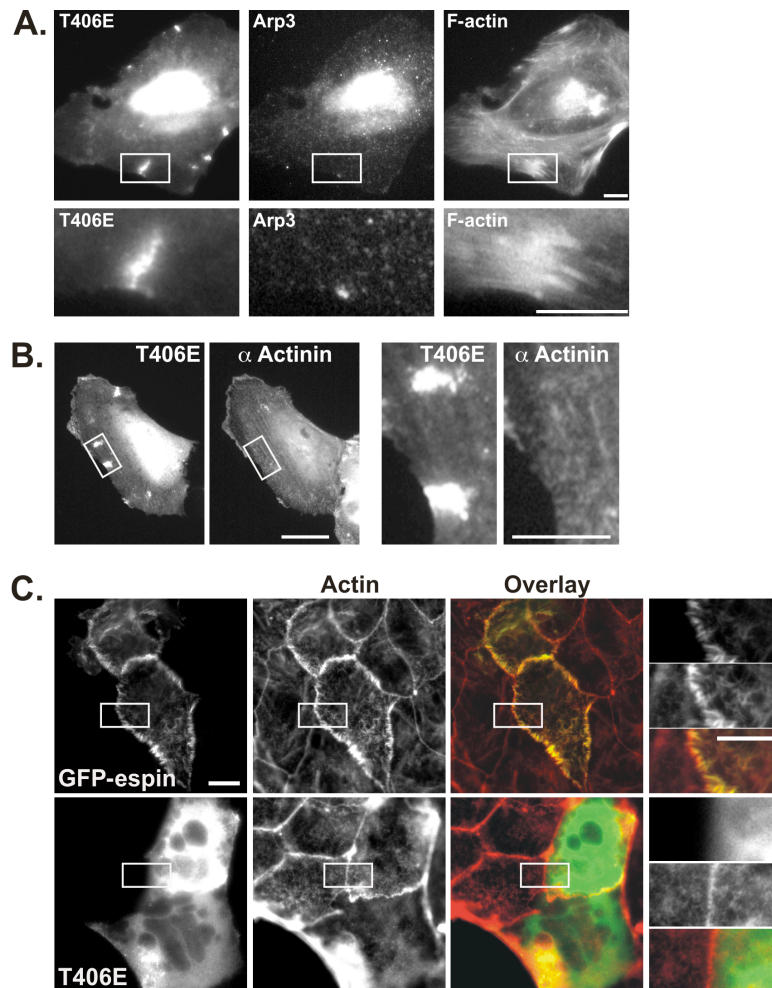


Figure 2.6. Actin rearrangements are not due to recruitment of actin polymerizing agents or actin crosslinking. (A) ARPE-19 cells expressing GFP-M6(T406E) were stained with antibody to Arp3. Cells exhibit GFP-M6(T406E)-associated clusters which do not colocalize with Arp3. The boxed area in the top panels are enlarged below. (B) Actin rearrangements are not due to recruitment of actin crosslinking agents. ARPE-19 cells expressing GFP-M6(T406E) were stained with antibody to α -actinin. Cells exhibit GFP-M6(T406E)-associated clusters which do not colocalize with α -actinin. The boxed area in the left handed panels are enlarged in the right handed panels. (C) Expression of GFP-espina, but not GFP-M6(T406E), has an effect on microvillar length. Caco-2 cells were transfected with the designated construct and stained for F-actin with rhodamine-phalloidin. Images are of the apical surface. The boxed area is enlarged in the right panels. Scale bars = 10 μ m.

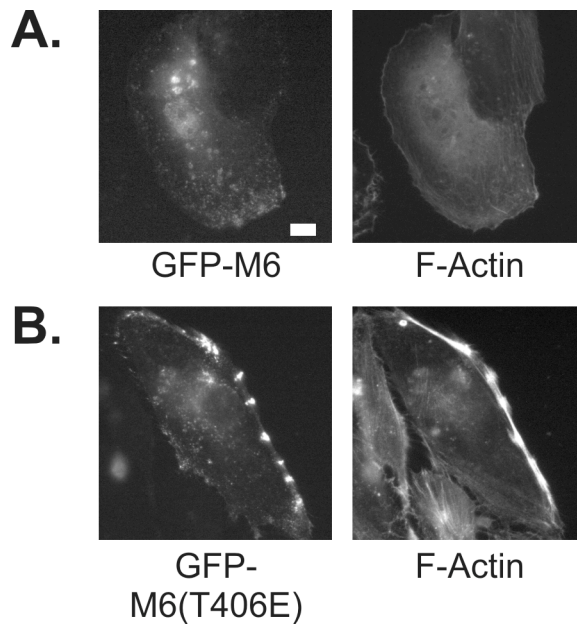
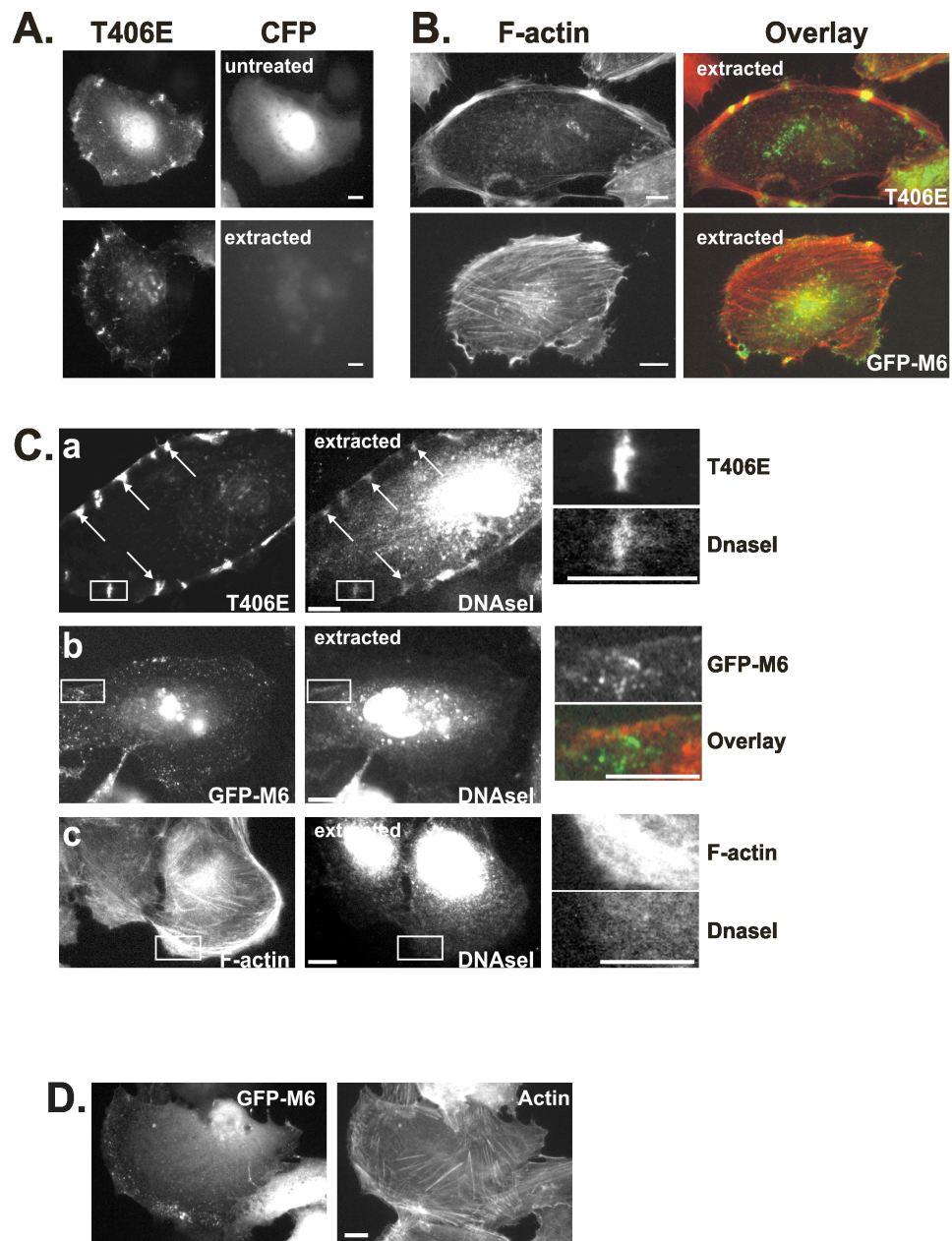


Figure 2.7. Modification at T406 results in changes in actin filament stability as judged by resistance to cytochalasin D. ARPE-19 cells expressing GFP-M6 (A) or GFP-M6(T406E) (B) were treated with 50 μ m cytochalasin D for 5 minutes. Fixed cells were stained with rhodamine-phalloidin to visualize F-actin. Scale bars = 10 μ m.

Figure 2.8. GFP-M6(T406E)-associated vesicles cluster at actin filament minus ends. (A) Extraction control – removal of soluble proteins: ARPE-19 cells co-expressing GFP-M6(T406E) and CFP were 0.05% saponin extracted in the presence of unlabeled phalloidin. (B) Extraction control – stability of the actin cytoskeleton: Cells expressing GFP-M6(T406E) (top) or GFP-M6 (bottom) extracted with 0.05% saponin and unlabeled phalloidin and counterstained with rhodamine- phalloidin to stain for actin. The rightmost panels are an overlay between the GFP and rhodamine channels. The left panel shows the actin cytoskeleton alone. Saponin extraction does not disrupt or significantly alter the actin cytoskeleton of transfected cells. (C) Cells expressing GFP-M6(T406E)(a), GFP-M6(b) or untransfected cells (c) were extracted with 0.05% saponin in the presence of phalloidin to remove G-actin, followed by incubation with rhodamine conjugated DNaseI and Coumarin-phalloidin. Arrows point to site of clusters and DNaseI enrichment. The boxed areas are enlarged in the rightmost panels. Scale bars = 10 μ m.



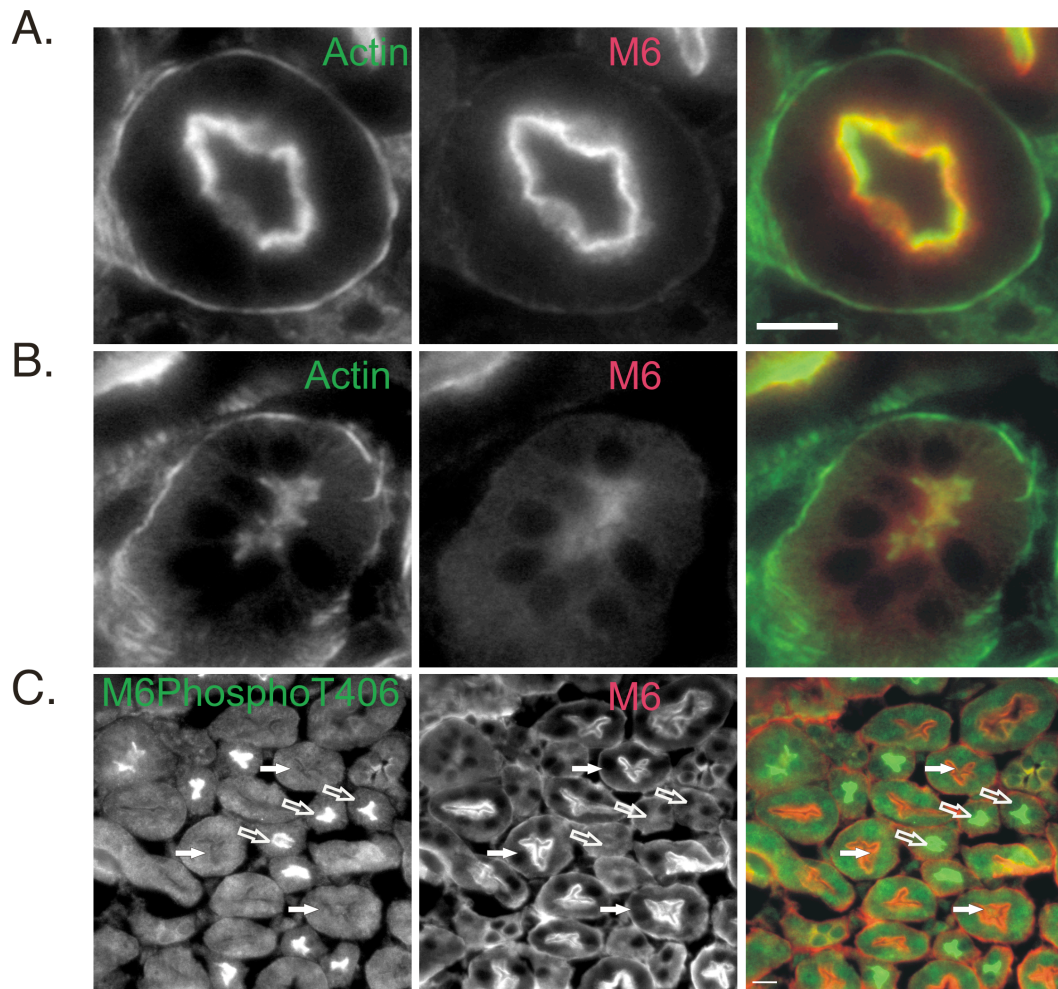


Figure 2.9. Antibody to phosphorylated threonine 406 on myosin VI recognizes distal tubules, not mouse kidney proximal tubules. (A) Mouse antibodies to the motor domain of myosin VI (M6) recognize the base of the kidney proximal tubule microvilli.. (B) Mouse antibodies to the motor domain of myosin VI do not recognize distal tubules. (C) Proximal tubule kidney sections include some distal tubule crosssections. Antibody to motor myosin VI stains for proximal tubules (closed arrows) but not distal tubules (open arrows). AntiM6PhosphoT406 does not recognize proximal tubules but instead it recognized a similar central region in distal tubules. Scale bar = 5 microns.

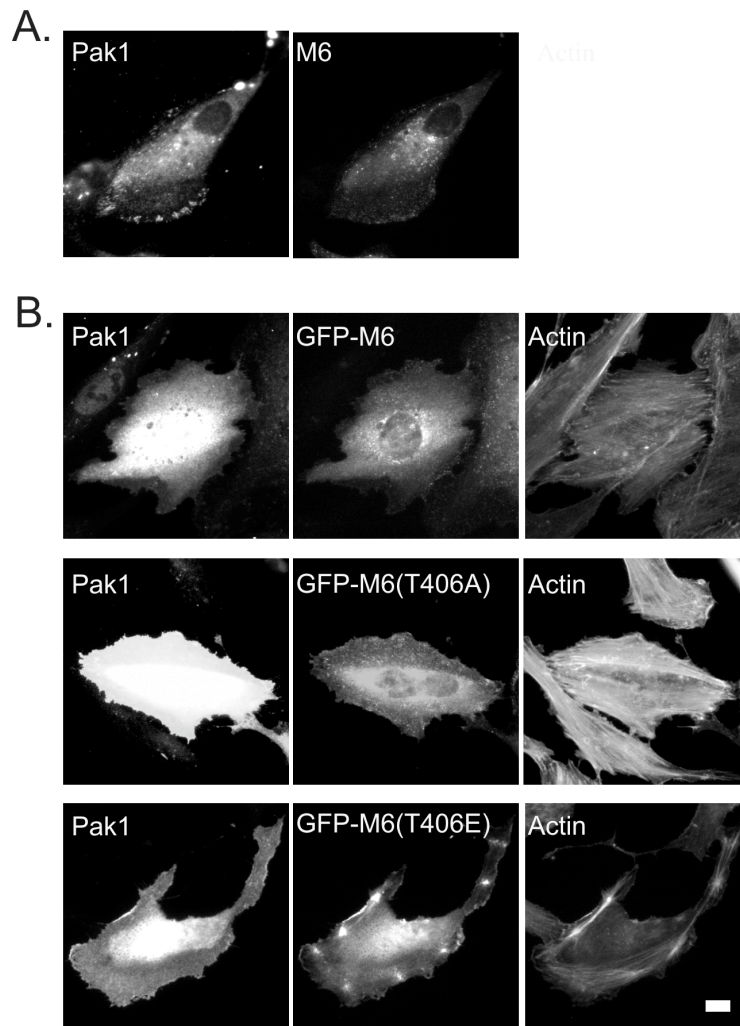
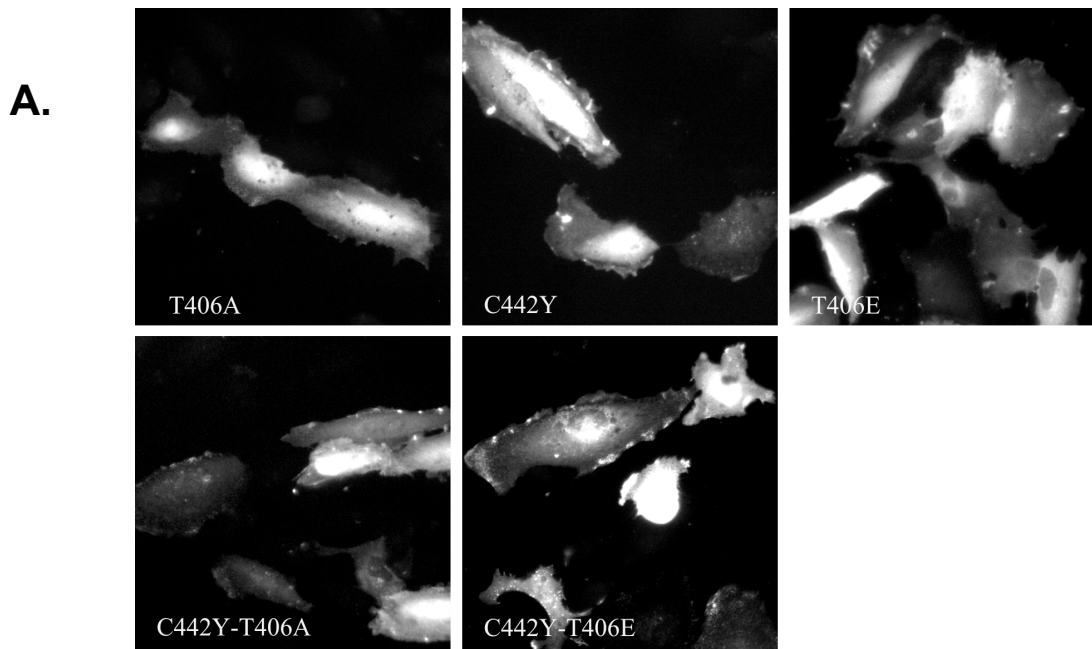


Figure 2.10. Expression of constitutively active hPak1T423E does not induce myosin VI-associated clusters in ARPE-19 cells expressing GFP-M6. (A) Cells were transfected with hPak1T423E and stained utilizing antibody to Pak1 and antibody to myosin VI. A low PAK expressor was chosen to demonstrate PAK targeting to focal adhesions. (B) ARPE19 cells were co-transfected with hPak1T423E and either GFP-M6, GFP-M6(T406A), or GFP-M6(T406E). Cells transfected with hPak1T423E were determined by staining with Pak1, and only cells with intense staining compared to neighboring cells were chosen. Cells were stained for actin utilizing coumarin phalloidin. Scale bar = 10 microns.



B.

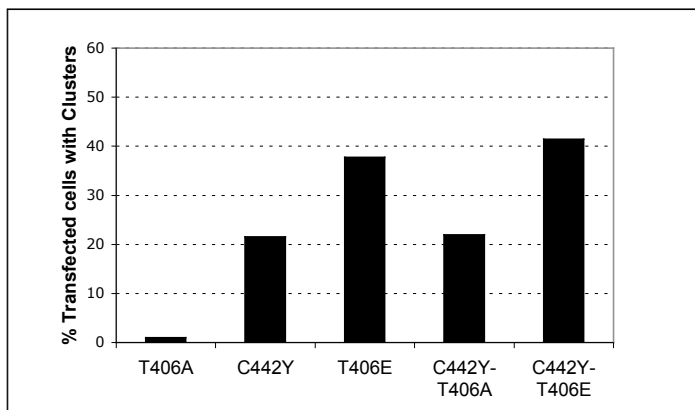


Figure 2.11. Expression of myosin VI constructs altered at T406 and C442. (A) ARPE-19 cells were transfected with GFP-M6(T406A), GFP-M6(C442Y), GFP-M6(T406E), GFP-M6(C442Y-T406A) and GFP-M6(C442Y-T406E). (B) Histogram depicting the percentage of cells transfected with each construct that exhibited the clustering phenotype. Scale bar = 10 microns.

Figure 2.12. Video Materials

Found at both <http://www.interscience.wiley.com/jpages/0886-1544/suppmat> and as supplementary material to this dissertation.

Movie 1 accompanying Figure 2.5A:

Time lapse movie monitoring the motility of GFP-M6(T406A)-associated vesicles in an ARPE-19 cell. This cell was monitored for 60 minutes, and the first 20 minutes are shown here. Images were acquired every 10 seconds. The exposure time was 2 seconds. The movie runs at 20 frames per second.

Movie 2 accompanying Figure 2.5B, parts (a,b):

Time lapse movie monitoring the motility of GFP-M6(T406E)-associated vesicles in an ARPE-19 cell. Focus on the lower right portion of the cell to visualize movement of these vesicles inwards to the early endosomes. This cell was monitored for 66 minutes and the first 60 minutes is shown here. Images were acquired every 10 seconds. The exposure time is 2 seconds. The movie runs at 20 frames per second.

Movie 3 accompanying Figure 2.5B, parts (c,e):

An enlargement of a portion of the cell presented in movie 2. This movie follows the motility of GFP-M6(T406E)-associated vesicles in an ARPE-19 cell as they assemble into a central cluster. Information is as described for movie 2.

CHAPTER THREE: Binding of Internalized receptors to the PDZ domain of GIPC/Synectin recruits myosin VI to endocytic vesicles.

INTRODUCTION

Unconventional myosins are actin-based molecular motors that have been implicated in vesicle and organelle movement (Soldati 2003) (Volkmann, Mori et al. 2003) (Ma, Fey et al. 2001). The motor domain of myosin VI is conserved among myosins and binds to F-actin to convert energy from ATP hydrolysis into directional motion along the actin filament. In contrast, the tail is divergent. It mediates cargo binding and can contain a variety of protein-protein and protein-lipid interaction motifs. Although associations between myosins and their cargoes are tail-specific, the mechanisms that govern the recruitment of myosins to their cargoes have not yet been fully determined.

Myosin V cargo sorting, for example, is mediated by organelle-specific Rab GTPases which reside on the organelle surface and interact with myosin V either directly or via an adapter protein (Wu, Rao et al. 2001; Fukuda, Kuroda et al. 2002; Wu, Wang et al. 2002; Westbroek, Lambert et al. 2003; Boldogh, Ramcharan et al. 2004). In addition, tail phosphorylation has been shown to regulate myosin V release

from cargo (Karcher, Roland et al. 2001). However, the regulation of myosin V recruitment to its cargo is still unknown.

The molecular motor myosin VI is involved in endocytic transport (reviewed in (Hasson 2003; Frank, Noguchi et al. 2004) and is the only actin-based molecular motor that translocates along actin filaments towards the minus end (Wells, Lin et al. 1999). In the cell, actin filaments are predominantly oriented with minus ends pointed inwards, supporting a role for myosin VI in endocytic trafficking. Indeed, the emerging picture is that myosin VI participates in two steps of trafficking as it is recruited to both clathrin-coated pits (CCP) and the ensuing uncoated endocytic vesicles (UCV) (Buss, Arden et al. 2001; Aschenbrenner, Lee et al. 2003; Dance, Miller et al. 2004).

Myosin VI associates with CCP via the adapter protein Dab2 (reviewed in (Hasson 2003). Dab2 binds directly to clathrin, to the clathrin adaptor protein AP-2 (Mishra, Keyel et al. 2002) and to myosin VI (Morris and Cooper 2001; Inoue, Sato et al. 2002). The protein likely involved in UCV recruitment, however, is GIPC (GAIP interacting protein, C terminus) (De Vries, Lou et al. 1998), a single Postsynaptic density 95, Disk large, Zona occludens-1 (PDZ) domain adaptor protein denoted also by several other names, including synectin (Gao, Li et al. 2000). Synectin's (as it will be referred throughout this chapter) central PDZ domain binds type I PDZ-binding motifs (PBMs) conforming to the consensus sequence (S/T)-X-(V/A) (Songyang, Fanning et al. 1997). Synectin is one of the most versatile PDZ proteins known to

date, with upwards of 20 binding partners, most of which are transmembrane receptors or adhesion molecules (e.g., (Cai and Reed 1999; Gao, Li et al. 2000; Blobel, Liu et al. 2001; Lou, Yano et al. 2001; El Mourabit, Poinat et al. 2002).

The Lutropin receptor (Hirakawa, Galet et al. 2003), Cystic Fibrosis Transmembrane Regulator (CFTR) (pers. Comm. B. Stanton), and Dopamine receptors 2 and 3 (Jeanneteau, Diaz et al. 2004) are among the receptors identified as binding partners to synectin. Another known PDZ-ligand of synectin is megalin (Gotthardt, Trommsdorff et al. 2000), a scavenger receptor of the LDL receptor family. Megalin is responsible for the uptake of a plethora of macromolecules (Christensen and Birn 2002) and megalin null mice exhibit easily detectable defects in renal function such as proteinuria (Lehste, Rolinski et al. 1999). Interestingly, the location of megalin at the base of microvilli in mouse proximal tubule kidney cells is very similar to that of myosin VI at the base of the microvilli (Biemesderfer et al 2002, Nagai et al 2005). Combined, these factors make megalin a promising candidate for myosin VI-synectin dependent trafficking through UCVs.

When used as the bait in yeast two-hybrid screens, synectin captured the carboxy-terminal “tail” domain of myosin VI (Bunn, Jensen et al. 1999). Synectin interacts with myosin VI in vivo as the two proteins collocate on UCV and can be coimmunoprecipitated from membrane fractions (Aschenbrenner, Lee et al. 2003). A portion of the carboxy-terminus tail domain of myosin VI is sufficient to associate with UCV (Aschenbrenner, Lee et al. 2003; Dance, Miller et al. 2004). Myosin VI is

mainly found in a cytoplasmic pool, where it is not complexed with synectin or Dab2 (Aschenbrenner, Lee et al. 2003), suggesting that its docking to cargoes is regulated. The docking mechanism remains unknown, however.

We found that myosin VI recruitment to UCV is synectin-dependent. PBM binding to the PDZ domain of synectin facilitates myosin VI binding to a site in the carboxy-terminus of synectin located outside of the PDZ domain. We determined that deletion of the PBM of megalin, a known synectin-binding receptor (Gotthardt, Trommsdorff et al. 2000), impairs synectin and myosin VI recruitment to UCV. Finally we found that synectin-null mice develop proteinuria, a condition consistent with defective megalin trafficking.

MATERIALS and METHODS

Expression constructs

Mouse synectin cDNA (Gao, Li et al. 2000) was subcloned into pEYFP-N1 vector (BD Biosciences) between the XhoI and BamHI sites. Deletion mutants were produced by PCR amplification of the desired fragments and subcloning into pECFP, pEGFP, or pEYFP plasmids (BD Biosciences) as required, using suitable primers (Table 3.2). These plasmids are collectively referred to in the text as visual fluorescent proteins (VFP). The GFP-tagged megalin minireceptor plasmid, pGFP-MegTmT was generously provided by Dr. Maria-Paz Marzolo (Pontificia Universidad Católica de Chile, Santiago, Chile) (Marzolo, Yuseff et al. 2003). Point mutations were introduced in the synectin and megalin constructs with the QuikChange kit (Stratagene) and the primers listed in Table 3.2. Plasmids were transfected into ARPE-19 cells as described (Aschenbrenner, Lee et al. 2003).

The expression levels of the constructs were verified by immunoblotting with an antibody that recognizes all 3 VFP variants GFP-wt-CFTR was generously provided by Dr. Agnieszka Swiatecka-Urban (Dartmouth) (Swiatecka-Urban, Boyd et al. 2004). Myc-Lutropin-wt was kindly provided by Dr. Mario Ascoli (University of Iowa) (Hirakawa, Galet et al. 2003). The dopamine receptor constructs PCDNA3.1/Hygro alpha7GFPD2S and pCEP4alpha7GFPD3 were kindly provided by Dr. Freddy Jenneteau (INSERM, France). Quinpirole (Sigma), a dopamine 2-like

dopamine receptor agonist was utilized at 1mM and 3mM from 1-30 minutes at 37 degrees Celsius.

Antibodies

Rabbit affinity-purified antibody to myosin VI was produced as described (Hasson and Mooseker 1994) and used at 10 $\mu\text{g/ml}$ for immunofluorescence and 1 $\mu\text{g/ml}$ for immunoblotting. Rabbit affinity-purified antibody to synectin was produced as described (Dance, Miller et al. 2004) and used at 1 $\mu\text{g/ml}$ for both immunoblotting and immunofluorescence. Antibody AP.6 to the alpha chain of AP-2 was obtained from Dr. Sandy Schmid (The Scripps Research Institute, La Jolla, CA) and was used at a dilution of 1:200. Mouse monoclonal (20B) and polyclonal anti-megalin were provided by Dr. Daniel Biemesderfer (Yale University). The monoclonal antibody was used at 1:100, and the polyclonal at 1:5000. Antibodies to EEA1 and AP-2 were from BD Biosciences. Antibody to RBP was from Lab Vision. Rhodamine-, Coumarin-, and Alex-647-conjugated phalloidin were from Invitrogen and used at 1:40 to 1:500. Fluorescein isothiocyanate-, rhodamine-, and horseradish peroxidase-conjugated donkey anti-rabbit and donkey anti-mouse antibodies were from Jackson ImmunoResearch Laboratories. All purchased antibodies were used at concentrations recommended by the manufacturer.

Isolation of mouse kidney epithelial cells

Snell's Waltzer mice were obtained from Dr. Sally Camper (University of Michigan). Mice were sacrificed in accordance with NIH guidelines. Kidneys were removed, placed in Hank's buffered saline solution (HBSS) and the cortex was sliced off with a razor. After mincing, tissue fragments were incubated with 1 mg/ml collagenase IV (Invitrogen) in HBSS for 10 min at 37°C with agitation. Following digestion, samples were vortexed for 10 s at full speed and large tissue fragments removed. Cell clusters sedimented by gravity after 5 min incubation at room temperature were collected and plated in collagen IV-coated flasks (BD Biosciences) in DMEM with nonessential amino acids (Sigma) supplemented with 10% fetal bovine serum (Invitrogen), 2.5 µg/ml Fungizone (Invitrogen) and 2 mM L-glutamine (Invitrogen). Cells were plated on glass coverslips coated with 50 mg/ml collagenase IV (BD Biosciences) when used for immunofluorescence experiments.

Fixation of mouse kidneys

WT and synectin-null mice (a gift of M. Simons, generated by disruption of the synectin gene by the gene-trap method) were anesthetized by injection of avertin and perfused through the left ventricle with phosphate buffered saline (PBS), followed by 4% paraformaldehyde (PFA) in PBS. Kidneys were excised and the cortex was cut into ~2×2 mm blocks and fixed in PBS containing 20 mM EGTA and 4% PFA for 5 min. After rinsing in PBS/20 mM EGTA, tissue blocks were quenched in 0.05%

NaBH₄/PBS/EGTA for 10 min and infiltrated with 1 M sucrose/PBS/EGTA for 2 hrs on ice. Tissue blocks were embedded in OCT (Tissue-Tek) and frozen in liquid nitrogen.

Analysis of urine samples

Urine was collected and pooled from 3 WT and 3 synectin-null mice. All mice had the same access to water before collection of urine samples. Urine from WT or synectin-null mice were analyzed by coomassie staining (20 μ l/lane) or by immunoblotting for RBP (10 μ l/lane). Samples were resolved by SDS-PAGE on 12% gel.

Uptake of R-Tfn or R-EGF

Cells were serum-starved for 1-2 hr then chilled on ice for 30 min before incubation with ligand. Pulse-chase rhodamine transferring (R-Tfn) uptake assays were performed as described (Aschenbrenner, Lee et al. 2003) and identical methods were utilized for rhodamine EGF (R-EGF uptake). To surface-label receptors, cells were incubated in serum-free medium on ice for 20 min, then in serum free media containing 50 μ g/ml R-Tfn or 1 μ g/ml R-EGF (Invitrogen) for 30 min on ice. Once surface-labeled, the cells were washed 3 times with ice-cold serum-free medium before chasing at 37°C in prewarmed medium containing serum for 0-8 min. Cells were fixed and permeabilized with PFA as described below. Steady-state R-Tfn

uptake assays were performed as described (Aschenbrenner, Lee et al. 2003). Cells were serum-starved for 2 hr, and then incubated at 37°C in serum-free media containing 50 µg/ml R-Tfn for 10 min before fixation as described below.

Collocation of R-EGF containing vesicles and endogenous synectin or endogenous AP-2 was quantified by counting the number of vesicles where the corresponding fluorescence emissions overlapped. At least 50 vesicles from three different cells were quantified for each time point.

Immunofluorescence microscopy

Cultured cells: cells grown on coverslips were fixed as described (Aschenbrenner, Lee et al. 2003). For AP-2 immunostaining, rhodamine-phalloidin staining, and R-Tfn uptakes, cells were fixed in 4% electron microscopy grade PFA (EM Scientific) for 25 min at room temperature and permeabilized in 4% PFA with 0.1% Triton X-100 (Pierce) for 5 min at room temperature. For synectin immunostaining, cells were fixed as described above but permeabilized with 1% Triton X-100. Coverslips were blocked with 3% bovine serum albumin (BSA, Sigma), before staining as described (Aschenbrenner, Lee et al. 2003). Samples were observed with a Leica DMR light microscope fitted with an ORCA digital camera well as with separate excitation and emission filters. Digital images were analyzed in Adobe Photoshop.

Collocation of vesicles associated with VFP-synectin constructs and endogenous myosin VI or R-Tfn was quantified by counting the number of vesicles where the corresponding fluorescence emissions overlapped. At least 50 vesicles from three different cells were quantified for each time point.

Kidney sections: frozen kidney blocks were cryo-sectioned (CM1850 cryostat, Leica) to a thickness of 4 μ m, and placed on microscope slides (Colorfrost, Fisher). OCT was removed by immersion in acetone at -20°C for 5 min, and the sections were transferred to room temperature and rehydrated by 0.5% BSA/PBS. Sections were blocked in 2% BSA/PBS for 20 min, incubated with primary antibodies for 1 hr, washed by 0.5% BSA/PBS, incubated with secondary antibodies, washed again, and incubated with phalloidin-Alexa-647 for 20 min. After a final wash, sections were mounted with coverslips and ProLong medium (Invitrogen). Sections were imaged by laser-scanning confocal microscopy (Zeiss LSM 510 Meta) with a 63 \times objective.

GST pull-down assays

Pulldown assays were conducted by Dr. Arie Horowitz. Glutathione-S-Transferase-tagged myosin VI tail domain (GST-M6tail) was expressed in bacteria, purified as described (Hasson and Mooseker 1994) and stored coupled to glutathione-sepharose at a concentration of $\sim 1\text{mg}/100\text{ml}$ beads. A poly-histidine-tagged synectin fragment (syn-120-333) was prepared as described (Dance, Miller et al. 2004). ARPE-19 cells were lysed in RIPA buffer containing 300mM sucrose, 5mM ATP and a

protease inhibitors cocktail (Complete, Roche), a buffer shown to maximize association between myosin VI and synectin (Aschenbrenner, Lee et al. 2003). Lysates were incubated for 1 hr on rotator at 4°C either in absence or presence of 50 mM peptide corresponding to the cytoplasmic tail of syndecan-4 (S4; RMKKKDEGSYDLGKKPIYKKAPTNEFYA), or of a similar peptide lacking the carboxy-terminus alanine (S4D). This peptide concentration saturated the endogenous synectin in ARPE-19 cells, as the latter was estimated to be at ~150 nM based on densitometric calibration of bands of immunoblotted recombinant synectin (Fig S5). Peptides were synthesized by Genemed Synthesis (South San Francisco, CA). Lysates were incubated with 40 ml GST-M6tail coupled to glutathione-sepharose beads (Amersham Biosciences) for 1 hr on rotator at 4°C. Bound proteins were eluted from beads by boiling in SDS-PAGE sample buffer, separated on 10% acrylamide gel (Biorad), transferred to PVDF membrane (Pierce), and probed with synectin or VFP antibody followed by secondary peroxidase-conjugated antibody. Signal was detected with SuperSignal West Pico enhanced chemiluminescent substrate (Pierce). TotalLab (Nonlinear) software was used for band densitometry. Nonlinear regression was performed with Prism (GraphPad).

Subcellular fractionation

ARPE-19 cells grown in 6 well dishes were transfected with 3 mg per well of pEGFP, pGFP-MegTmT, or pGFP-MegTmTDPDZ. Cells were washed 36 hr post

transfection with PBS and scraped into PBS containing 5mM EDTA. Cells were collected by centrifugation at 500× g. For whole cell lysates, the pellet was lysed in RIPA buffer with protease inhibitors (Aschenbrenner, Lee et al. 2003). To separate the cytoplasmic and membrane fractions, cells were lysed in 100 ml of RIPA for 20 min on ice, followed by centrifugation for 5 min at 1000×g to remove nuclei. The supernatant was spun further at 14,000×g for 20 min. The pellet comprised the plasma membrane fraction. Samples were separated on 4-20% gradient SDS-polyacrylamide gels and immunoblotted as described (Aschenbrenner, Lee et al. 2003).

Biotinylation assay

Cells were transfected in 6-well dishes as described above. Before labeling, cells were washed with ice cold PBS containing 1mM CaCl₂ and 0.1 mM MgCl₂ (PBS-CM) then placed on ice in PBS-CM for 20 min. To surface-label, cells were incubated with 0.5mg/ml EZ-link Sulfo-NHS-SS-biotin (Pierce) in PBS-CM on ice for 30 min with rotation. Cells were then washed 3 times with cold PBS-CM. In some cell samples the disulfide bonds on Sulfo-NHS-SS-biotinylated proteins remaining in the apical membrane were reduced by incubation in a fresh solution of 45 mM glutathione, 75 mM NaCl, 1 mM MgCl₂, 0.1 mM CaCl₂, 75 mM NaOH, 1% BSA for 90 min on ice with shaking. Following labeling, cells were washed 3 times in ice-cold PBS, then scraped into PBS with 5mM EDTA and spun at 500×g for 5 min. Cells in each 6-well were lysed in 400 ml of RIPA buffer and the cleared lysates mixed with

100 ml streptavidin-agarose beads (50% slurry in RIPA; Sigma) for 3 hrs. The washed beads were boiled in 5× sample buffer supplemented with 100mM DTT before SDS-PAGE and immunoblotting.

RESULTS

Synectin precedes myosin VI on UCV

We hypothesized two scenarios for myosin VI recruitment to UCV: (1) synectin is required for myosin VI recruitment to UCV, serving as an essential bridge to the UCV; (2) synectin performs only an auxiliary role and is not required for myosin VI recruitment. In order to test these alternatives we took advantage of the *Snell's waltzer (sv)* mouse (Avraham, Hasson et al. 1995), which does not express myosin VI. In both wild type (WT) and *sv* kidney epithelial cells, synectin was evident on punctae that had all the established identifiers of UCV (Aschenbrenner, Lee et al. 2003): they did not collocate with markers for clathrin-coated vesicles (e.g. the clathrin-adaptor AP-2; not shown), or with early endosome markers (e.g. EEA1; not shown), but could be internally labeled with endocytosed rhodamine-conjugated EGF (R-EGF) after 2-4 min of endocytosis (Figure 3.1A, B). Moreover, at this time point, R-EGF was no longer present in CCP (not shown), confirming that the R-EGF/synectin-labeled punctae were UCV. Peak R-EGF/synectin collocation occurred after two min at which $39.6 \pm 5.5\%$ and $42 \pm 2\%$ of the synectin-associated vesicles in WT and *sv* kidney cells, respectively, contained R-EGF. We concluded that myosin VI was not required for synectin recruitment to the UCV surface.

The presence of both the amino-terminus and the PDZ domain of synectin are required for synectin targeting to UCV

To identify the minimal region required for synectin targeting to UCV, we expressed a series of VFP-tagged domain-deletion constructs of synectin in ARPE-19 cells, a human retinal epithelial cell line (Figure 3.3A and Table 3.1; from here on in this manuscript we will use the term VFP- for visual fluorescent protein, as a generic term for GFP, CFP, or YFP). In ARPE-19 cells, UCV can also be labeled internally with rhodamine-conjugated transferrin (R-Tfn) two min after the initiation of endocytosis; at this time point the labeled transferrin has exited CCP as it no longer collocates with the CCP markers AP-2 or clathrin (Aschenbrenner, Lee et al. 2003) but has not yet reached the EEA1-positive early endosome (Aschenbrenner, Lee et al. 2003; Dance, Miller et al. 2004). Full length VFP-synectin targeted specifically to UCV in ARPE-19 cells, where it collocated with labeled transferrin after two min of pulse chase uptake (Figure 3.2C) and with myosin VI (Figure 3.3B) (Table 3.1) but does not collocate with AP-2 or EEA1 (Figure 3.2 A,B).

Interestingly, the PDZ domain alone (VFP-syn-P) was not sufficient for UCV-association and its expression had no effect on myosin VI targeting to UCV (Figure 3.3C). Furthermore, VFP-syn-P did not collocate with endocytosed Tfn (not shown). Instead, the PDZ domain was recruited to focal adhesions (FA), overlapping with vinculin (Figure 3.3D). A truncated synectin containing both the PDZ and carboxy-

terminus domains but lacking the amino-terminus (VFP-syn-PC) was also targeted to FA (not shown), suggesting that in the absence of the amino-terminus targeting was altered, permitting association with FA-resident PBMs.

The smallest fragment of synectin capable of targeting to R-Tfn-containing UCV consisted of the amino-terminus and the PDZ domain (VFP-syn-NP; Figure 3E). The UCV-targeting of this construct was as efficient as that of VFP-fused intact synectin; the extent of collocation of the two VFP-fused constructs with R-Tfn-containing vesicles after 2 min of pulse-chase uptake was virtually identical: $68.6 \pm 7.57\%$ and $68 \pm 7.2\%$, respectively (Table 3.1). VFP-syn-N expressing the amino-terminus alone was diffusely distributed in the cytoplasm, however (Table 3.1). Thus both the amino-terminus and the PDZ binding domains, but not the carboxy-terminus domain, are required and sufficient for synectin targeting to UCV (Table 3.1). Since the amino-terminus domain self-associates (Gao, Li et al. 2000; Jeanneteau, Diaz et al. 2004), dimerization appears to be required for synectin binding to UCV.

The myosin VI binding site is located in the carboxy-terminus of synectin

While VFP-syn-NP was capable of vesicle association, it apparently lacked the myosin VI binding site as upon expression in ARPE-19 cells, myosin VI was no longer recruited to UCV (Figure 3.3F). Only $20.5 \pm 8\%$ of VFP-syn-NP punctae collocated with myosin VI, versus $70 \pm 2\%$ of VFP-synectin punctae (Table 3.1).

Moreover, whereas R-Tfn endocytosis was normal (Figure 3.3E), R-Tfn reached early endosomes only in $24.5 \pm 6.2\%$ of VFP-syn-NP-expressing cells after 15 min of uptake versus $\sim 90\%$ of untransfected cells and cells expressing all other VFP-synectin constructs (Figure 3.4 A,B). This phenotype suggests a block in the inwards transport of UCV and is similar to that seen upon expression of myosin VI motor domain mutants (Aschenbrenner, Lee et al. 2003). We concluded that the myosin VI binding site is located in the carboxy-terminus domain of synectin, and that VFP-syn-NP expression blocked trafficking by displacing endogenous synectin from UCV, thus preventing myosin VI docking.

Co-immunoprecipitation experiments with a series of truncated synectin constructs narrowed down the location of the essential part of the myosin VI binding motif to the last 29 residues in the carboxy-terminus (Figure 3.5A). A construct lacking these residues no longer collocated with myosin VI (not shown).

A functional PDZ domain is required for synectin targeting to UCV

Uncoated endocytic vesicles carry numerous types of cell surface receptors from CCP to early endosomes. As a large number of transmembrane receptors bind to the PDZ domain of synectin, it seemed likely that this domain is required for synectin association with UCV. To test this hypothesis we replaced two consecutive residues in the carboxylate binding loop of the PDZ domain of synectin (L142A/G143E) to produce VFP-syn-PDZ-. This mutation was previously shown to impair the binding

between synectin and $G\alpha_i$ -interacting protein (Lou, Yano et al. 2001). When expressed in ARPE-19 cells, the mutant synectin (VFP-syn-PDZ⁻) did not affect trafficking (Figure 3.4B) but no longer targeted to UCV (Figure 3.5B) confirming that UCV association requires binding of the PDZ domain of synectin to PBMs on the UCV surface.

Ligand binding to the PDZ domain of synectin facilitates myosin VI binding to the synectin carboxy-terminus

Surprisingly, although the VFP-syn-PDZ⁻ construct possessed an intact myosin VI-binding site, which was far removed from the two point mutations in the PDZ domain, it did not co-immunoprecipitate with myosin VI (Figure 3.5A, lane 8). We hypothesized therefore that binding of the PDZ domain of synectin to its ligand on the UCV surface is required for myosin VI binding to synectin and recruitment to UCV.

In order to gain insight into the effect of ligand-binding to the PDZ domain on the interaction between synectin and myosin VI, we estimated the binding coefficients of the tail domain of myosin VI to synectin in the presence of a peptide corresponding to the cytoplasmic tail of syndecan-4 (S4), previously shown to bind synectin (Gao, Li et al. 2000). As a control, we used a syndecan-4 peptide lacking the carboxy-terminus alanine, which does not bind synectin (Horowitz, Tkachenko et al. 2002). Immobilized GST-fused myosin VI tail domain (GST-M6tail) was used to pull down endogenous synectin from ARPE-19 cell lysates in the presence of each peptide (Figure 3.6A). In

order to estimate the binding coefficients between myosin VI and synectin under these conditions, we constructed a saturation-binding curve by varying the fraction of ARPE-19 cell lysate in the constant total volume used in each pull-down experiment. Nonlinear regression of the ensuing saturation-binding curves yielded similar dissociation constants in the presence of S4 or S4D – 1.2 nM and 1.7 nM, respectively (Figure 3.6B). However, the B_{\max} of the binding was more than twice larger in the presence of S4 than in the presence S4D (0.82 versus 0.35 nM-s⁻¹, respectively). These results suggest that ligand binding to the PDZ domain stabilizes synectin in a conformation favorable for myosin VI binding. As an additional test for the dependence of myosin VI binding to synectin on engagement of the latter's PDZ domain, we repeated the pull down on lysate of ARPE-19 cells expressing VFP-syn-PDZ⁻. While endogenous synectin was precipitated, GST-M6tail failed to bind and pull down VFP-syn-PDZ⁻ (Figure 3.6C).

Search for receptors that would engage synectin and recruit myosin VI on the UCV *in vivo*

We had so far shown that activation of the PDZ domain of synectin increased its binding to myosin VI *in vitro*. We next embarked on a search for PDZ binding motif-containing receptors that would similarly activate myosin VI binding, following PDZ domain engagement on UCV *in vivo*. The basic criteria for these receptors was that they had to be known to bind synectin via a C terminal PDZ binding motif and

exist as VFP fusion constructs. They also had to be endocytosed through receptor mediated endocytosis when expressed in ARPE-19 cells, meaning they had to be expressed properly in ARPE-19 cells, be able to target to the cytoplasmic membrane, undergo endocytosis and target to UCV as measured by association with UCV markers. In addition, when the PDZ binding motif was mutated on these receptors, they still had to target similarly to wild type to the endocytic pathway.

Our first candidate was the cystic fibrosis transmembrane conductance regulator (CFTR), generally expressed in airway epithelial cells. CFTR was chosen because it was shown to bind synectin (pers. Comm. B. Stanton), and because it recycles to the cytoplasmic membrane in a myosin VI-dependent fashion (Swiatecka-Urban, Boyd et al. 2004). In order to determine whether CFTR targeted to UCV in ARPE-19 cells, we expressed GFP tagged CFTR (GFP-CFTR) and stained for GIPC or Myosin VI. GFP-CFTR was expressed mostly in the E.R. and golgi region and did not colocalize at all with UCV markers and was thus discounted (data not shown).

Next we attempted to analyze the location of the lutropin receptor, shown to bind synectin (Hirakawa, Galet et al. 2003). We expressed the myc tagged version of the lutropin receptor in ARPE-19 cells. Utilizing multiple myc antibodies and permeabilization conditions, it was still difficult to distinguish lutropin receptor specific staining from background to a specific enough level to be able to measure the colocalization of anti-myc staining with UCV markers. At the optimal time of expression, which we found to be 36 hours post transfection, most of the receptor was in the

endoplasmic reticulum. To determine whether the receptor was ever on the cytoplasmic membrane or in UCV we moved to biochemical experiments to ascertain membrane targeting. Western blots using anti-myc antibody showed that lutropin was in an aggregate that ran at 220 KD instead of 85 KD (data not shown). We attempted different elution conditions that would bypass the formation of aggregates (M. Ascoli pers Comm), by increasing the reducing agent concentration of the sample buffer, and removing the boiling step, but these steps made it very difficult for lutropin to be eluted off beads. Given the general uncertainty involved in potential readouts from this system, it was discounted as well.

Dopamine receptors were investigated next. Dopamine receptors 2 and 3 were also found to bind to megalin via their PDZ binding motifs (Jeanneteau, Diaz et al. 2004). Both GFP-D2 and GFP-D3 targeted to vesicles in ARPE-19 cells. However neither of them targeted significantly to UCV markers. (Figure 3.7 A and B). Since this might be due to the fact that dopamine is not normally expressed in ARPE-19 cells and might need an agonist to recycle through the endocytic system properly, we stimulated ARPE-19 cells with quinpirole, a dopamine 2 agonist. Quinpirole did not increase the number of GFP-D2 associated vesicles nor their association with UCV markers (data not shown). GFP-D2 and D3 were discounted as well.

Synectin-null mice exhibit perturbed megalin targeting and proteinuria

We next investigated the scavenger receptor megalin, which binds synectin (Gotthardt, Trommsdorff et al. 2000) and collocates with it on the lumen of kidney proximal tubules (Lou, McQuistan et al. 2002). This location is shared by myosin VI (Biemesderfer, Mentone et al. 2002). Given the well-documented defects in the renal function of megalin-null mice (Kozyraki, Fyfe et al. 2001), we sought to determine if the binding of megalin to synectin is essential for megalin's function in renal physiology. One of the renal defects found in megalin-null mice is low molecular weight proteinuria caused by tubular resorption deficiency (Leheste, Rolinski et al. 1999). Urine analysis of synectin-null mice by SDS-PAGE revealed the presence of proteins in the urine of these mice, which resolved into a band pattern similar to that seen in megalin-null mice. For example, urine from synectin-null mice contained retinol binding protein (RBP) (Figure 3.8A), a known megalin ligand (Christensen, Moskaug et al. 1999). However, the level of megalin found in the kidneys of synectin null mice was equivalent to that seen in WT mice (Figure 3.8B). The increased protein presence in the urine of synectin-null mice despite the normal expression of megalin in the proximal tubules of their kidneys supported the possibility that megalin recycling is defective in these mice, and suggested that synectin is required for proper megalin trafficking in vivo. Interestingly, myosin VI expression level was 6-fold higher in synectin-null than in WT kidneys (Figure 3.8B) reflecting a possible compensatory

response to the impaired trafficking of megalin in the proximal tubules of synectin-null mice

To further determine if proteinuria in synectin-null mice was due to defective megalin trafficking, we analyzed the distribution of myosin VI and megalin in the proximal tubules of these mice. In WT mice (Figure 3.8C) megalin was primarily detected in the endocytic region at the base of the proximal tubule cell microvilli, as also noted in other studies (Lou, McQuistan et al. 2002). In synectin-null mice, however, megalin extended along the length of the microvilli (Figure 3.8C). A low level of megalin is normally present in microvilli (Biemesderfer, DeGray et al. 2001). Therefore, the elevated presence of megalin in the microvilli of synectin-null mice most likely reflects impairment in megalin recycling, possibly caused by the loss of its interaction with myosin VI, rather than a complete alteration of its targeting. Neither myosin VI targeting nor CCP location (Figure 3.8D) appeared to be perturbed by the absence of synectin.

Megalín recruits synectin to UCV via PDZ domain interaction

In order to substantiate the previous observation concerning the inability of VFP-syn-PDZ⁻ (lacking a functional PDZ domain) to associate with UCV, we asked whether a complementary approach - removal of the PBM of a synectin-binding cell surface receptor - would impair receptor trafficking by preventing the docking of synectin and the recruitment of myosin VI. To test this premise, we used a chimeric

GFP-tagged megalin “mini-receptor”, GFP-MegTmT, where GFP is fused to the transmembrane and cytoplasmic domains of human megalin (Marzolo, Yuseff et al. 2003). We generated a truncated construct, GFP-MegTmT Δ PDZ, lacking the four residue (DSEV) PBM and as a result unable to bind synectin (Figure 3.9C). We hypothesized that GFP-MegTmT Δ PDZ would inhibit both synectin and myosin VI recruitment to UCV if synectin binding to the PBM were required for targeting to UCV.

The cytoplasmic domain of megalin is sufficient for apical membrane targeting of the fusion protein in MDCK epithelial cells (Marzolo, Yuseff et al. 2003). We first sought to verify that the GFP-MegTmT mini-receptor is similarly present on the cell surface and undergoes recycling in ARPE-19 cells, our model system for UCV trafficking. Surface biotinylation (Figure 9A) as well as subcellular fractionation (Figure 9B) confirmed that both GFP-MegTmT and GFP-MegTmT Δ PDZ reached the plasma membrane in ARPE-19 cells. Both were effectively endocytosed (Figure 9A) and collocated to an equivalent level with the CCP marker AP-2 (Figures 11.3, Figure 3.12A), and with endocytosed R-Tfn (Figure 1.10A, Figure 11). In addition, GFP-MegTmT was present in UCV, as both endogenous synectin and myosin VI overlapped with GFP-MegTmT-labeled vesicles (Figure 3.10B, Figure 3.11).

Expression of GFP-MegTmT Δ PDZ drastically reduced the ability of exogenously expressed synectin to associate with UCV (Figure 3.10B, Figure 3.11). Nearly 90% of GFP-MegTmT-containing vesicles present in the cell periphery

recruited VFP-synectin, whereas the synectin recruitment level was less than 10% when GFP-MegTmT Δ PDZ was expressed (Figure 3.10A, Figure 3.11). Unlike exogenously-expressed synectin, part of the endogenous synectin population, as well as that of myosin VI, was still recruited to UCV in GFP-MegTmT Δ PDZ-expressing cells, though significantly less than in GFP-MegTmT-expressing cells (Figure 3.10B, 11.3). This suggests that the population of cell surface receptors present in UCV is heterogeneous, frequently containing more than a single synectin-binding species. Finally, CFP-syn-NP, which cannot associate with myosin VI, associated with GFP-MegTmT and did not associate with GFP-MegTmT Δ PDZ, confirming that the ability of megalin to recruit synectin to UCV was not myosin VI dependent (Figure 3.12B).

DISCUSSION

In this study we investigated the recruitment of myosin VI to its adapter, synectin, as well as the mechanism that synectin uses to recognize cargo. We conclude that myosin VI binding to synectin is dependent on the engagement of synectin's PDZ domain: (1) while myosin VI can complex with synectin, myosin VI does not co-immunoprecipitate with VFP-syn-PDZ⁻, a synectin construct which has a non-functional PDZ domain but still contains a potential myosin VI binding site; (2) expression of VFP-syn-PDZ⁻ does not block myosin VI recruitment to UCV, an event that would be predicted if binding of myosin VI to the carboxy-terminus of synectin could occur in the absence of PDZ-domain engagement; (3) the binding of the myosin VI tail domain to synectin in vitro is enhanced in the presence of a synectin PDZ ligand.

With regards to the mechanism of cargo selection, three lines of evidence suggest that recruitment of myosin VI requires interaction between the PBMs of engulfed receptors and synectin's PDZ domain: (1) as mentioned above, engagement of synectin's PDZ domain facilitated its binding to myosin VI in vitro; (2) the PBM of megalin was required for synectin and myosin VI recruitment to megalin-containing UCV; (3) megalin targeting to the apical endocytic region of proximal tubule epithelial cells, presumably a myosin VI dependent process, was disrupted in kidneys of synectin-null mice, resulting in an impairment of megalin function.

The PDZ domain may regulate myosin VI binding to the carboxy-terminus domain of synectin in two possible ways. Synectin may predominantly reside in a conformation where the PDZ domain interacts with the carboxy-terminus, physically blocking access to the myosin VI binding site. Alternatively, ligand binding to the PDZ domain may be transmitted to the carboxy-terminus by an allosteric mechanism. In either scenario, engagement of the PDZ domain would stabilize synectin in a conformation in which the myosin VI binding site is exposed. Without the interaction of a PDZ-binding ligand, synectin appears to favor a conformation where the myosin VI binding site is inaccessible. Thus, the PDZ domain of synectin functions as an active regulatory component conditioning myosin VI binding to synectin upon synectin's association with UCV.

PDZ domains occur in a large number of proteins where they are thought to function primarily as passive binding modules (reviewed in (Nourry, Grant et al. 2003)). The only known instance of a ligand-dependent intramolecular regulation by a PDZ domain is the activation of protease activity of the bacterial protein DegS (Walsh, Alba et al. 2003). Conceivably, cooperative binding mechanisms similar to the ones occurring in DegS and synectin may be more prevalent than currently appreciated.

Evidence from yeast two-hybrid assays suggests that synectin dimerizes in a manner requiring the participation of its amino-terminus (Gao, Li et al. 2000; Jeanneteau, Diaz et al. 2004). In support, we detected by size exclusion

chromatography that synectin is present as a dimer in solution under physiological conditions (data not shown). The functional significance of synectin dimerization has become particularly intriguing in light of a recent study suggesting that myosin VI exists primarily as a monomer but can dimerize when in very close proximity to another myosin VI molecule (Park, Ramamurthy et al. 2006). Myosin VI dimerization was inhibited by the myosin VI cargo binding domain *in vitro*, indicating that a cargo binding-dependent mechanism is required for proximity based dimerization. It is thus likely that a mechanism that allows two myosin VI molecules to be in close proximity such as synectin dimerization, would promote both the recruitment and subsequent dimerization of myosin VI.

Myosins from classes I, V, VI, VII, and X participate in intracellular organelle trafficking including endocytosis and exocytosis (reviewed in (Krendel and Mooseker 2005)). The cargo docking mechanism for myosin Va is the only one fully elucidated (Wu, Rao et al. 2001; Fukuda, Kuroda et al. 2002; Wu, Wang et al. 2002; Westbroek, Lambert et al. 2003; Boldogh, Ramcharan et al. 2004). Myosin V targeting to a variety of organelles is mediated by organelle-specific Rab GTPases, some of which bind to myosin Va directly, and some via adaptor proteins. For example Rab27a, involved in exocytic vesicle sorting, is the receptor for myosin V on the melanocyte surface (Jung, Remmert et al. 2001), and recruits melanophilin (Fukuda, Kuroda et al. 2002; Strom, Hume et al. 2002; Wu, Wang et al. 2002), an adaptor protein that can also link to the actin cytoskeleton (Kuroda, Ariga et al. 2003), in a GTPase dependent manner. The

carboxy-terminus of melanophilin can then recruit myosin Va to the Rab27a-melanophilin complex. Clearly this cargo recruitment mechanism is different from that described here for myosin VI. The myosin VI-UCV docking scenario derived from our study (Figure 3.13A) suggests that shortly after clathrin uncoating, synectin binds to the carboxy-termini of endocytosed transmembrane receptors present in UCV as a dimer. Once the PDZ domain is engaged, synectin stabilizes in a conformation where the myosin VI binding site in the synectin carboxy-terminus is accessible, and myosin VI is recruited to the UCV.

In studying myosin VI's specific role in endocytic vesicle trafficking, it has been shown that myosin VI can be recruited to two distinct cargoes, UCV and CCP, though it is recruited to UCV in most cell types (Buss, Arden et al. 2001; Dance, Miller et al. 2004). Two mechanisms modulate the ability of myosin VI to target to CCP, the alternative splicing of the myosin VI tail domain and the expression level of Dab2, an adapter protein that binds to clathrin, clathrin adaptors and myosin VI (Dance, Miller et al. 2004); only under conditions where Dab2 levels are high is targeting of myosin VI to CCP seen. Relevant to this study, Dab2 can also bind megalin (Oleinikov and Makker 2000) and as such may link megalin to myosin VI in CCP. Unlike synectin, Dab2 binds to the internalization FXNPXY motif in megalin's cytoplasmic domain (Oleinikov and Makker 2000). Notably, renal proximal tubule epithelial cells from Dab2-null mice are defective in protein uptake (Morris, Arden et al. 2002), however this is due to decreased synthesis or increased turnover of megalin

(Nagai, Christensen et al. 2005). In contrast, in the absence of synectin, megalin levels remain unchanged. Therefore synectin and Dab2 clearly play different roles with regards to megalin function.

Based on these differences we suggest that Dab2 and synectin perform non-overlapping functions with regards to megalin's endocytosis and transport. Dab2 likely plays a role early in endocytosis, perhaps to cluster the receptor in CCP or to signal receptor endocytosis. Synectin in turn may act at two stages. As presented in Figure 3.13, synectin may act after the completion of endocytosis and vesicle uncoating. This may explain why myosin VI location appeared essentially unchanged in synectin-null mice, as Dab2 could still recruit myosin VI to CCP. The lack of myosin VI association with UCV would be hard to discern in the dense apical endocytic region of the proximal tubule epithelial cells. Alternatively, synectin could be required earlier for megalin translocation down microvilli towards CCP located near the microvillus base (Figure 3.13B). Actin filaments are oriented with their minus ends at the microvillus base, facilitating the retrograde translocation of myosin VI and its cargo towards the base. Indeed, myosin VI was reported to serve a similar function in the microvillar transport of the sodium proton exchanger NHE3 during acute renal hypertension (Yang, Maunsbach et al. 2005). Loss of myosin VI-driven translocation may explain the redistribution of megalin seen in synectin-null mice, causing accumulation of the protein in microvilli rather than at the base of these structures.

According to our last count there are currently 28 known ligands to the PDZ domain of synectin, most of which, though not all, are membrane proteins. There does not seem to be a common functional theme to this large group of ligands, whose members are as diverse as semaphorin (Wang, Kalb et al. 1999), TGF β (Blobe, Liu et al. 2001) and the RhoA guanine exchange factor Syx1 (Liu and Horowitz 2006). The only known binding partner of synectin that does not interact with the PDZ domain is myosin VI. It is conceivable therefore that this interaction underlies synectin function, namely that synectin serves as a “universal” adapter of myosin VI to a myriad of cargoes. The association of synectin with myosin VI is not necessarily confined to UCV, as both synectin (Liu, Kandala et al. 2001) and myosin VI (Buss, Kendrick-Jones et al. 1998) are present in the Golgi apparatus. We also cannot rule out the interaction of other motor proteins with synectin, e.g. the kinesin superfamily protein 1B detected as ligand of the synectin PDZ domain in a yeast two-hybrid screen (Reed, Cefalu et al. 2005). Two separate yeast two-hybrid screens, however, ((Reed, Cefalu et al. 2005); M. Simons, personal communication) did not identify additional unconventional myosins or other molecular motors as putative synectin binding partners.

ACKNOWLEDGEMENTS

The text of Chapter Three is in part derived from Naccache, Hasson and Horowitz, submitted to PNAS. Dr. Tama Hasson is acknowledged for her work on creating the synectin constructs and analyzing their localization. Dr. Arie Horowitz (Dartmouth College) is acknowledged for his exclusive work on saturation binding curves, kidney cryosection and staining, and urine analysis. Drs. Sally Camper and Jill Karolyi (University of Michigan), and Dr. Michael Simons (Dartmouth College) are acknowledged for sharing with us the Snell's Waltzer mice and the synectin-null mice, respectively. Further acknowledgment is extended to Dr. Daniel Biemesderfer (Yale University) for use of megalin antibodies, Dr. Maria Paz Marzolo (Pontificia Universidad Católica de Chile, Santiago, Chile) for sharing with us the megalin minireceptor construct, Dr. Agnieszka Swiatecka-Urban (Dartmouth College) for sharing the GFP-wt-CFTR construct, Dr. Mario Ascoli (University of Iowa) for the myc-hLHR-lutropin construct, Dr. Freddy Jeanneteau (INSERM) for the GFP tagged dopamine receptor constructs, Dr. Sassan Hajmohammadi (Dartmouth College) for help with preparation of mouse kidneys, and Dr. Colin Jamora for use of the cryosection.

FIGURES

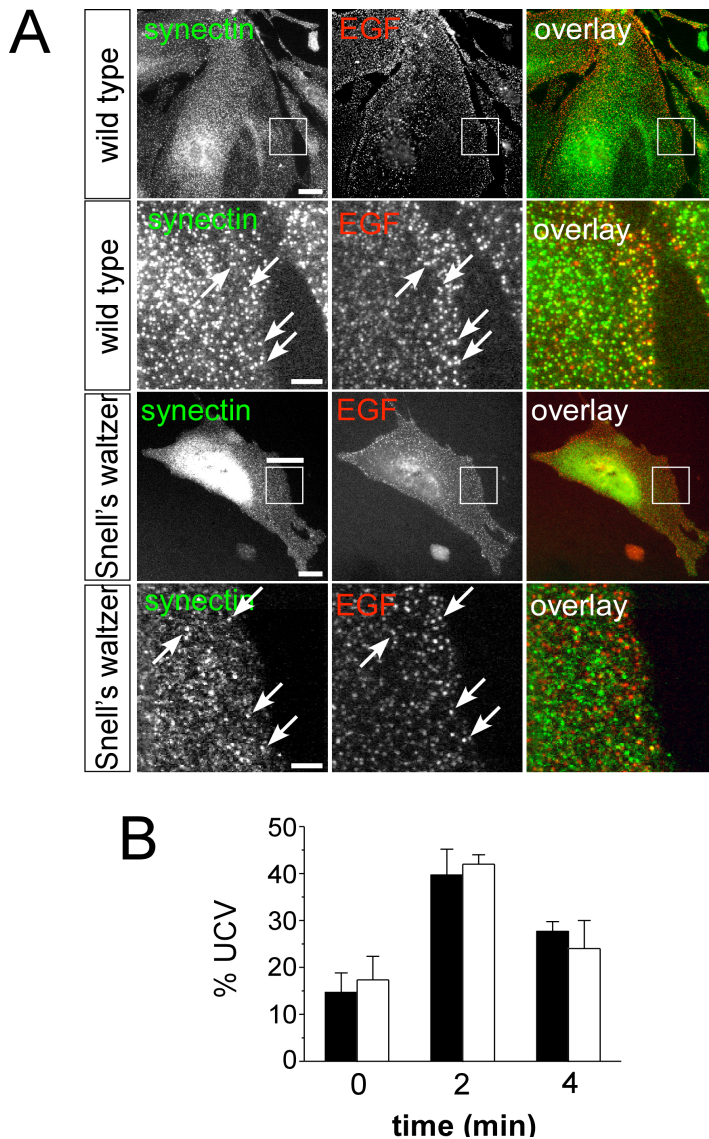


Figure 3.1. Myosin VI is not required for the targeting of synectin to UCV. (A) Location of synectin (visualized with rabbit-anti-synectin; green) in WT and Snell's waltzer (*sv*) mouse kidney epithelial cells after 4 min uptake of R-EGF (red). The bottom panels are enlargements of the boxed areas in the top panels of each cell type (scale bars: 10 mm; 2.5 mm in enlarged panels). (B) Histogram representing quantified collocation in WT kidney epithelial cells (black bars) or *sv* cells (white bars) of R-EGF-containing vesicles and synectin-associated vesicles. R-EGF was endocytosed by pulse-chase and cells were fixed at 0, 2, and 4 min of endocytosis. Synectin was detected by indirect immunofluorescence. N=150 vesicles were counted from 3 different cells.

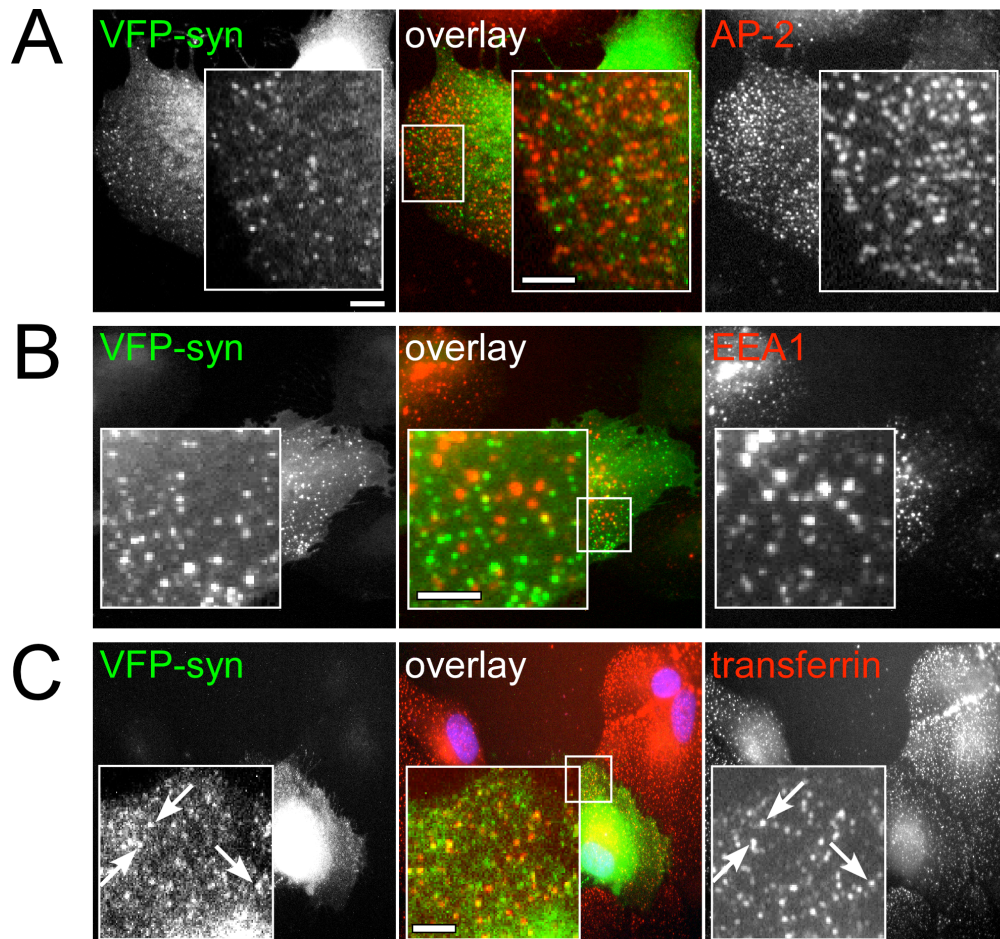
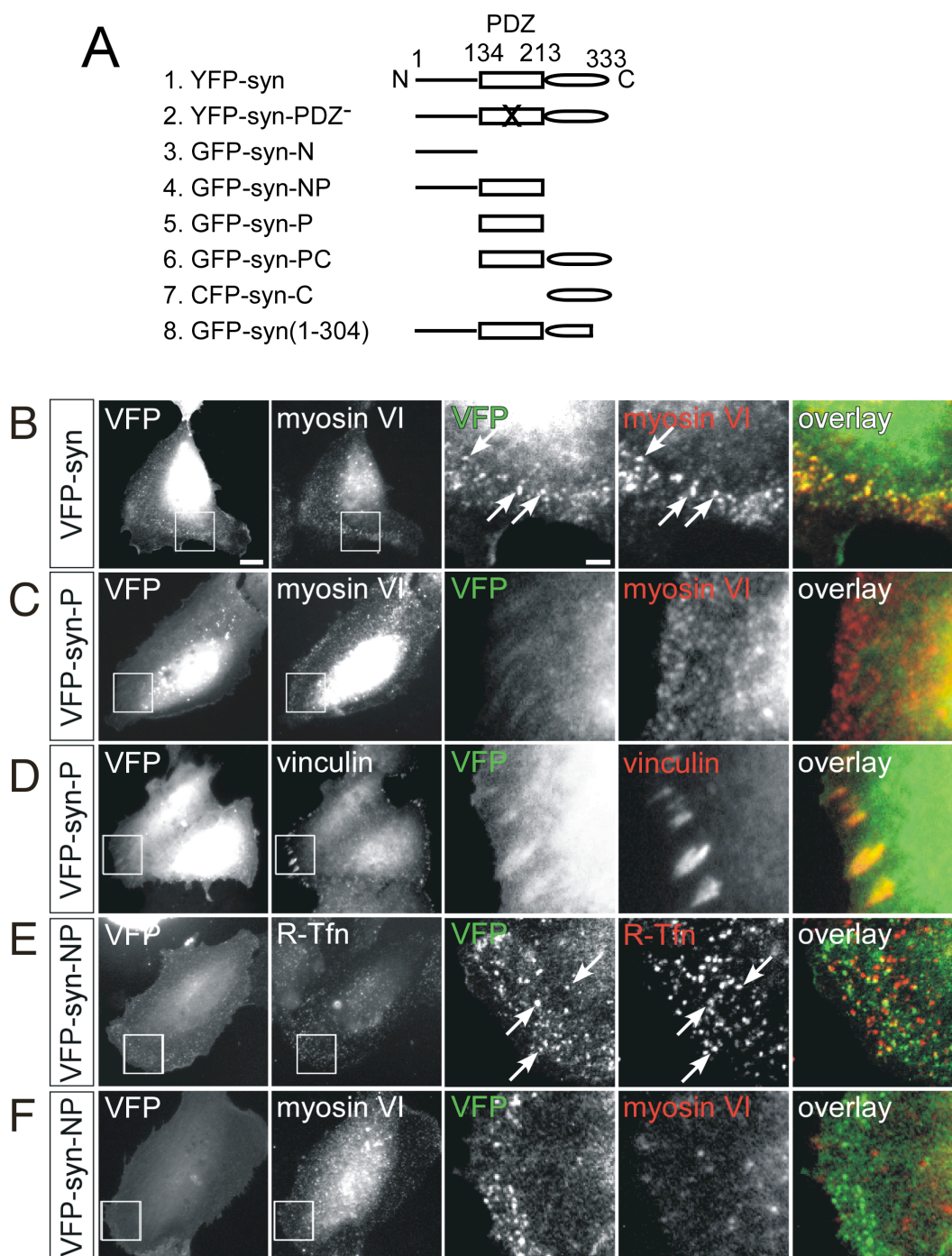
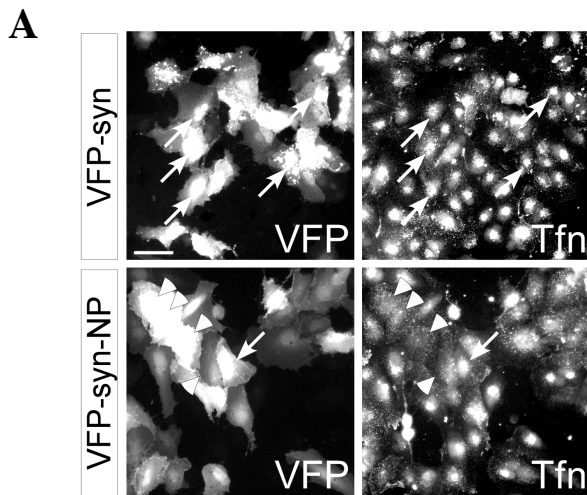


Figure 3.2. VFP-fused synectin targets to UCV. Similar to endogenous synectin, YFP-fused synectin (green; VFP-synectin) had a peripheral distribution in ARPE-19 epithelial cells and did not collocate with AP-2 (A, red) or with EEA1 (B, red). R-Tfn (red) uptake was similar in cells expressing high or low levels of VFP-synectin (green) (C). Cell nuclei in C are stained by DAPI (blue). Arrows indicate vesicles with collocated VFP-synectin and R-Tfn (scale bars: 10 μm , 2.5 μm in insets).

Figure 3.3. Both the amino-terminus and PDZ domains of synectin are required for UCV binding. (A) Schematic of GFP-, YFP- and CFP-fused synectin constructs used in this study. Residue numbers at the boundaries of the amino-terminus (N), PDZ (P) and carboxy-terminus (C) domains are shown above the full length YFP-synectin construct. B-F: ARPE-19 cells expressing VFP-fused synectin constructs (green). Boxed area in the two left hand panels are enlarged in the right hand panels. The furthestmost panel to the right represents the overlay between the two enlarged fields to its left. Vesicles showing collocation are indicated by arrows. (B) VFP-synectin expressing cells were stained for myosin VI (rabbit-anti myosin VI, red), revealing significant collocation. (C) The PDZ domain (VFP-syn-P, green) was not recruited to UCV and its expression did not interfere with myosin VI targeting to vesicles in ARPE-19 cells (anti-myosin VI, red). (D) VFP-syn-P collocated with the focal adhesion marker vinculin (visualized with mouse anti-vinculin; red). (E) VFP-syn-NP targeted to peripheral vesicles internally labeled with R-Tfn (red) after 2 min pulse-chase uptake, a characteristic of UCV. (F) Expression of VFP-syn-NP (green) prevented myosin VI (red) recruitment to UCV (scale bars: 10 μm , 2.5 μm in enlarged panels).





B.

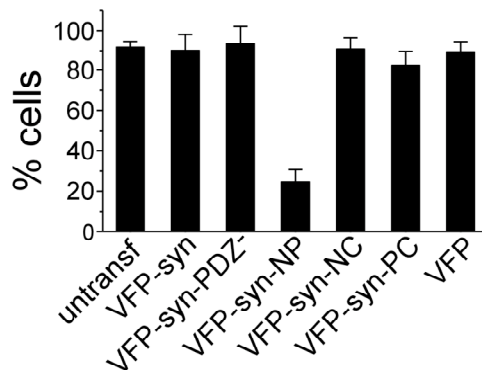


Figure 3.4. Expression of VFP-syn-NP disrupted trafficking of UCV to the early endosome. (A) Transfected ARPE-19 cells were incubated for 15 min at 37°C with R-Tfn (red), resulting in Tfn uptake and accumulation in pericentriolar endosomes. VFP-syn-expressing cells endocytosed R-Tfn and exhibited pericentriolar R-Tfn accumulation. VFP-syn-NP-expressing cells endocytosed R-Tfn but mostly lacked the pericentriolar accumulation, consistent with a block in vesicle transport (arrows, arrowheads: presence or absence, respectively, of pericentriolar Tfn accumulation; scale bar: 50 mm). (B) Histogram showing the percentage of transfected and untransfected cells exhibiting R-Tfn labeling of pericentriolar endosomes after 15 min of uptake. More than 100 cells were counted per transfection. See Fig 2A for schemes of the constructs.

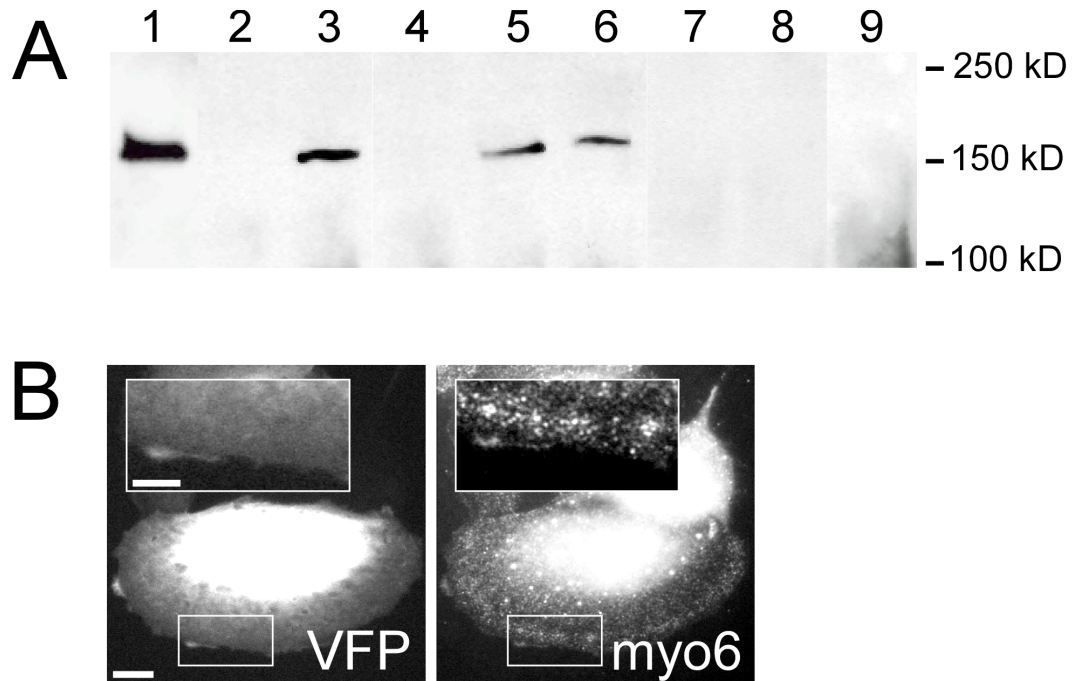


Figure 3.5. Myosin VI binds to the carboxy-terminus of synectin but requires a functional synectin PDZ domain for in situ interaction. (A) Myosin VI immunoblot of ARPE-19 cell lysates transfected with the indicated synectin constructs and immunoprecipitated with anti-VFP (which recognizes all three GFP variants). The lysate lane was loaded with 10% of the immunoprecipitated samples volume. Myosin VI was co-immunoprecipitated only by synectin constructs that contained the full-length carboxy-terminus domain. Coimmunoprecipitation was abolished by the deletion of the last 29 carboxy-terminus residues (CFP-syn(1-304)) or by inactivation of the PDZ domain by two point mutations (denoted by X on the scheme of the YFP-syn-PDZ- construct in Fig 2A). (B) Expression of synectin containing the PDZ domain mutations L142A/G143E (VFP-syn-PDZ-) in ARPE-19 cells. Cells were counterstained with anti-myosin VI. The PDZ domain mutations eliminated UCV recruitment, but had no effect on the targeting of endogenous myosin VI to UCV (scale bars: 10 μ m, 5 μ m in insets).

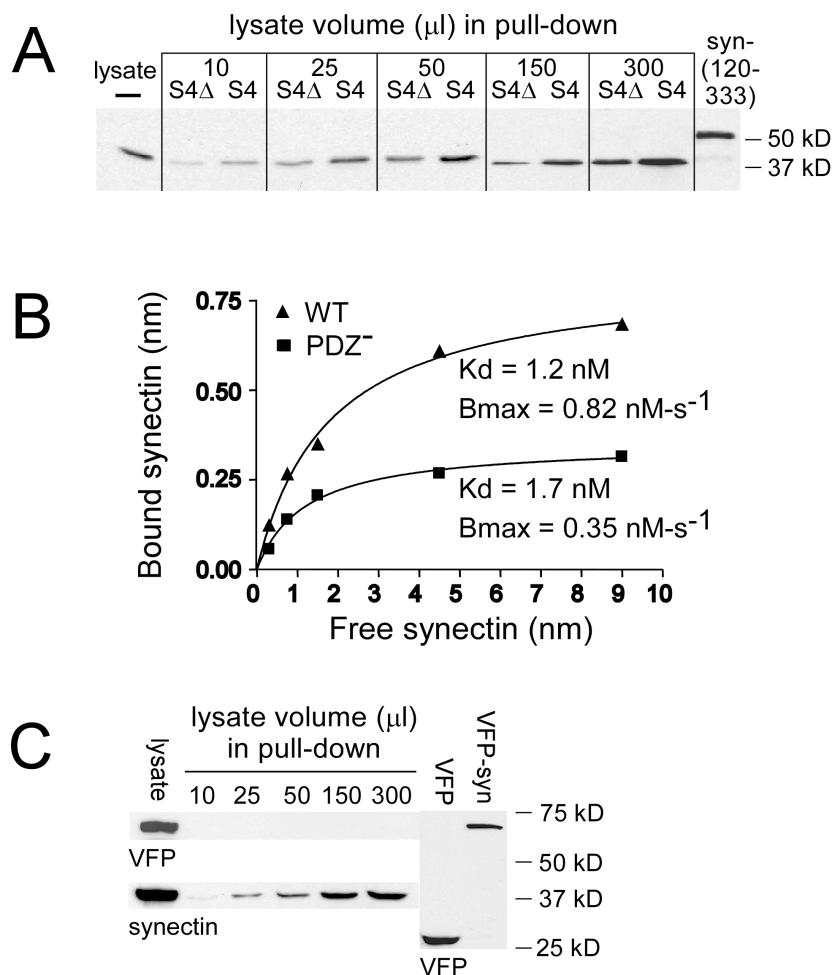


Figure 3.6. PDZ ligand binding regulates myosin VI binding to synectin. (A) Pull-down assay with immobilized GST-M6tail and varying volumes of ARPE-19 cell lysate, as shown above each pair of lanes, in the presence of either WT (S4) or truncated (S4D) syndecan-4 cytoplasmic tail peptides. The bands in the immunoblots (IB) correspond to synectin in the lysate (left lane, 3% of pull-down input volume), synectin eluted from GST-M6tail, and the synectin fragment syn (120-333), which migrated as a dimer. The syn (120-333) band served as a densitometric reference value for quantification of the other bands. (B) Saturation-binding curves derived from the densitometric values of the synectin bands in A, and binding constants calculated from these curves. (C) Pull-down assay as in A with lysates of cells expressing VFP-syn-PDZ⁻. The top part of the membrane was probed with anti-VFP, and the bottom with anti-synectin, as indicated. Lanes a-b: pull-down of cell expressing VFP and VFP-syn respectively. Lane c: lysate (3% of pull-down input volume) of cells expressing VFP-syn-PDZ⁻.

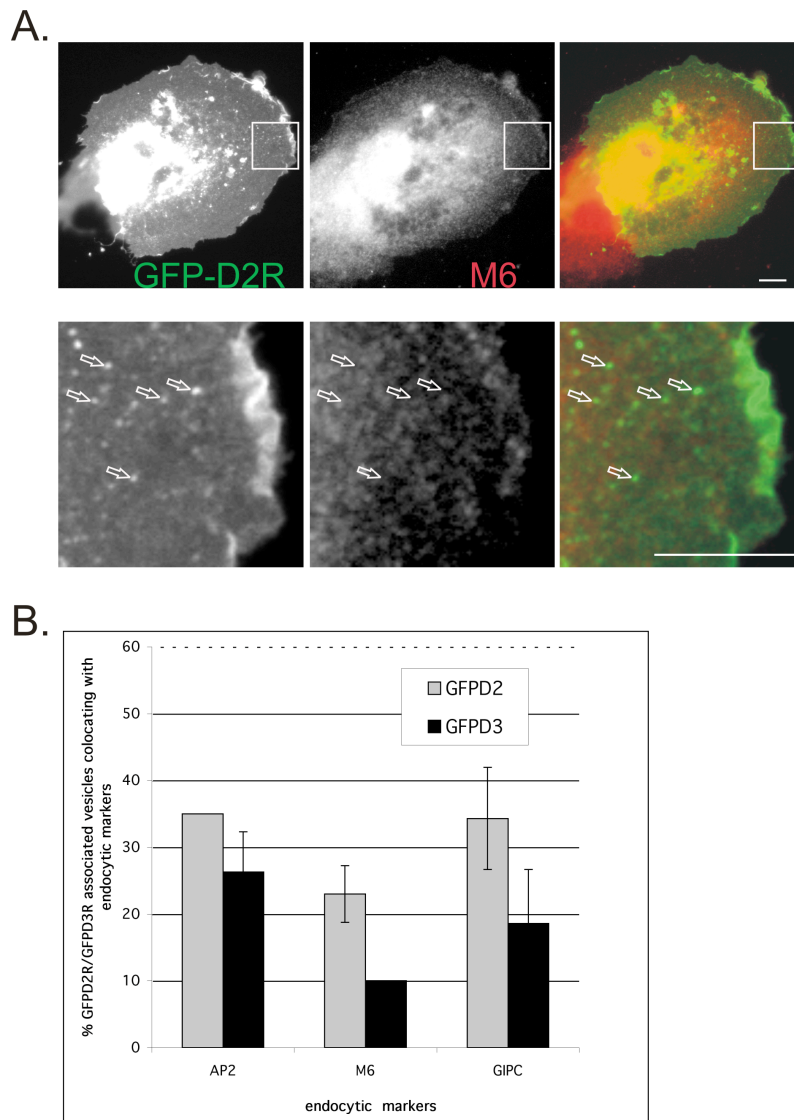
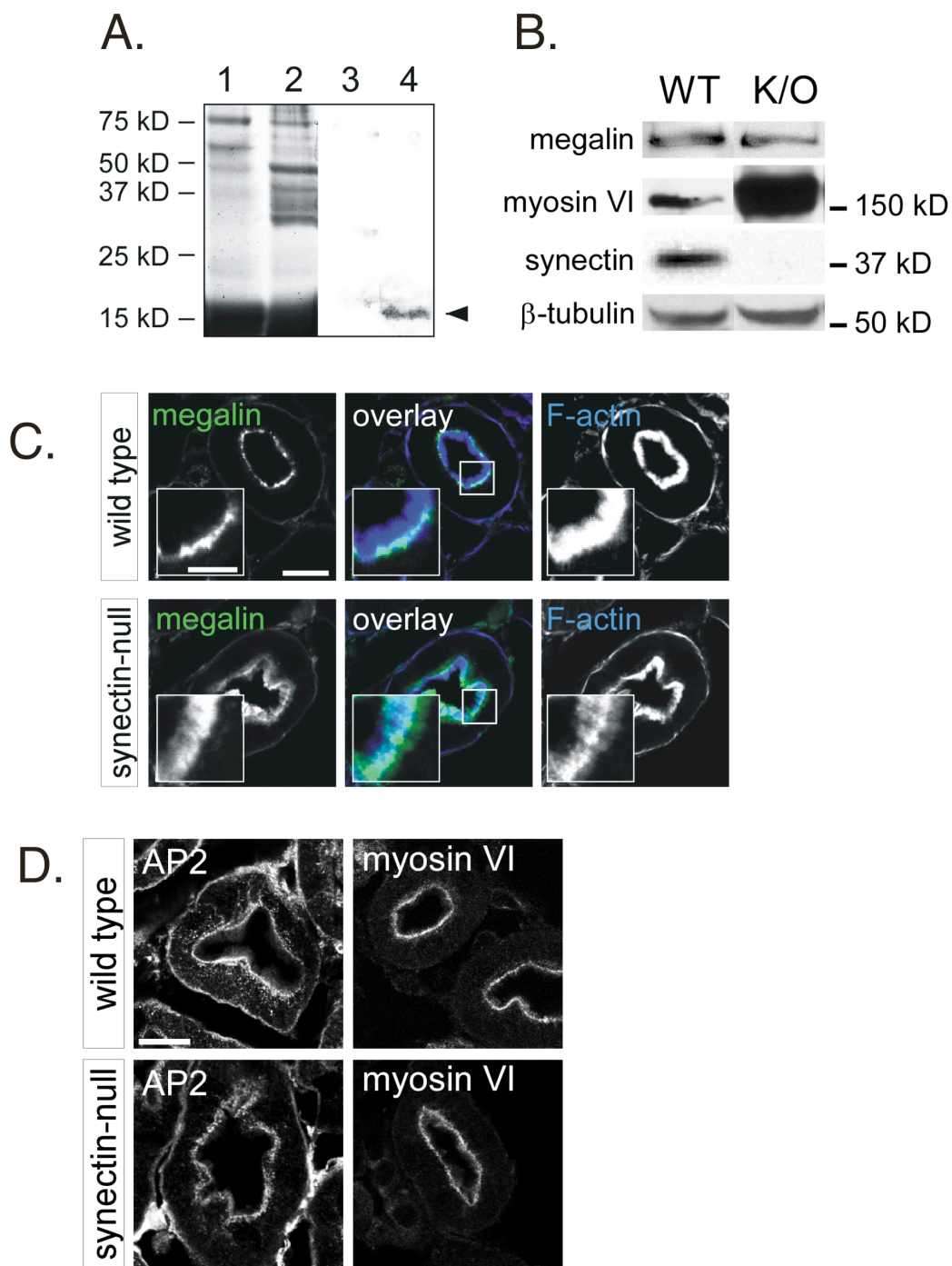


Figure 3.7. Dopamine Receptor 2 targets minimally to the myosin VI associated endocytic vesicle population. (A) GFP-D2R shows unconvincing overlap with M6 on endocytic vesicles. Lower panels are magnifications of the boxed regions above. Scale bar = 10 microns. arrows indicate representative GFP-D2R-associated vesicles that do not overlap with myosin VI. (B) Histogram representing the percentage of overlap between the endocytic vesicle markers AP2 (adaptor protein to clathrin), Myosin VI or GIPC and GFP tagged Dopamine receptor 2 (GFPD2) and GFP tagged Dopamine receptor 3 (GFPD3). 150 vesicles were counted for each data point, n=2 where SD are available.

Figure 3.8. Proteinuria and altered megalin distribution in synectin-null mice.

(A) Coomassie-stained gel of urine samples from WT and from synectin-null mice revealed the presence of multiple bands in the synectin-null sample which were absent from the WT samples, indicative of proteinuria. Immunoblotting of similar urine samples detected the presence of the megalin ligand RBP in the synectin-null urine sample. (B) Immunoblots of synectin, myosin VI, and megalin in WT and synectin-null mice. 50 mg of total protein were loaded in each lane. The synectin-null myosin VI band was ~6-fold heavier than the WT one, as measured by densitometry. β -tubulin immunoblot was used as a loading control. (C) Confocal images of 4 μ m cryosections of WT and synectin-null mouse kidneys stained for megalin (green, left panels) and F-actin (blue, center panels). Megalin was enriched at the base of the actin-rich microvilli in WT kidney. In synectin-null kidney, however, megalin was distributed along the length of microvilli/brush border where it collocated with F-actin. (D) Confocal images of 4 μ m cryosections of formaldehyde-fixed WT and synectin-null mouse kidneys stained for AP-2 and F-actin. There were no significant differences in AP-2 and myosin VI distribution between WT and synectin-null proximal tubules (scale bars: 5 μ m, 2.5 μ m in insets).



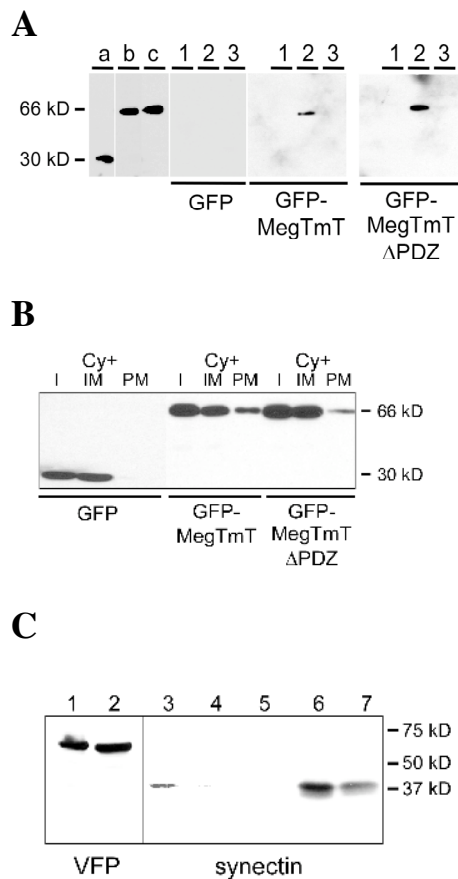
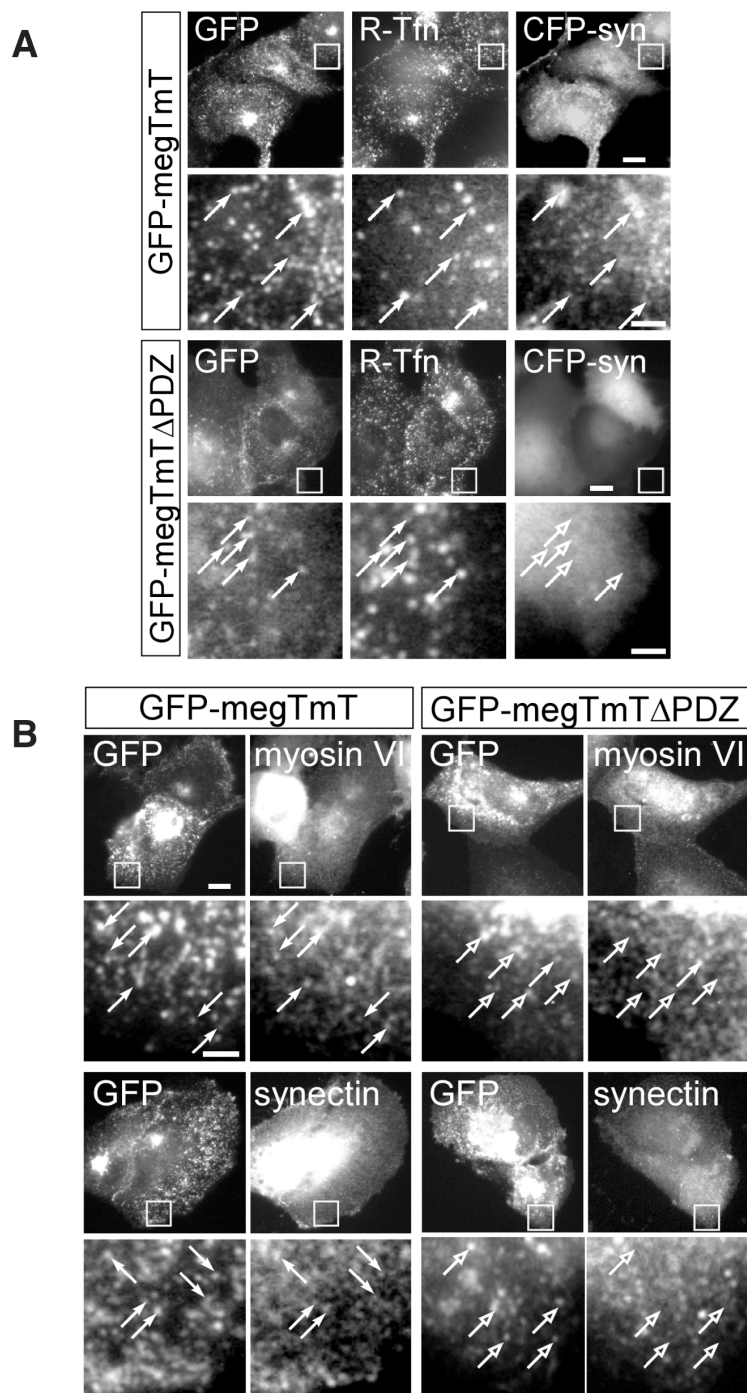


Figure 3.9. Confirmation of the correct targeting of GFP-MegTmT and GFP-MegTmT Δ PDZ constructs. (A) Effect of megalin PBM deletion on megalin targeting to the plasma membrane. ARPE-19 cells transiently expressing GFP, GFP-MegTmT, or GFP-MegTmT Δ PDZ (see total lysate lanes a, b, and c, respectively) were left untreated on ice (lane 1), biotinylated on ice (2), or biotinylated on ice followed by reduction to release surface biotin (3). See Materials and Methods for details. Biotinylated proteins were isolated by incubation with streptavidin-agarose beads, separated by SDS-PAGE and immunoblotted with anti-VFP. (B) Subcellular fractionation of ARPE-19 cells expressing GFP, GFP-MegTmT or pGFP-MegTmT Δ PDZ confirmed membrane association of the megalin constructs. See Materials and Methods for details (I, whole cell lysates; Cy+IM, cytoplasmic fraction derived from the post nuclear supernatant including internal membranes; PM, plasma membrane fraction). (C) Coimmunoprecipitation of synectin with GFP-MegTmT or GFP-MegTmT Δ PDZ. ARPE-19 cells expressing GFP-MegTmT (lanes 1, 3, 5, 6) or GFP-MegTmT Δ PDZ (lanes 2, 4, 7) were lysed and immunoprecipitated with anti-VFP (lanes 3, 4) or non-immune IgG (lane 5), and probed with the indicated antibodies. GFP-MegTmT Δ PDZ did not coimmunoprecipitate with synectin (lane 4).

Figure 3.10. Synectin binding to the PBM of megalin is required for synectin and myosin VI recruitment to UCV. (A) ARPE-19 cells co-expressing GFP-MegTmT or pGFP-MegTmT Δ PDZ and CFP-Synectin were subjected to 2 min R-Tfn pulse-chase uptake, fixed and imaged. (B) Indirect immunofluorescence staining of ARPE-19 cells expressing GFP-MegTmT or GFP-MegTmT Δ PDZ labeled with anti-myosin VI or anti synectin. The panels in the 2nd and 4th rows in B and C are enlargements of the boxed regions in the 1st and 3rd rows. Filled arrows indicate collocation of GFP constructs, CFP constructs, and R-Tfn; open arrows indicate absence of collocation (scale bars: 10 μ m, 2.5 μ m in enlarged panels).



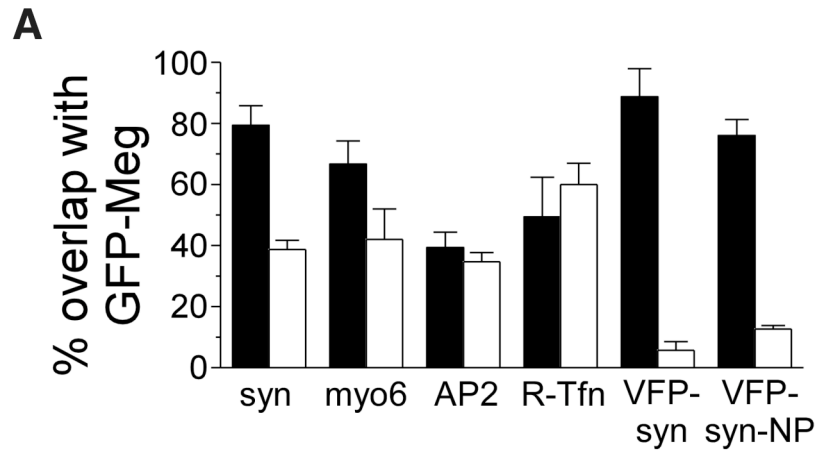


Figure 3.11. Quantification of the collocation of GFP-MegTmT- or GFP-MegTmT Δ PDZ- and endocytic markers. Quantification of the collocation of GFP-MegTmT- (black bars) or GFP-MegTmT Δ PDZ- (white bars) containing vesicles with endogenous synectin (syn), myosin VI (myo6), AP-2 (see also Fig 11A), R-Tfn, VFP-synectin, and VFP-syn-NP (see also Fig 11B). N=150 vesicles were counted from at least three cells.

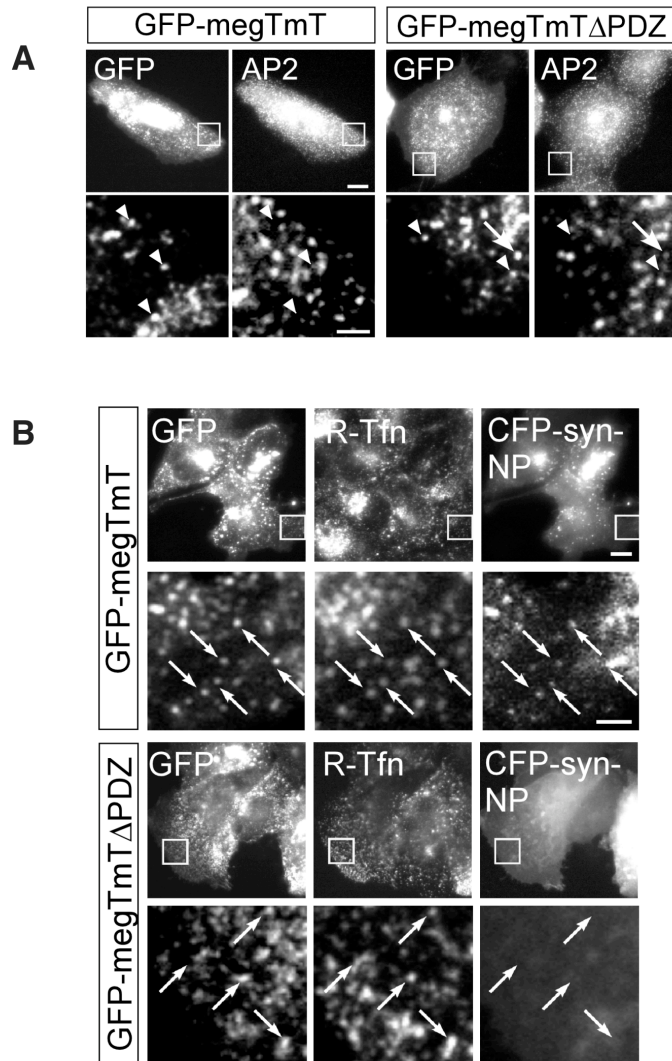


Figure 3.12. Confirmation of the correct targeting of GFP-MegTmT and GFP-MegTmT Δ PDZ constructs. (A) Indirect immunofluorescence staining of endogenous AP-2 in cells transiently expressing GFP-MegTmT or GFP-MegTmT Δ PDZ. The panels in the bottom row are enlargements of the boxed regions in the top row. (B) ARPE-19 cells co-expressing GFP-MegTmT or pGFP-MegTmT Δ PDZ and CFP-Syn-NP were subjected to 2 min R-Tfn pulse-chase uptake, fixed and imaged. The panels in the 2nd and 4th rows are enlargements of the boxed regions in the 1st and 3rd rows (scale bars: 10 μ m, 2.5 μ m in enlarged panels). Data in A and B is quantified in Fig 9C.

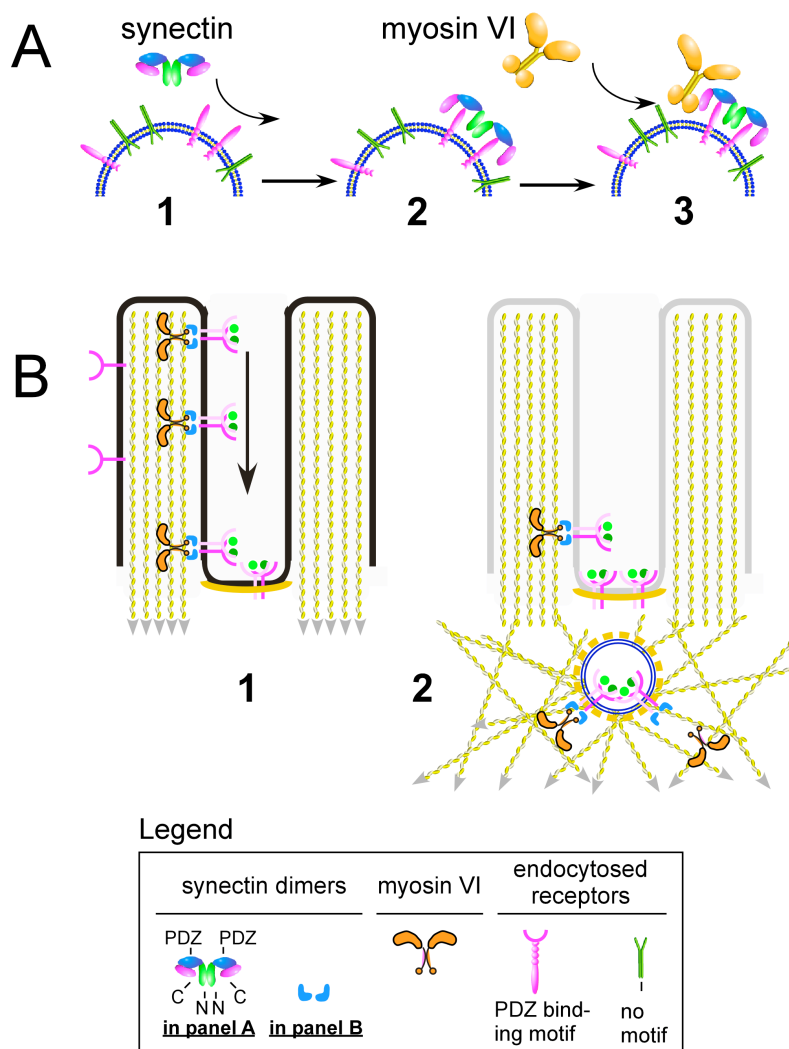


Figure 3.13. Scheme of myosin VI docking to UCV and synectin function in kidney proximal tubules. A. (1) following vesicle uncoating, PBMs at the carboxy-termini of endocytosed dimerized receptors are exposed; (2) the PDZ domains of cytoplasmic synectin dimers engage the carboxy-termini of the endocytosed receptors. This interaction stabilizes synectin in a conformation where its carboxy-terminus is accessible for binding myosin VI; (3) the globular tails of myosin VI monomers bind to the now-available carboxy-termini of synectin dimers; myosin VI dimerizes. B. Hypothetically, synectin participates in two myosin VI-driven stages of megalin recycling: (1) translocation of dimeric megalin towards the minus end of microvillar actin filaments; (2) translocation of megalin-containing UCV through the cortical F-actin mesh of the proximal tubule epithelial cells.

Table 3.1. Synectin constructs expressed in ARPE-19 cells, their expression patterns, and their uptake characteristics (n/a – not applicable).

Synectin constructs	Expression pattern in ARPE-19 cells	Overlap with R-Tfn after 2 min pulse-chase uptake	Overlap with endogenous myosin VI
VFP-syn	UCV	68%±7.2	70%±2%
VFP-syn-PDZ ⁻	diffuse	n/a	n/a
VFP-syn-N	diffuse	n/a	n/a
VFP-syn-NP	UCV	68.6±%7.57%	20.5%±8%
VFP-syn-P	FA	none	3.00%
VFP-syn-PC	FA	none	n/a
VFP-syn-C	diffuse	n/a	n/a

Table 3.2. List of primers used for generation of synectin constructs. Primers for pEYFP-N1-syn-PDZ⁻ and pGFP-MegTmT-ΔPDZ were used for site-directed mutagenesis.

Construct	5' primer	3' primer
pECFP-N1-syn-N	GGAATTCCGACGAGGACCGAGCAGGG	GGGATCCAACCTCTTTG CGCTGCCCTTC
pEGFP-N3-syn-NP	GGAATTCCGACGAGGACCGAGCAGGG	CGGGATCCGGCCTTTC GAGGTTCTGTGAGTT
pEGFP-N3-syn-P	GGAATTCATGCAGCGCAAAGAGGTGG AAG	CGGGATCCGGCCTTTC GAGGTTCTGTGA
pEGFP-N3-syn-PC	GGAATTCATGCAGCGCAAAGAGGTGG AAG	CGGGATCCGTAGCGGC CAACCTTGG
pECFP-C1-syn-C	GGAATTCGAACCTCGAAAGGCCTTTGA TATG	CGGGATCCGTAGCGGC CAACCTTGGC
pECFP-N1-syn(1-304)	GGAATTCCGACGAGGACCGAGCAGGG	GGGATCCAACAGGGCT TCTGCCAGCTCGT
pEYFP-N1-syn-PDZ ⁻	GTCGGAGGAGGCTGCGGAGCTACCA TCACCGAC	GTCGGTGATGGTGAGC TCCGCAGCCTCCTCCG AC
pGFP-MegTmT-ΔPDZ	CGCAAATCTTGTTAAAGAATAGTCTGAA GTATAGTCTAGAGG	CCTCTAGACTATACTTC AGACTATTCTTTAACAA GATTTGCG

CONCLUSION

Myosin VI targets to uncoated endocytic vesicles in our model system, the retinal pigmented epithelial cell line ARPE-19 (Aschenbrenner, Lee et al. 2003). We had already tested the role of myosin VI in vesicle transport and cargo trafficking by characterizing the motile properties of uncoated vesicles using GFP-tagged versions of myosin VI as markers. Timelapse microscopy revealed that myosin VI-associated uncoated vesicles were motile, and that in the absence of myosin VI motor activity, uncoated vesicles remain trapped in the actin mesh. In the first chapter of this dissertation, I tested the importance of cortical F-actin in endocytic vesicle trafficking to determine whether actin is a barrier to myosin VI-associated vesicle trafficking, and if myosin VI is the motor used to cross that barrier. Depolymerization of the actin cytoskeleton rescued the block in transferrin trafficking to the pericentriolar region imposed by myosin VI motor mutants. Depolymerization also specifically accelerated transferrin delivery to the early endosome without affecting earlier steps in endocytosis. Therefore we showed that actin is a physical barrier impeding inward uncoated vesicle trafficking, and myosin VI is recruited to move the vesicles through this barrier for fusion with the early endosome.

Recent kinetic studies have shown that myosin VI displays altered ADP release kinetics under different load conditions allowing myosin VI to serve alternately as a transporter, as in the previous chapter, or as a tension sensor that tethers

membrane and protein elements to actin. In the second chapter of this dissertation, I theorized that one potential regulatory event to modulate between these kinetic choices is phosphorylation at a conserved site, threonine 406 (T406) in the myosin VI motor domain. Alterations mimicking the phosphorylated (T406E) and dephosphorylated state (T406A) were introduced into a GFP-myosin VI fusion construct (GFP-M6). Live cell imaging revealed that GFP-M6(T406E) expression changed the path myosin VI took in its transport of UCVs. Rather than routing vesicles inwards as seen in GFP-M6 and GFP-M6(T406A) expressing cells, GFP-M6(T406E) moved vesicles into clusters at distinct peripheral sites. GFP-M6(T406E) expression also increased the density of the actin cytoskeleton. Filaments were enriched at the vesicle cluster sites. This was not due to redistribution of the actin polymerization machinery and instead correlated with tight binding of GFP-M6(T406E) to F-actin, leading to inhibition of depolymerization at actin filament minus ends. Our study suggests that phosphorylation at T406 changes the nature of myosin VI's interaction with actin *in vivo*. By entering into the actin bound state more quickly, it is possible that myosin VI now acts as an anchor onto actin. Future studies would have to include determining the systems in which myosin VI is phosphorylated *in vivo* at threonine 406. In addition, actin depolymerization studies *in vitro* would need to be conducted to determine if M6(T406E) stabilizes the filament *in vitro*. For this purpose we would require dimerized M6(T406E) bound to cargo in order to recreate the conditions we think are necessary for myosin VI to initiate actin filament stabilization.

Myosin VI is mainly found in a cytoplasmic pool suggesting that its docking to cargoes is regulated. While we have investigated the method of regulation of myosin VI interaction with the actin filament, regulation must also occur at the level of myosin VI targeting to its cargo. Myosin VI participates in two steps of endocytic trafficking; it is recruited to both clathrin-coated pits and to ensuing uncoated endocytic vesicles (UCV). While there is evidence suggesting that the PDZ adaptor protein GIPC/synectin is involved in the association of myosin VI with UCV, the recruitment mechanism is unknown. In the final chapter of this dissertation, I have shown that GIPC/synectin is required for both the internalization of cell surface receptors and for the coupling of myosin VI to UCV. This coupling occurs via a novel mechanism wherein engagement of the GIPC/synectin PDZ domain by the carboxy-termini of internalized receptors facilitates *in trans* myosin VI binding to the GIPC/synectin carboxy-terminus which is located outside of the PDZ domain. Analysis of megalin, a prototypical GIPC/synectin-binding receptor, revealed that deletion of its PDZ-binding motif drastically reduces GIPC/synectin and myosin VI recruitment to UCV. Furthermore, interaction with GIPC/synectin is required for megalin's function, as megalin was mistargeted in the renal proximal tubules of GIPC/synectin-null mice and these mice exhibited proteinuria, a condition consistent with defective megalin trafficking.

In summary, we conclude that myosin VI functions to transport uncoated endocytic vesicles through the actin meshwork in our model retinal pigmented epithelial cell system. We provide evidence that *in vivo*, myosin VI is regulated to act

as a transporter or tension sensing anchor to actin by alteration at threonine 406. Finally, we provide a mechanism for myosin VI recruitment to the UCV cargo through its adapter GIPC/synectin via activation of the GIPC/synectin PDZ domain by PDZ motif containing receptors.

REFERENCES

- Ahmed, Z. M., R. J. Morell, S. Riazuddin, A. Gropman, S. Shaukat, M. M. Ahmad, S. A. Mohiddin, L. Fananapazir, R. C. Caruso, T. Husnain, S. N. Khan, A. J. Griffith, T. B. Friedman and E. R. Wilcox (2003). "Mutations of MYO6 are associated with recessive deafness, DFNB37." Am J Hum Genet **72**(5): 1315-22.
- Altman, D., H. L. Sweeney and J. A. Spudich (2004). "The mechanism of myosin VI translocation and its load-induced anchoring." Cell **116**(5): 737-49.
- Anderson, B. L., I. Boldogh, M. Evangelista, C. Boone, L. A. Greene and L. A. Pon (1998). "The Src homology domain 3 (SH3) of a yeast type I myosin, Myo5p, binds to verprolin and is required for targeting to sites of actin polarization." J Cell Biol **141**(6): 1357-70.
- Apodaca, G. (2001). "Endocytic traffic in polarized epithelial cells: role of the actin and microtubule cytoskeleton." Traffic **2**(3): 149-59.
- Aschenbrenner, L. (2004). "Myosin VI moves nascent uncoated endocytic vesicles." PhD Dissertation, University of California, San Diego. Chapter 4.
- Aschenbrenner, L., T. Lee and T. Hasson (2003). "Myo6 facilitates the translocation of endocytic vesicles from cell peripheries." Mol Biol Cell **14**(7): 2728-43.
- Aschenbrenner, L., S. N. Naccache and T. Hasson (2004). "Uncoated endocytic vesicles require the unconventional myosin, Myo6, for rapid transport through actin barriers." Mol Biol Cell **15**(5): 2253-63.
- Avraham, K. B., T. Hasson, T. Sobe, B. Balsara, J. R. Testa, A. B. Skvorak, C. C. Morton, N. G. Copeland and N. A. Jenkins (1997). "Characterization of unconventional MYO6, the human homologue of the gene responsible for deafness in Snell's waltzer mice." Hum Mol Genet **6**(8): 1225-31.

- Avraham, K. B., T. Hasson, K. P. Steel, D. M. Kingsley, L. B. Russell, M. S. Mooseker, N. G. Copeland and N. A. Jenkins (1995). "The mouse Snell's waltzer deafness gene encodes an unconventional myosin required for structural integrity of inner ear hair cells." Nature genetics **11**: 369-375.
- Bahler, J. and P. Nurse (2001). "Fission yeast Pom1p kinase activity is cell cycle regulated and essential for cellular symmetry during growth and division." Embo J **20**(5): 1064-73.
- Bahloul, A., G. Chevreux, A. L. Wells, D. Martin, J. Nolt, Z. Yang, L. Q. Chen, N. Potier, A. Van Dorsselaer, S. Rosenfeld, A. Houdusse and H. L. Sweeney (2004). "The unique insert in myosin VI is a structural calcium-calmodulin binding site." Proc Natl Acad Sci U S A **101**(14): 4787-92.
- Barylko, B., D. D. Binns and J. P. Albanesi (2000). "Regulation of the enzymatic and motor activities of myosin I." Biochim Biophys Acta **1496**(1): 23-35.
- Barylko, B., G. Jung and J. P. Albanesi (2005). "Structure, function, and regulation of myosin 1C." Acta Biochim Pol **52**(2): 373-80.
- Bement, W. M. and M. S. Mooseker (1995). "TEDS rule: a molecular rationale for differential regulation of myosins by phosphorylation of the heavy chain head." Cell Motil Cytoskeleton **31**(2): 87-92.
- Berg, J. S., B. C. Powell and R. E. Cheney (2001). "A millennial myosin census." Mol Biol Cell **12**(4): 780-94.
- Biemesderfer, D., B. DeGray and P. S. Aronson (2001). "Active (9.6 s) and inactive (21 s) oligomers of NHE3 in microdomains of the renal brush border." J Biol Chem **276**(13): 10161-7.
- Biemesderfer, D., S. A. Mentone, M. Mooseker and T. Hasson (2002). "Expression of myosin VI within the early endocytic pathway in adult and developing proximal tubules." Am J Physiol Renal Physiol **282**(5): F785-94.
- Blobe, G. C., X. Liu, S. J. Fang, T. How and H. F. Lodish (2001). "A novel mechanism for regulating transforming growth factor beta (TGF-beta)

- signaling. Functional modulation of type III TGF-beta receptor expression through interaction with the PDZ domain protein, GIPC." J Biol Chem **276**(43): 39608-17.
- Bohrmann, J. (1997). "Drosophila unconventional myosin VI is involved in intra- and intercellular transport during oogenesis." Cell Mol Life Sci **53**(8): 652-62.
- Boldogh, I. R., S. L. Ramcharan, H. C. Yang and L. A. Pon (2004). "A type V myosin (Myo2p) and a Rab-like G-protein (Ypt11p) are required for retention of newly inherited mitochondria in yeast cells during cell division." Mol Biol Cell **15**(9): 3994-4002.
- Booth, R. A., C. Cummings, M. Tiberi and X. J. Liu (2002). "GIPC participates in G protein signaling downstream of insulin-like growth factor 1 receptor." J Biol Chem **277**(8): 6719-25.
- Bose, A., A. Guilherme, S. I. Robida, S. M. Nicoloso, Q. L. Zhou, Z. Y. Jiang, D. P. Pomerleau and M. P. Czech (2002). "Glucose transporter recycling in response to insulin is facilitated by myosin Myo1c." Nature **420**(6917): 821-4.
- Brzeska, H., R. Young, U. Knaus and E. D. Korn (1999). "Myosin I heavy chain kinase: cloning of the full-length gene and acidic lipid-dependent activation by Rac and Cdc42." Proceedings of the National Academy of Science USA **96**(2): 394-399.
- Brzeska, H., R. Young, C. Tan, J. Szczepanowska and E. D. Korn (2001). "Calmodulin-binding and autoinhibitory domains of Acanthamoeba myosin I heavy chain kinase, a p21-activated kinase (PAK)." The Journal of Biological Chemistry **276**(50): 47468-47473.
- Bunn, R. C., M. A. Jensen and B. C. Reed (1999). "Protein interactions with the glucose transporter binding protein GLUT1CBP that provide a link between GLUT1 and the cytoskeleton." Mol Biol Cell **10**(4): 819-32.
- Buss, F., S. D. Arden, M. Lindsay, J. P. Luzio and J. Kedrick-Jones (2001). "Myosin VI isoform localized to clathrin-coated vesicles with a role in clathrin-mediated endocytosis." EMBO Journal **20**(14): 3676-3684.

- Buss, F., S. D. Arden, M. Lindsay, J. P. Luzio and J. Kendrick-Jones (2001). "Myosin VI isoform localized to clathrin-coated vesicles with a role in clathrin-mediated endocytosis." Embo J **20**(14): 3676-84.
- Buss, F., J. Kendrick-Jones, C. Lionne, A. E. Knight, G. P. Cote and J. P. Luzio (1998). "The localization of myosin VI at the golgi complex and leading edge of fibroblasts and its phosphorylation and recruitment into membrane ruffles of A431 cells after growth factor stimulation." The Journal of Cell Biology **143**: 1535-1545.
- Buss, F., J. Kendrick-Jones, C. Lionne, A. E. Knight, G. P. Cote and J. Paul Luzio (1998). "The localization of myosin VI at the golgi complex and leading edge of fibroblasts and its phosphorylation and recruitment into membrane ruffles of A431 cells after growth factor stimulation." J Cell Biol **143**(6): 1535-45.
- Cai, H. and R. R. Reed (1999). "Cloning and characterization of neuropilin-1-interacting protein: a PSD-95/Dlg/ZO-1 domain-containing protein that interacts with the cytoplasmic domain of neuropilin-1." J Neurosci **19**(15): 6519-27.
- Chavrier, P. (2002). "May the force be with you: Myosin-X in phagocytosis." Nat Cell Biol **4**(7): E169-71.
- Christensen, E. I. and H. Birn (2002). "Megalin and cubilin: multifunctional endocytic receptors." Nat Rev Mol Cell Biol **3**(4): 256-66.
- Christensen, E. I., J. O. Moskaug, H. Vorum, C. Jacobsen, T. E. Gundersen, A. Nykjaer, R. Blomhoff, T. E. Willnow and S. K. Moestrup (1999). "Evidence for an essential role of megalin in transepithelial transport of retinol." J Am Soc Nephrol **10**(4): 685-95.
- Clague, M. J. (1998). "Molecular aspects of the endocytic pathway." Biochem J **336** (Pt 2): 271-82.
- Coluccio, L. M. (1997). "Myosin I." Am J Physiol **273**(2 Pt 1): C347-59.

- Dance, A. L., M. Miller, S. Seragaki, P. Aryal, B. White, L. Aschenbrenner and T. Hasson (2004). "Regulation of myosin-VI targeting to endocytic compartments." Traffic **5**(10): 798-813.
- De La Cruz, E. M., E. M. Ostap and H. L. Sweeney (2001). "Kinetic mechanism and regulation of myosin VI." J Biol Chem **276**(34): 32373-81.
- De Vries, L., X. Lou, G. Zhao, B. Zheng and M. G. Farquhar (1998). "GIPC, a PDZ domain containing protein, interacts specifically with the C terminus of RGS-GAIP." Proc Natl Acad Sci U S A **95**(21): 12340-5.
- Deng, W., K. Leaper and M. Bownes (1999). "A targeted gene silencing technique shows that *Drosophila* myosin VI is required for egg chamber and imaginal disc morphogenesis." J Cell Sci **112** (Pt 21): 3677-90.
- Desnos, C., J. S. Schonn, S. Huet, V. S. Tran, A. El-Amraoui, G. Raposo, I. Fanget, C. Chapuis, G. Menasche, G. de Saint Basile, C. Petit, S. Cribier, J. P. Henry and F. Darchen (2003). "Rab27A and its effector MyRIP link secretory granules to F-actin and control their motion towards release sites." J Cell Biol **163**(3): 559-70.
- Dunn, K. C., A. E. Aotaki-Keen, F. R. Putkey and L. M. Hjelmeland (1996). "ARPE-19, a human retinal pigment epithelial cell line with differentiated properties." Exp Eye Res **62**(2): 155-69.
- Durrwang, U., S. Fujita-Becker, M. Erent, F. J. Kull, G. Tsiavaliaris, M. A. Geeves and D. J. Manstein (2006). "Dictyostelium myosin-IE is a fast molecular motor involved in phagocytosis." J Cell Sci **119**(Pt 3): 550-8.
- Eitzen, G. (2003). "Actin remodeling to facilitate membrane fusion." Biochim Biophys Acta **1641**(2-3): 175-81.
- El Mourabit, H., P. Poinat, J. Koster, H. Sondermann, V. Wixler, E. Wegener, E. Laplantine, D. Geerts, E. Georges-Labouesse, A. Sonnenberg and M. Aumailley (2002). "The PDZ domain of TIP-2/GIPC interacts with the C-terminus of the integrin alpha5 and alpha6 subunits." Matrix Biol **21**(2): 207-14.

- Eskelinen, S., J. W. Kok, R. Sormunen and D. Hoekstra (1991). "Coated endosomal vesicles: sorting and recycling compartment for transferrin in BHK cells." Eur J Cell Biol **56**(2): 210-22.
- Evangelista, M., B. M. Klebl, A. H. Tong, B. A. Webb, T. Leeuw, E. Leberer, M. Whiteway, D. Y. Thomas and C. Boone (2000). "A role for myosin-I in actin assembly through interactions with Vrp1p, Bee1p, and the Arp2/3 complex." J Cell Biol **148**(2): 353-62.
- Frank, D. J., T. Noguchi and K. G. Miller (2004). "Myosin VI: a structural role in actin organization important for protein and organelle localization and trafficking." Curr Opin Cell Biol **16**(2): 189-94.
- Fujimoto, L. M., R. Roth, J. E. Heuser and S. L. Schmid (2000). "Actin assembly plays a variable, but not obligatory role in receptor-mediated endocytosis in mammalian cells." Traffic **1**(2): 161-71.
- Fukuda, M., T. S. Kuroda and K. Mikoshiba (2002). "Slac2-a/melanophilin, the missing link between Rab27 and myosin Va: implications of a tripartite protein complex for melanosome transport." J Biol Chem **277**(14): 12432-6.
- Gaidarov, I., F. Santini, R. A. Warren and J. H. Keen (1999). "Spatial control of coated-pit dynamics in living cells." Nat Cell Biol **1**(1): 1-7.
- Gao, Y., M. Li, W. Chen and M. Simons (2000). "Synectin, syndecan-4 cytoplasmic domain binding PDZ protein, inhibits cell migration." J Cell Physiol **184**(3): 373-9.
- Geisbrecht, E. R. and D. J. Montell (2002). "Myosin VI is required for E-cadherin-mediated border cell migration." Nat Cell Biol **4**(8): 616-20.
- Gorvel, J. P., P. Chavrier, M. Zerial and J. Gruenberg (1991). "rab5 controls early endosome fusion in vitro." Cell **64**(5): 915-25.
- Gotthardt, M., M. Trommsdorff, M. F. Nevitt, J. Shelton, J. A. Richardson, W. Stockinger, J. Nimpf and J. Herz (2000). "Interactions of the low density

lipoprotein receptor gene family with cytosolic adaptor and scaffold proteins suggest diverse biological functions in cellular communication and signal transduction." J Biol Chem **275**(33): 25616-24.

Gottlieb, T. A., I. E. Ivanov, M. Adesnik and D. D. Sabatini (1993). "Actin microfilaments play a critical role in endocytosis at the apical but not the basolateral surface of polarized epithelial cells." J Cell Biol **120**(3): 695-710.

Grosshans, B. L., H. Grotzsch, D. Mukhopadhyay, I. M. Fernandez, J. Pfannstiel, F. Z. Idrissi, J. Lechner, H. Riezman and M. I. Geli (2006). "TEDS site phosphorylation of the yeast myosins I is required for ligand-induced but not for constitutive endocytosis of the G protein-coupled receptor Ste2p." J Biol Chem **281**(16): 11104-14.

Gruenberg, J. (2001). "The endocytic pathway: a mosaic of domains." Nat Rev Mol Cell Biol **2**(10): 721-30.

Hanover, J. A., M. C. Willingham and I. Pastan (1984). "Kinetics of transit of transferrin and epidermal growth factor through clathrin-coated membranes." Cell **39**(2 Pt 1): 283-93.

Harsfalvi, J., L. Fesus, E. Tarcsa, J. Laczko and A. G. Loewy (1991). "The presence of a covalently cross-linked matrix in human platelets." Biochim Biophys Acta **1073**(2): 268-74.

Hasson, T. (2003). "Myosin VI: two distinct roles in endocytosis." J Cell Sci **116**(Pt 17): 3453-61.

Hasson, T., P. G. Gillespie, J. A. Garcia, R. B. MacDonald, Y. Zhao, A. G. Yee, M. S. Mooseker and D. P. Corey (1997). "Unconventional myosins in inner-ear sensory epithelia." J Cell Biol **137**(6): 1287-307.

Hasson, T. and M. S. Mooseker (1994). "Porcine myosin-VI: characterization of a new mammalian unconventional myosin." J Cell Biol **127**(2): 425-40.

- Hayden, S. M., J. S. Wolenski and M. S. Mooseker (1990). "Binding of brush border myosin I to phospholipid vesicles." J Cell Biol **111**(2): 443-51.
- Heintzelman, M. B., T. Hasson and M. S. Mooseker (1994). "Multiple unconventional myosin domains of the intestinal brush border cytoskeleton." J Cell Sci **107** (Pt **12**): 3535-43.
- Hicks, J. L., W. M. Deng, A. D. Rogat, K. G. Miller and M. Bownes (1999). "Class VI unconventional myosin is required for spermatogenesis in *Drosophila*." Mol Biol Cell **10**(12): 4341-53.
- Higgins, M. K. and H. T. McMahon (2002). "Snap-shots of clathrin-mediated endocytosis." Trends Biochem Sci **27**(5): 257-63.
- Hirakawa, T., C. Galet, M. Kishi and M. Ascoli (2003). "GIPC binds to the human lutropin receptor (hLHR) through an unusual PDZ domain binding motif, and it regulates the sorting of the internalized human choriogonadotropin and the density of cell surface hLHR." J Biol Chem **278**(49): 49348-57.
- Hopkins, C. R. (1983). "The importance of the endosome in intracellular traffic." Nature **304**(5928): 684-5.
- Horowitz, A., E. Tkachenko and M. Simons (2002). "Fibroblast growth factor-specific modulation of cellular response by syndecan-4." J Cell Biol **157**(4): 715-25.
- Inoue, A., O. Sato, K. Homma and M. Ikebe (2002). "DOC-2/DAB2 is the binding partner of myosin VI." Biochem Biophys Res Commun **292**(2): 300-7.
- Iwaki, M., H. Tanaka, A. H. Iwane, E. Katayama, M. Ikebe and T. Yanagida (2006). "Cargo-binding makes a wild-type single-headed myosin-VI move processively." Biophys J **90**(10): 3643-52.
- Jackman, M. R., W. Shurety, J. A. Ellis and J. P. Luzio (1994). "Inhibition of apical but not basolateral endocytosis of ricin and folate in Caco-2 cells by cytochalasin D." J Cell Sci **107** (Pt **9**): 2547-56.

- Jeanneteau, F., J. Diaz, P. Sokoloff and N. Griffon (2004). "Interactions of GIPC with dopamine D2, D3 but not D4 receptors define a novel mode of regulation of G protein-coupled receptors." Mol Biol Cell **15**(2): 696-705.
- Jung, E. J., G. Liu, W. Zhou and X. Chen (2006). "Myosin VI is a mediator of the p53-dependent cell survival pathway." Mol Cell Biol **26**(6): 2175-86.
- Jung, G., K. Remmert, X. Wu, J. M. Volosky and J. A. Hammer, 3rd (2001). "The Dictyostelium CARMIL protein links capping protein and the Arp2/3 complex to type I myosins through their SH3 domains." J Cell Biol **153**(7): 1479-97.
- Kachar, B., A. Battaglia and J. Fex (1997). "Compartmentalized vesicular traffic around the hair cell cuticular plate." Hear Res **107**(1-2): 102-12.
- Kappler, J. A., C. J. Starr, D. K. Chan, R. Kollmar and A. J. Hudspeth (2004). "A nonsense mutation in the gene encoding a zebrafish myosin VI isoform causes defects in hair-cell mechanotransduction." Proc Natl Acad Sci U S A **101**(35): 13056-61.
- Karcher, R. L., J. T. Roland, F. Zappacosta, M. J. Huddleston, R. S. Annan, S. A. Carr and V. I. Gelfand (2001). "Cell cycle regulation of myosin-V by calcium/calmodulin-dependent protein kinase II." Science **293**(5533): 1317-20.
- Kelleher, J. F., M. A. Mandell, G. Moulder, K. L. Hill, S. W. L'Hernault, R. Barstead and M. A. Titus (2000). "Myosin VI is required for asymmetric segregation of cellular components during *C. elegans* spermatogenesis." Curr Biol **10**(23): 1489-96.
- Kitamoto, J., R. T. Libby, D. Gibbs, K. P. Steel and D. S. Williams (2005). "Myosin VI is required for normal retinal function." Exp Eye Res **81**(1): 116-20.
- Kozyraki, R., J. Fyfe, P. J. Verroust, C. Jacobsen, A. Dautry-Varsat, J. Gburek, T. E. Willnow, E. I. Christensen and S. K. Moestrup (2001). "Megalin-dependent cubilin-mediated endocytosis is a major pathway for the apical uptake of transferrin in polarized epithelia." Proc Natl Acad Sci U S A **98**(22): 12491-6.

- Krendel, M. and M. S. Mooseker (2005). "Myosins: tails (and heads) of functional diversity." Physiology (Bethesda) **20**: 239-51.
- Kreplak, L., U. Aebi and H. Herrmann (2004). "Molecular mechanisms underlying the assembly of intermediate filaments." Exp Cell Res **301**(1): 77-83.
- Kuroda, T. S., H. Ariga and M. Fukuda (2003). "The actin-binding domain of Slac2-a/melanophilin is required for melanosome distribution in melanocytes." Mol Cell Biol **23**(15): 5245-55.
- Lamaze, C., L. M. Fujimoto, H. L. Yin and S. L. Schmid (1997). "The actin cytoskeleton is required for receptor-mediated endocytosis in mammalian cells." J Biol Chem **272**(33): 20332-5.
- Lechler, T., A. Shevchenko and R. Li (2000). "Direct involvement of yeast type I myosins in Cdc42-dependent actin polymerization." J Cell Biol **148**(2): 363-73.
- Lee, S. F., T. T. Egelhoff, A. Mahasneh and G. P. Cote (1996). "Cloning and characterization of a Dictyostelium myosin I heavy chain kinase activated by Cdc42 and Rac." The Journal of Biological Chemistry **271**(43): 27044-27048.
- Leheste, J. R., B. Rolinski, H. Vorum, J. Hilpert, A. Nykjaer, C. Jacobsen, P. Aucouturier, J. O. Moskaug, A. Otto, E. I. Christensen and T. E. Willnow (1999). "Megalin knockout mice as an animal model of low molecular weight proteinuria." Am J Pathol **155**(4): 1361-70.
- Lister, I., S. Schmitz, M. Walker, J. Trinick, F. Buss, C. Veigel and J. Kendrick-Jones (2004). "A monomeric myosin VI with a large working stroke." Embo J **23**(8): 1729-38.
- Liu, M. and A. Horowitz (2006). "A PDZ-binding motif as a critical determinant of Rho guanine exchange factor function and cell phenotype." Mol Biol Cell **17**(4): 1880-7.

- Liu, T. F., G. Kandala and V. Setaluri (2001). "PDZ domain protein GIPC interacts with the cytoplasmic tail of melanosomal membrane protein gp75 (tyrosinase-related protein-1)." J Biol Chem **276**(38): 35768-77.
- Liu, X., N. Osherov, R. Yamashita, H. Brzeska, E. D. Korn and G. S. May (2001). "Myosin I mutants with only 1% of wild-type actin-activated MgATPase activity retain essential in vivo function(s)." Proc Natl Acad Sci U S A **98**(16): 9122-7.
- Loomis, P. A., L. Zheng, G. Sekerkova, B. Changyaleket, E. Mugnaini and J. R. Bartles (2003). "Espin cross-links cause the elongation of microvillus-type parallel actin bundles in vivo." J Cell Biol **163**(5): 1045-55.
- Lou, X., T. McQuistan, R. A. Orlando and M. G. Farquhar (2002). "GAIP, GIPC and Galphai3 are concentrated in endocytic compartments of proximal tubule cells: putative role in regulating megalin's function." J Am Soc Nephrol **13**(4): 918-27.
- Lou, X., H. Yano, F. Lee, M. V. Chao and M. G. Farquhar (2001). "GIPC and GAIP form a complex with TrkA: a putative link between G protein and receptor tyrosine kinase pathways." Mol Biol Cell **12**(3): 615-27.
- Ma, S., P. Fey and R. L. Chisholm (2001). "Molecular motors and membrane traffic in Dictyostelium." Biochim Biophys Acta **1525**(3): 234-44.
- Marzolo, M. P., M. I. Yuseff, C. Retamal, M. Donoso, F. Ezquer, P. Farfan, Y. Li and G. Bu (2003). "Differential distribution of low-density lipoprotein-receptor-related protein (LRP) and megalin in polarized epithelial cells is determined by their cytoplasmic domains." Traffic **4**(4): 273-88.
- Melchionda, S., N. Ahituv, L. Bisceglia, T. Sobe, F. Glaser, R. Rabionet, M. L. Arbones, A. Notarangelo, E. Di Iorio, M. Carella, L. Zelante, X. Estivill, K. B. Avraham and P. Gasparini (2001). "MYO6, the human homologue of the gene responsible for deafness in Snell's waltzer mice, is mutated in autosomal dominant nonsyndromic hearing loss." Am J Hum Genet **69**(3): 635-40.

- Menetrey, J., A. Bahloul, A. L. Wells, C. M. Yengo, C. A. Morris, H. L. Sweeney and A. Houdusse (2005). "The structure of the myosin VI motor reveals the mechanism of directionality reversal." Nature **435**(7043): 779-85.
- Mermall, V., J. G. McNally and K. G. Miller (1994). "Transport of cytoplasmic particles catalysed by an unconventional myosin in living *Drosophila* embryos." Nature **369**(6481): 560-2.
- Mermall, V. and K. G. Miller (1995). "The 95F unconventional myosin is required for proper organization of the *Drosophila* syncytial blastoderm." J Cell Biol **129**(6): 1575-88.
- Merrifield, C. J., S. E. Moss, C. Ballestrem, B. A. Imhof, G. Giese, I. Wunderlich and W. Almers (1999). "Endocytic vesicles move at the tips of actin tails in cultured mast cells." Nat Cell Biol **1**(1): 72-4.
- Merrifield, C. J., D. Perrais and D. Zenisek (2005). "Coupling between clathrin-coated-pit invagination, cortactin recruitment, and membrane scission observed in live cells." Cell **121**(4): 593-606.
- Millo, H., K. Leaper, V. Lazou and M. Bownes (2004). "Myosin VI plays a role in cell-cell adhesion during epithelial morphogenesis." Mech Dev **121**(11): 1335-51.
- Mishra, S. K., P. A. Keyel, M. J. Hawryluk, N. R. Agostinelli, S. C. Watkins and L. M. Traub (2002). "Disabled-2 exhibits the properties of a cargo-selective endocytic clathrin adaptor." Embo J **21**(18): 4915-26.
- Mohiddin, S. A., Z. M. Ahmed, A. J. Griffith, D. Tripodi, T. B. Friedman, L. Fananapazir and R. J. Morell (2004). "Novel association of hypertrophic cardiomyopathy, sensorineural deafness, and a mutation in unconventional myosin VI (MYO6)." J Med Genet **41**(4): 309-14.
- Morris, S. M., S. D. Arden, R. C. Roberts, J. Kendrick-Jones, J. A. Cooper, J. P. Luzio and F. Buss (2002). "Myosin VI binds to and localises with Dab2, potentially linking receptor-mediated endocytosis and the actin cytoskeleton." Traffic **3**(5): 331-41.

- Morris, S. M. and J. A. Cooper (2001). "Disabled-2 colocalizes with the LDLR in clathrin-coated pits and interacts with AP-2." Traffic **2**(2): 111-23.
- Mukherjee, S., R. N. Ghosh and F. R. Maxfield (1997). "Endocytosis." Physiol Rev **77**(3): 759-803.
- Nagai, J., E. I. Christensen, S. M. Morris, T. E. Willnow, J. A. Cooper and R. Nielsen (2005). "Mutually dependent localization of megalin and Dab2 in the renal proximal tubule." Am J Physiol Renal Physiol **289**(3): F569-76.
- Nishikawa, S., K. Homma, Y. Komori, M. Iwaki, T. Wazawa, A. Hikikoshi Iwane, J. Saito, R. Ikebe, E. Katayama, T. Yanagida and M. Ikebe (2002). "Class VI myosin moves processively along actin filaments backward with large steps." Biochem Biophys Res Commun **290**(1): 311-7.
- Noguchi, T., M. Lenartowska and K. G. Miller (2006). "Myosin VI Stabilizes an Actin Network during Drosophila Spermatid Individualization." Mol Biol Cell.
- Nourry, C., S. G. Grant and J. P. Borg (2003). "PDZ domain proteins: plug and play!" Sci STKE **2003**(179): RE7.
- Novak, K. D. and M. A. Titus (1998). "The myosin I SH3 domain and TEDS rule phosphorylation site are required for in vivo function." Mol Biol Cell **9**(1): 75-88.
- Okten, Z., L. S. Churchman, R. S. Rock and J. A. Spudich (2004). "Myosin VI walks hand-over-hand along actin." Nat Struct Mol Biol **11**(9): 884-7.
- Oleinikov, A. V. and S. P. Makker (2000). "Increased expression of cytoplasmic tail-containing form of gp600/megalyn in active Heymann nephritis." J Pathol **192**(2): 251-6.
- Ostap, E. M., T. Lin, S. S. Rosenfeld and N. Tang (2002). "Mechanism of regulation of Acanthamoeba myosin-IC by heavy-chain phosphorylation." Biochemistry **41**(41): 12450-6.

- Osterweil, E., D. G. Wells and M. S. Mooseker (2005). "A role for myosin VI in postsynaptic structure and glutamate receptor endocytosis." J Cell Biol **168**(2): 329-38.
- Park, H., B. Ramamurthy, M. Travaglia, D. Safer, L. Q. Chen, C. Franzini-Armstrong, P. R. Selvin and H. L. Sweeney (2006). "Full-length myosin VI dimerizes and moves processively along actin filaments upon monomer clustering." Mol Cell **21**(3): 331-6.
- Petritsch, C., G. Tavosanis, C. W. Turck, L. Y. Jan and Y. N. Jan (2003). "The Drosophila myosin VI Jaguar is required for basal protein targeting and correct spindle orientation in mitotic neuroblasts." Dev Cell **4**(2): 273-81.
- Pfeffer, S. R., A. B. Dirac-Svejstrup and T. Soldati (1995). "Rab GDP dissociation inhibitor: putting rab GTPases in the right place." J Biol Chem **270**(29): 17057-9.
- Qualmann, B., M. M. Kessels and R. B. Kelly (2000). "Molecular links between endocytosis and the actin cytoskeleton." J Cell Biol **150**(5): F111-6.
- Reed, B. C., C. Cefalu, B. H. Bellaire, J. A. Cardelli, T. Louis, J. Salamon, M. A. Bloecher and R. C. Bunn (2005). "GLUT1CBP(TIP2/GIPC1) interactions with GLUT1 and myosin VI: evidence supporting an adapter function for GLUT1CBP." Mol Biol Cell **16**(9): 4183-201.
- Robblee, J. P., A. O. Olivares and E. M. de la Cruz (2004). "Mechanism of nucleotide binding to actomyosin VI: evidence for allosteric head-head communication." J Biol Chem **279**(37): 38608-17.
- Rock, R. S., B. Ramamurthy, A. R. Dunn, S. Beccafico, B. R. Rami, C. Morris, B. J. Spink, C. Franzini-Armstrong, J. A. Spudich and H. L. Sweeney (2005). "A flexible domain is essential for the large step size and processivity of myosin VI." Mol Cell **17**(4): 603-9.
- Rock, R. S., S. E. Rice, A. L. Wells, T. J. Purcell, J. A. Spudich and H. L. Sweeney (2001). "Myosin VI is a processive motor with a large step size." Proc Natl Acad Sci U S A **98**(24): 13655-9.

- Rogat, A. D. and K. G. Miller (2002). "A role for myosin VI in actin dynamics at sites of membrane remodeling during *Drosophila* spermatogenesis." J Cell Sci **115**(Pt 24): 4855-65.
- Rose, S. D., T. Lejen, L. Casaletti, R. E. Larson, T. D. Pene and J. M. Trifaro (2002). "Molecular motors involved in chromaffin cell secretion." Ann N Y Acad Sci **971**: 222-31.
- Rudolf, R., T. Kogel, S. A. Kuznetsov, T. Salm, O. Schlicker, A. Hellwig, J. A. Hammer, 3rd and H. H. Gerdes (2003). "Myosin Va facilitates the distribution of secretory granules in the F-actin rich cortex of PC12 cells." J Cell Sci **116**(Pt 7): 1339-48.
- Ruppel, K. M. and J. A. Spudich (1996). "Structure-function studies of the myosin motor domain: importance of the 50-kDa cleft." Mol Biol Cell **7**(7): 1123-36.
- Sahlender, D. A., R. C. Roberts, S. D. Arden, G. Spudich, M. J. Taylor, J. P. Luzio, J. Kendrick-Jones and F. Buss (2005). "Optineurin links myosin VI to the Golgi complex and is involved in Golgi organization and exocytosis." J Cell Biol **169**(2): 285-95.
- Sankaranarayanan, S., P. P. Atluri and T. A. Ryan (2003). "Actin has a molecular scaffolding, not propulsive, role in presynaptic function." Nat Neurosci **6**(2): 127-35.
- Sato, O., H. D. White, A. Inoue, B. Belknap, R. Ikebe and M. Ikebe (2004). "Human deafness mutation of myosin VI (C442Y) accelerates the ADP dissociation rate." J Biol Chem **279**(28): 28844-54.
- Schmid, S. L. (1997). "Clathrin-coated vesicle formation and protein sorting: an integrated process." Annu Rev Biochem **66**: 511-48.
- Schott, D. H., R. N. Collins and A. Bretscher (2002). "Secretory vesicle transport velocity in living cells depends on the myosin-V lever arm length." J Cell Biol **156**(1): 35-9.

- Seiler, C., O. Ben-David, S. Sidi, O. Hendrich, A. Rusch, B. Burnside, K. B. Avraham and T. Nicolson (2004). "Myosin VI is required for structural integrity of the apical surface of sensory hair cells in zebrafish." Dev Biol **272**(2): 328-38.
- Self, T., T. Sobe, N. G. Copeland, N. A. Jenkins, K. B. Avraham and K. P. Steel (1999). "Role of myosin VI in the differentiation of cochlear hair cells." Dev Biol **214**(2): 331-41.
- Sheff, D. R., R. Kroschewski and I. Mellman (2002). "Actin dependence of polarized receptor recycling in Madin-Darby canine kidney cell endosomes." Mol Biol Cell **13**(1): 262-75.
- Shurety, W., N. L. Stewart and J. L. Stow (1998). "Fluid-phase markers in the basolateral endocytic pathway accumulate in response to the actin assembly-promoting drug Jasplakinolide." Mol Biol Cell **9**(4): 957-75.
- Smith, D. A. and R. M. Simmons (2001). "Models of motor-assisted transport of intracellular particles." Biophys J **80**(1): 45-68.
- Smythe, E., T. E. Redelmeier and S. L. Schmid (1992). "Receptor-mediated endocytosis in semiintact cells." Methods Enzymol **219**: 223-34.
- Soldati, T. (2003). "Unconventional myosins, actin dynamics and endocytosis: a menage a trois?" Traffic **4**(6): 358-66.
- Songyang, Z., A. S. Fanning, C. Fu, J. Xu, S. M. Marfatia, A. H. Chishti, A. Crompton, A. C. Chan, J. M. Anderson and L. C. Cantley (1997). "Recognition of unique carboxyl-terminal motifs by distinct PDZ domains." Science **275**(5296): 73-7.
- Spector, I., N. R. Shochet, Y. Kashman and A. Groweiss (1983). "Latrunculins: novel marine toxins that disrupt microfilament organization in cultured cells." Science **219**(4584): 493-5.
- Spudich, J. A. (2001). "The myosin swinging cross-bridge model." Nat Rev Mol Cell Biol **2**(5): 387-92.

- Strom, M., A. N. Hume, A. K. Tarafder, E. Barkagianni and M. C. Seabra (2002). "A family of Rab27-binding proteins. Melanophilin links Rab27a and myosin Va function in melanosome transport." J Biol Chem **277**(28): 25423-30.
- Swiatecka-Urban, A., C. Boyd, B. Coutermarsh, K. H. Karlson, R. Barnaby, L. Aschenbrenner, G. M. Langford, T. Hasson and B. A. Stanton (2004). "Myosin VI regulates endocytosis of the cystic fibrosis transmembrane conductance regulator." J Biol Chem **279**(36): 38025-31.
- Tapon, N. and A. Hall (1997). "Rho, rac and cdc42 GTPases regulate the organization of the actin cytoskeleton." Current Opinion in Cell Biology **9**: 86-92.
- Taunton, J., B. A. Rowning, M. L. Coughlin, M. Wu, R. T. Moon, T. J. Mitchison and C. A. Larabell (2000). "Actin-dependent propulsion of endosomes and lysosomes by recruitment of N-WASP." J Cell Biol **148**(3): 519-30.
- Titus, M. A. (1999). "A class VII unconventional myosin is required for phagocytosis." Curr Biol **9**(22): 1297-303.
- Trifaro, J., S. D. Rose, T. Lejen and A. Elzagallaai (2000). "Two pathways control chromaffin cell cortical F-actin dynamics during exocytosis." Biochimie **82**(4): 339-52.
- Trischler, M., W. Stoorvogel and O. Ullrich (1999). "Biochemical analysis of distinct Rab5- and Rab11-positive endosomes along the transferrin pathway." J Cell Sci **112** (Pt 24): 4773-83.
- Van Dijk, J., M. Furch, C. Lafont, D. J. Manstein and P. Chaussepied (1999). "Functional characterization of the secondary actin binding site of myosin II." Biochemistry **38**(46): 15078-85.
- van Ham, M. and W. Hendriks (2003). "PDZ domains-glue and guide." Mol Biol Rep **30**(2): 69-82.

- Varadi, A., T. Tsuboi and G. A. Rutter (2005). "Myosin Va transports dense core secretory vesicles in pancreatic MIN6 beta-cells." Mol Biol Cell **16**(6): 2670-80.
- Volkman, D., T. Mori, U. K. Tirlapur, K. Konig, T. Fujiwara, J. Kendrick-Jones and F. Baluska (2003). "Unconventional myosins of the plant-specific class VIII: endocytosis, cytokinesis, plasmodesmata/pit-fields, and cell-to-cell coupling." Cell Biol Int **27**(3): 289-91.
- Walsh, N. P., B. M. Alba, B. Bose, C. A. Gross and R. T. Sauer (2003). "OMP peptide signals initiate the envelope-stress response by activating DegS protease via relief of inhibition mediated by its PDZ domain." Cell **113**(1): 61-71.
- Wang, F., E. V. Harvey, M. A. Conti, D. Wei and J. R. Sellers (2000). "A conserved negatively charged amino acid modulates function in human nonmuscle myosin IIA." Biochemistry **39**(18): 5555-5560.
- Wang, L. H., R. G. Kalb and S. M. Strittmatter (1999). "A PDZ protein regulates the distribution of the transmembrane semaphorin, M-SemF." J Biol Chem **274**(20): 14137-46.
- Wang, Z. Y., F. Wang, J. R. Sellers, E. D. Korn and J. A. Hammer, 3rd (1998). "Analysis of the regulatory phosphorylation site in *Acanthamoeba* myosin IC by using site-directed mutagenesis." Proc Natl Acad Sci U S A **95**(26): 15200-5.
- Warner, C. L., A. Stewart, J. P. Luzio, K. P. Steel, R. T. Libby, J. Kendrick-Jones and F. Buss (2003). "Loss of myosin VI reduces secretion and the size of the Golgi in fibroblasts from Snell's waltzer mice." Embo J **22**(3): 569-79.
- Wells, A. L., A. W. Lin, L. Chen, D. Safer, S. M. Cain, T. Hasson, B. O. Carragher, R. A. Milligan and H. L. Sweeny (1999). "Myosin Vi is an actin-based motor that moves backwards." Nature **401**: 505-507.
- Wells, A. L., A. W. Lin, L. Q. Chen, D. Safer, S. M. Cain, T. Hasson, B. O. Carragher, R. A. Milligan and H. L. Sweeney (1999). "Myosin VI is an actin-based motor that moves backwards." Nature **401**(6752): 505-8.

- Westbroek, W., J. Lambert, P. Bahadoran, R. Busca, M. C. Herteleer, N. Smit, M. Mommaas, R. Ballotti and J. M. Naeyaert (2003). "Interactions of human Myosin Va isoforms, endogenously expressed in human melanocytes, are tightly regulated by the tail domain." J Invest Dermatol **120**(3): 465-75.
- Wu, C., V. Lytvyn, D. Y. Thomas and E. Leberer (1997). "The phosphorylation site for Ste20p-like protein kinases is essential for the function of myosin-I in yeast." The Journal of Biological Chemistry **272**(49): 30623-30626.
- Wu, X., K. Rao, M. B. Bowers, N. G. Copeland, N. A. Jenkins and J. A. Hammer, 3rd (2001). "Rab27a enables myosin Va-dependent melanosome capture by recruiting the myosin to the organelle." J Cell Sci **114**(Pt 6): 1091-100.
- Wu, X., F. Wang, K. Rao, J. R. Sellers and J. A. Hammer, 3rd (2002). "Rab27a is an essential component of melanosome receptor for myosin Va." Mol Biol Cell **13**(5): 1735-49.
- Xu, P., K. I. Mitchelhill, B. Kobe, B. E. Kemp and H. G. Zot (1997). "The myosin-I-binding protein Acan125 binds the SH3 domain and belongs to the superfamily of leucine-rich repeat proteins." Proc Natl Acad Sci U S A **94**(8): 3685-90.
- Yamashita, R. A. and G. S. May (1998). "Constitutive activation of endocytosis by mutation of myoA, the myosin I gene of *Aspergillus nidulans*." The Journal of Biological Chemistry **273**(23): 14644-14648.
- Yang, L. E., A. B. Maunsbach, P. K. Leong and A. A. McDonough (2005). "Redistribution of myosin VI from top to base of proximal tubule microvilli during acute hypertension." J Am Soc Nephrol **16**(10): 2890-6.
- Yarmola, E. G., T. Somasundaram, T. A. Boring, I. Spector and M. R. Bubb (2000). "Actin-latrunculin A structure and function. Differential modulation of actin-binding protein function by latrunculin A." J Biol Chem **275**(36): 28120-7.
- Yildiz, A., H. Park, D. Safer, Z. Yang, L. Q. Chen, P. R. Selvin and H. L. Sweeney (2004). "Myosin VI steps via a hand-over-hand mechanism with its lever arm undergoing fluctuations when attached to actin." J Biol Chem **279**(36): 37223-6.

Yoshimura, M., K. Homma, J. Saito, A. Inoue, R. Ikebe and M. Ikebe (2001). "Dual regulation of mammalian myosin VI motor function." J Biol Chem **276**(43): 39600-7.

Zerial, M. and H. McBride (2001). "Rab proteins as membrane organizers." Nat Rev Mol Cell Biol **2**(2): 107-17.